STRESS SEPARATION IN DIGITAL PHOTOELASTICITY BY INTEGRATION OF EQUILIBRIUM EQUATIONS

A thesis Submitted
in partial fulfilment of the requirements
for the degree of

MASTER OF TECHNOLOGY

February, 1999

by
DHISH KUMAR SAXENA

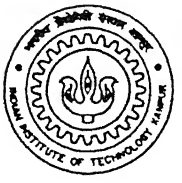

DEPARTMENT OF MECHANICAL ENGINEERING
INDIAN INSTITUTE OF TECHNOLOGY
KANPUR - 208 016 (INDIA)

01 JUN 1999 /ME
CENTRAL LIBRARY
I. I. T., KANPUR
Acc. No. A 128076

TH
ME|1999|M
Sa98s

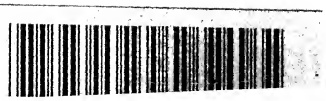

Submitted on 22.02.99

CERTIFICATE

This is to certify that the thesis entitled, **STRESS SEPARATION IN DIGITAL PHOTOELASTICITY BY INTEGRATION OF EQUILIBRIUM EQUATIONS** by *Dhish Kumar Saxena* is a record of the work carried out under my supervision and has not been submitted elsewhere for a degree.

February, 1999.

22/2/99

Dr. K. Ramesh

(Associate Professor)

Department Of Mechanical Engineering,

Indian Institute Of Technology,Kanpur.

ABSTRACT

Photoelasticity is an optical method of experimental stress analysis which yields a whole-field representation of the principal-stress difference and its orientations. Though a large class of problems can be solved using the information of difference in principal stress alone, a certain class of problems need the value of individual stress components.The process of obtaining the individual values of the principal stresses separately is referred to as stress separation. Several separation methods have been developed to determine the individual values of the principal stresses.

The present work discusses two methods of stress separation namely: shear difference method and Trebuna's method for stress separation. Before the advent of widespread use of digital computers, shear difference technique was widely used for stress separation. The purpose of the present thesis is to have a relook on the applicability of this technique in digital photoelasticity. The various issues related to the digital implementation of the techniques are discussed in this thesis. To verify the implementation, initially fringe order and principal stress direction for the problem of a disc under diametral compression are used from theory of elasticity solution. The results compare very well with theory. Experimental data for the problem of disc under diametral compression is obtained using the phase shifting technique. As the phase shifting technique generally gives better values of isochromatic fringe order than the isoclinic value, initially stress components are obtained using experimental isochromatic fringe order and theoretical isoclinic value. Quantitative results for few arbitrary lines are compared with theoretical solutions. To verify the whole field implementation pseudo fringe patterns were plotted for individual stress components and compared with theory.

In order to fully utilize the experimental data, the suitability of various methods for evaluating isoclinic value by phase shifting technique is discussed. The use of multiple load method for isoclinic determination, provided better values of isoclinic parameter for stress separation. Separation of stress components is then carried out for the problem of a finite plate with a hole in uniaxial tension.

ACKNOWLEDGEMENTS

I wish to express my deep sense of gratitude and indebtedness towards Dr.K.Ramesh for his inspiring guidance, invaluable suggestions and constructive criticism, without which this work would not have materialized. He has always been a constant source of encouragement throughout my thesis work. "Plan, well" and "Framing question is an art. The better you try to frame it, more chances you have to reach the solution yourself". These messages of his, I'm sure will always help me in life ahead.

I am extremely thankful to Shri S.K.Mangal for his constant support and help, whenever I needed it. I heartily appreciate the keen interest shown by Dheeraj, Vinayak & Kulkarni in the Lab and their support to me.I also thank Radheshyamji for his invariable readiness to help me. I've had a great company with them, all through.

I must not skip to mention the gift of nature to me, here in IIT.K. I got two brother friends - Tariq Bhai and Samar. Their support cannot be expressed through words. I look forward to a never-lasting relationship with them. Nema's dream of being most versatile, Amreesh's running to phonebooth, Sandeep's large-criteria, Neeraj's dedication & Asit's moustaches will always be remembered. Maneesh and Praveen will be missed for their lively moods.

Last but not the least, my indebtedness towards my parents, my brother & sister, whose love affection & support has always been behind me, is worthmentioning.

Om

Om Ram, Shri Ram, Jai Jai Ram,
Jai Raghuvar, Jai Krishna,
Jai Shyam, Jai Jai Ram.

Dedicated to....

MY GRANDPARENTS.

...who are the guiding spirits of my life.

LIST OF CONTENTS

ABSTRACT

LIST OF FIGURES

LIST OF TABLES

CHAPTER 1 INTRODUCTION

1.1 Introduction 1

1.2 Present work 2

1.3 Thesis layout 3

CHAPTER 2 STRESS SEPARATION TECHNIQUES IN PHOTOELASTICITY

2.1 Introduction 5

2.2 Methods of stress separation 6

2.3 Need for application of shear difference scheme in digital photoelasticity 9

2.4 Shear difference method 10

2.5 Trebuna's method 13

2.6 Generation of theoretical data and application of stress separation schemes 14

2.6.1 Physical significance of the grid 15

2.6.2 User's input data 17

2.6.3 Scheme for horizontal scanning 17

2.6.4 Scheme for vertical scanning 18

2.7 Effect of grid size 30

2.8 Comparitive analysis of accuracy aspects of shear difference and Trebuna's method 35

CHAPTER 3 STRESS SEPARATION IN DIGITAL PHOTOELASTICITY

3.1 Introduction 36

3.2 Need for automation of data acquisition 37

3.3 Phase shifting in photoelasticity 38

3.3.1 Patterson and Wang's scheme: Use of circular polariscope 40

3.3.2 Plane polariscope arrangement 43

3.4 Image processing set-up 44

3.5 Experimental evaluation and whole field representation of fractional retardation 45

3.6 Boundary detection 48

3.6.1 Utility of boundary information 51

3.7 The grid system in digital domain 55

3.8 Digital implementation of stress separation techniques

3.8.1 Verification of algorithm,using theoretical data 60

3.8.1.1 Transformation law 61

3.8.1.2 The free boundary 61

3.8.2 Use of N from phase shifting; θ from theory 68

3.8.3 Use of N from phase shifting; θ from plane polariscope 72

3.8.4 Use of N from phase shifting;

θ from plane polariscope;

use of multiple loads 72

3.8.5 Whole field representation of

the results 85

3.8.6 Plate with a hole 90

3.9.1 Boundary information 90

CHAPTER 4 CONCLUSIONS AND SUGGESTIONS FOR FUTURE WORK

4.1 Conclusions 95

4.2 Suggestions for future work 96

REFERENCES 97

APPENDIX-I 100

APPENDIX-II 101

APPENDIX-III 102

LIST OF FIGURES

Fig. 2.1 Oblique incidence method. 7

Fig. 2.2 Direction of scan along a horizontal grid. 12

Fig. 2.3 Concept of a grid system. 16

Fig. 2.4 Scheme for horizontal scanning: (a) All grids of equal size (b) Unequal grid at boundary. 18

Fig. 2.5 Variation of stresses over various horizontal lines: (a) y = 0 (mm) (b) y = R/2 (mm) (c) y = 3R/4 (mm). 21

Fig. 2.6 Scheme for vertical scanning: (a) All grids of equal size (b) Unequal grid at boundary. 22

Fig. 2.7 Assignment of starting point in vertical scanning. 24

Fig. 2.8 Variation of stresses over various vertical lines with initial horizontal scan at y = R/2, (a) x = 0 (mm) (b) x = R/2 (mm) (c) x = 3R/4 (mm) 28

Fig. 2.9 Full field variation of stresses by shear difference method (a) σ_x (b) σ_y 29

Fig. 2.10 Effect of grid size over accuracy of stresses for horizontal scan at y = R/2 (mm) (a) Pixel dimensions (b) 5 times pixel dimensions (c) 10 times pixel dimensions. 31

Fig. 2.11 Effect of grid size over accuracy of stresses for vertical scan at x = R/2 (mm), for an initial horizontal scan at y = R/2 (mm), (a)Pixel dimensions (b) 5 times pixel dimensions (c) 10 times pixel dimensions. 32

Fig. 2.12 Comparitive study of Trebuna vs Shear difference method

for horizontal scan at y = R/2 with erroneous Isoclinic data: (a) 10% error (b) 20% error (c) 50% error. 33

Fig. 2.13 Comparitive study of Trebuna vs Shear difference method for vertical scans with: 20% error in isoclinic data, Initial horizontal scan at y= R/2. (a) x = 0 (mm) (b) x = R/2 (mm) (c) x = 3R/4 (mm). 34

Fig. 3.1 Circular polariscope arrangement for phase shifting technique. 39

Fig. 3.2 Plane polariscope arrangement for phase shifting technique. 42

Fig. 3.3 The sequence of six images of a circular disc under diametral compression recorded for phase shifting technique, by plane polariscope arrangement. 46

Fig. 3.4 Figure showing the various representations of the phase retardation. (a) Simulated dark field (b) Simulated bright field (c) Phase map. 47

Fig. 3.5 Histogram of the bright field image of the circular disc undar diametral compression. 50

Fig. 3.6 Magnified pixel representation of a curved segment on the screen 50

Fig. 3.7 Boundary detection for a circular disc. 50

Fig. 3.8 Utility of boundary information. 52

Fig. 3.9 Boundary simulated by pixel location. 54

Fig. 3.10 Averaging scheme for a particular grid. 56

Fig. 3.11 The grid system in digital domain. 58

Fig. 3.12 Generation of spatial coordinates for a pixel in the region of interest. 61

Fig. 3.13 Transformation of stress along a new set of axes. 62

Fig. 3.14 The free boundary. 63

Fig. 3.15 Use of theoretical data. Variation of stresses over horizontal scan line at y = 0 (mm).(a) variation of σ_x, σ_y.(b) variation of τ_{xy} 64

Fig. 3.16 Use of theoretical data. Variation of stresses over horizontal scan line at y = R/2 (mm). (a) variation of σ_x, σ_y. (b) variation of τ65 65

Fig. 3.17 Use of theoretical data. Variation of stresses over horizontal scan line at y = 3R/4 (mm).(a) variation of σ_x, σ_y.(b) variation of τ_{xy} 66

Fig. 3.18 Variation of Isochromatic parameter (N), obtained from phase shifting technique, for horizontal scan lines at (a) y = 0 (mm) (b) y = R/2 (mm) (c) y = 3R/4 (mm) 67

Fig. 3.19 Variation of Isochromatic parameter (N), along the boundary of the quarter disc. 68

Fig. 3.20 Use of N: phase shifting; θ: theoretical. Variation of stresses over horizontal scan line at y = 0 (mm). (a) variation of σ_x, σ_y. (b) variation of τ_{xy} 69

Fig. 3.21 Use of N: phase shifting; θ: theoretical. Variation of stresses over horizontal scan line at y = R/2 (mm). (a) variation of σ_x, σ_y. (b) variation of τ_{xy} 70

Fig. 3.22 Use of N: phase shifting; θ: theoretical. Variation of

stresses over horizontal scan line at y = 3R/4 (mm). (a) variation of σ_x, σ_y.(b) variation of τ_{xy} 71

Fig. 3.23 Comparative study of Isoclinic parameter θ: circular polariscope vs. plane polariscope arrangement, for various horizontal scan lines. (a) y = 0 (mm) (b) y = R/2 (mm) (c) y = 3R/4 (mm). 73

Fig. 3.24 Comparative study of Isoclinic parameter θ, obtained from plane polariscope arrangement: Single load vs. Multiple load, for various horizontal scan lines.(a) y = 0 (mm) (b) y = R/2 (mm) (c) y = 3R/4 (mm) 74

Fig. 3.25 Variation of Isochromatic parameter (N), along the boundary of the quarter disc. 76

Fig. 3.26 Use of N: phase shifting; θ: plane polariscope / multiple loads. Variation of stresses over horizontal scan line at y = 0 (mm). (a) variation of σ_x, σ_y. (b) variation of τ_{xy} 77

Fig. 3.27 Use of N: phase shifting; θ: plane polariscope / multiple loads. Variation of stresses over horizontal scan line at y = R/2 (mm). (a) variation of σ_x, σ_y. (b) variation of τ_{xy} 78

Fig. 3.28 Use of N: phase shifting; θ: plane polariscope / multiple loads. Variation of stresses over horizontal scan line at y = 3R/4 (mm). (a) variation of σ_x, σ_y. (b)variation of τ_{xy} 79

Fig. 3.29 Use of N: phase shifting; θ: plane polariscope / multiple loads. Variation of stresses over horizontal scan line at y = R/4 (mm). (a) variation of σ_x, σ_y. (b) variation of τ_{xy} 80

Fig. 3.30 Variation of photoelastic data for horizontal scan line at y

= R/4 (mm). (a)variation of N: phase shifting. (b) variation of θ: plane polariscope arrangement using multiple loads. 81

Fig. 3.31 Modification of Isoclinic parameter (θ), along the boundary (a) the proposed scheme (b) improved variation along the boundary. 83

Fig. 3.32 Use of N: phase shifting; θ: modified form of - plane polariscope / multiple loads. Variation of stresses over various horizontal scan lines. (a) y = 0 (mm) (b) y = R/2 (mm) (c) y = 3R/4 (mm) 84

Fig. 3.33 Pseudo fringe patterns showing variation of stresses, determined using theoretical data and standard solution for disc under diametral compression. 86

Fig. 3.34 Pseudo fringe patterns for σ_x for various sets of input data.(a) N:theory; θ:theory - shear diff. (b) N:theory; θ:theory - Trebuna (c) N:p-sftg; θ:theory - shear diff. (d) N:p-sftg; θ:theory - Trebuna (f) N:p-sftg; θ:mult.loads - shear diff.(f) N:p-sftg; θ:mult.loads-Trebuna 87

Fig. 3.35 Pseudo fringe patterns for σ_y for various sets of input data. (a) N:theory; θ:theory - shear diff. (b) N:theory; θ:theory - Trebuna (c) N:p-sftg; θ:theory - shear diff. (d) N:p-sftg; θ:theory - Trebuna (f) N:p-sftg; θ:mult.loads - shear diff.(f) N:p-sftg; θ:mult.loads-Trebuna 88

Fig. 3.36 Pseudo fringe patterns for τ_{xy} for various sets of input data. (a) N:theory; θ:theory - shear diff. (b) N:theory;

θ:theory - Trebuna (c) N:p-sftg; θ:theory - shear diff. (d) N:p-sftg; θ:theory - Trebuna (f) N:p-sftg; θ:mult.loads - shear diff.(f) N:p-sftg; θ:mult.loads-Trebuna 89

FIG.3.37 The sequence of six images of a plate with a hole under uni-axial tension recorded for phase shifting technique, by plane polariscope arrangement 92

Fig. 3.38 Field variation of principal stresses for the plate with a hole (a) σ_1: FEM (b) σ_2: FEM (c) σ_1: shear diff. (d) σ_2: shear diff. (e) σ_1: Trebuna (f) σ_2: Trebuna 93

LIST OF TABLES

Table 3.1 Table showing intensity equations for various optical arrangements used in phase shifting algorithm, with circular polariscope arrangement 41

Table 3.2 Table showing that only six intensity equations are independent . . 43

Table 3.3 Table showing the intensity equations for the different orientations of the polariser and the analyser 44

Chapter 1

INTRODUCTION

1.1 Introduction

Photoelasticity deals with determination of stress fields by the use of polarised light. This method is based on the temporary or artificial birefringence effect. Certain transparent, non crystalline materials like Plexiglas, celluloid, homolite, epoxy[1] etc., are optically isotropic when not loaded but become optically anisotropic and display characteristics similar to crystals when they are stressed[2]. The birefringence in the material is retained only during the application of the loads and disappears when they are removed. Measurements of this birefringence provides data adequate for quantitative determination of the corresponding state of stress.

The measurements are made with the help of an optical instrument called the polariscope. A polariscope could be used to find out, namely, the maximum shear stress i.e. the difference in principal stresses and the orientation of principal stresses. The corresponding contours seen by the polariscope are called isochromatics and isoclinic fringes. The experimentation in photoelasticity involves acquisition of these images and their interpretation. To interpret the photoelastic images, data should be collected from the images and these data should be analyzed. The main merit of photoelasticity is its simplicity in experimentation as well as in the evaluation of the stress field.

1.2 Present work

It is well known that a direct photoelastic approach cannot solve completely a general stress problem. The conventional photoelastic method provides two independent equations for a two-dimensional problem and five independent equations for a three dimensional problem[3]. Since there are three unknown stress components for a two dimensional problem and six unknown stress components for a three dimensional problem, the equations obtained by photoelasticity are not sufficient to determine the complete state of stress at any interior point. Hence, with a view to obtain additional relation, several auxiliary methods have been developed both for two and three dimensional problems, which in conjunction with photoelastic analysis provides the complete information for solving a general stress problem. Since all such methods provide additional information and enable the evaluation of stress components separately, these are referred to as stress separation methods. Each of these methods have their own advantage, limitation and application.

The present work focuses on the shear difference technique. This method is relatively easier to employ for both two and three dimensional problems. This also happens to be one of the most widely used method, however it inherently bears the property of accumulation of errors, which further go on increasing, as one proceeds along the line of interest. Trebuna has modified the shear difference technique to minimize error accumulation. This method works on the principle of Block Integration. The isoclinic parameter which is the chief source of error is averaged along the 3 lines of the grid (the grid being employed as an integral feature of these methods) and assumed to represent the isoclinic along the centre line. With the noisy points of

isoclinic data being "smoothened out", this method is supposed to offer better results.

A comparative analysis of these two methods is done for a disc under diametral compression. For this purpose first an error free set of data is theoretically generated through the standard solution of the stress field of circular disc under diametral compression. Trebuna's method hardly shows any improvement over the conventional shear difference technique Error is intentionally introduced in the value of isoclinic parameter and it is observed that the averaging effect in Trebuna's method does improve the accuracy of evaluation.

Then use of experimentally obtained photoelastic data is studied. Use of phase-shifting technique, which uses the intensity data in spatial domain to extract the isochromatics over the field, is employed. In this technique, one has to record a few images corresponding to different optical arrangements for a given experimental set up. Phase-shifting technique, in general provides the estimation of fringe orders with reasonable accuracy. However the isoclinic parameter is not quite accurate. Hence, different optical arrangements to evaluate the isoclinic parameter such as a circular polariscope and a plane polariscope arrangement, are studied. The isoclinic parameter obtained by plane polariscope arrangement is found to be more accurate as against the circular polariscope arrangement and hence is suggested for analysis. The analysis is further improved by using multiple loads in plane polariscope arrangement for obtaining isoclinic data.

With the two methods established for the disc under diametral compression, in the light of various combinations of photoelastic data, a similar analysis is performed for a plate with a hole, subjected to uniaxial tension, using completely experimental data.

1.3 THESIS LAYOUT

In chapter 2, first an overview of some of the well established methods of stress separation is presented. It then discusses in detail the shear difference method and it's modified version i.e., Trebuna's method. Comparative analysis of the two methods is made by intentionally introducing error in the isoclinic parameter (θ). The results have been graphically recorded and presented. The effect of grid size on the accuracy of the results has also been discussed.

Chapter 3 focuses on the use of experimental data for stress separation. The analysis starts with theoretical solutions, being used as input data. Then partly realistic data is used for the analysis. This partly realistic data is in the form of the isochromatic parameter (N) which is obtained by the phase-shifting technique. Finally completely realistic data is employed for the analysis, with the isoclinic parameter (θ), which in real sense is the main cause of errors, being experimentally determined using the circular polariscope arrangement and the plane polariscope arrangement. Here it is proved that θ obtained from plane polariscope arrangement is better than that obtained from circular polariscope arrangement. The superiority of θ obtained by superimposition of two images (grabbed with plane polariscope arrangement) over θ obtained by a single image is also discussed here. The analysis for the case of plate with a hole, using completely realistic data is also discussed in this chapter.

CHAPTER 2

STRESS SEPARATION TECHNIQUES IN PHOTOELASTICITY

2.1 INTRODUCTION

Photoelasticity is an experimental method for analyzing stress fields which yields the principal stress difference and its orientation in the form of fringes that are known as isochromatics and isoclinics respectively.

The fringe pattern obtained by normal incidence in a circular polariscope can be related to principal stress difference using stress optic law as,

$$\sigma_1 - \sigma_2 = \frac{NF_\sigma}{t} \tag{2.1}$$

where F_σ is material stress fringe value (N/mm/fringe), N is fringe order at the point of interest and t is model thickness in mm.

It is evident that the pure photoelastic method cannot solve completely a general stress problem. The conventional photoelastic method provides two independent equations for a two-dimensional problem and five independent equations for a three dimensional problem. Since there are three unknown stress components for a two dimensional problem and six unknown stress components for a three dimensional problem, the equations obtained by photoelasticity are not sufficient to determine the complete state of stress at any interior point. Hence with a view to obtain additional

relations, several auxiliary methods are required for both two and three dimensional problems, which in conjunction with photoelastic analysis can provide the complete information for solving a general stress problem. Determination of $\sigma 1$ and $\sigma 2$ separately by utilising additional information is referred as stress-separation.

2.2 Methods of Stress-Separation

In a broad sense, the stress separation techniques can be divided into four main categories. These categories are

(i) Oblique Incidence Method.

(ii) Use of Compatibility Equation.

(iii) Shear difference Method or integration of the equilibrium condition.

(iv) Hybrid methods based on combination of experimental & numerical methods.

In oblique incidence method, additional equation for stress separation is obtained by making photoelastic measurements in oblique incidence,as shown in Fig. 2.1. To minimise refraction effects the model is to be immersed in a tank of liquid having same refractive index as the model. The secondary principal stresses along the light path are assumed to cause the formation of photoelastic fringes[4]. The method is basically a point by point technique.

If the model is viewed normally(the direction of incidence being along z axis in x-z plane) and obliquely (the directions of incidence being at angles $+\phi$ and $-\phi$ to the z axis) the data obtained is sufficient to yield the unknown stress components.

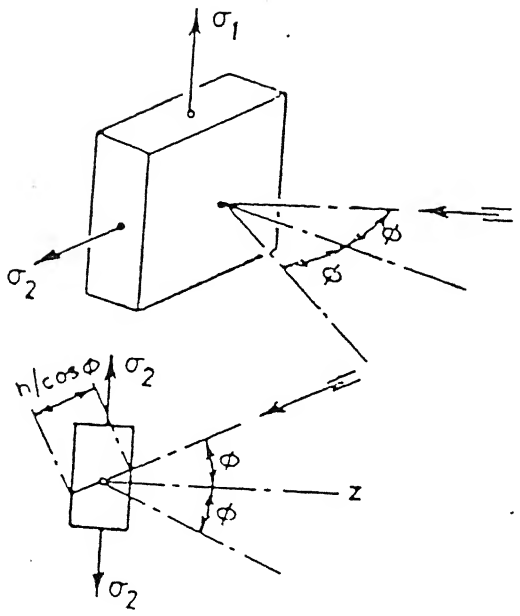

Fig. 2.1 Oblique incidence method.

Case a: Normal Incidence

N : Corresponding Fringe order

θ : Corresponding Isoclinic Parameter

Case b: Oblique Incidence at angle ϕ'

N': Corresponding Fringe Order

θ': Corresponding Isoclinic Parameter

Case c: Oblique Incidence at angle -ϕ'

N": Corresponding Fringe Order

θ": Corresponding Isoclinic Parameter

If the notation for the Fringe order and Isoclinic Parameter corresponding to the different directions of incidence, is as referred above and the material fringe value and the model thickness are represented by F_σ and h respectively, then the solution can be represented in the form:

$$\sigma_x - \sigma_y = \frac{N F_\sigma}{h} cos2\theta \tag{2.2}$$

$$\sigma_z - \sigma_x = \frac{F_\sigma}{2hsin^2\phi} (N'' cos2\theta'' \cos\phi' + N' cos2\theta' \cos\phi' - 2N cos2\theta) \tag{2.3}$$

$$\tau_{xy} = \frac{F_\sigma}{2h} Nsin2\theta \tag{2.4}$$

$$\tau_{yz} = \frac{F_\sigma \cos\phi'}{2h\sin\phi'} (Nsin2\theta - N' sin2\theta') \tag{2.5}$$

$$\tau_{zx} = \frac{F_\sigma}{4\sin\phi'} (N'' cos2\theta'' - N' cos2\theta') \tag{2.6}$$

This is the maximum information obtainable from photoelastic observations alone and enables the determination of the individual stress components. The biggest advantage of the method is that the stresses can be separated at all points in the model independent of neighbouring points.

In the compatibility equation method, separation of stresses is accomplished by using the solution of $\sigma_x + \sigma_y$, (the first stress invariant for constant body forces) and the photoelastic data $\sigma_1 - \sigma_2$. This offers greater accuracy since the isoclinic angle θ is not involved in the determination of principal stresses. The compatibility equation method requires a good knowledge of the boundary values of the model which may be difficult to achieve as time-edge effect or residual stresses due to machining are significant.

Before the advent of widespread use of digital computers, the shear difference method was widely used technique for stress separation. One of the main drawbacks of this is the accumulation of error, which builds up as one proceeds along the line of interest. This has been reported mainly due to the poor experimental evaluation of the

isoclinic angle. The recent modification by Trebuna on numerically integrating the shear component's differentials, has to a great extent diminished this problem. In conventional analysis the data is collected over discrete array of points. However, in digital photoelasticity, the data array could be finer and it can be just one pixel. The resolution of the pixel could be increased by appropriate optical magnification. The purpose of the present thesis is to have a relook on the applicability of shear difference technique for stress separation in digital photoelasticity.

The hybrid techniques[5] are extremely involved. Some techniques utilize the photoelastic results partially and rely on numerical procedures while some attempt to obtain the required information based entirely on experimental data. The technique of using only the experimentally determined surface stresses and numerical methods for interior stresses facilitates important applications. These techniques have been utilized for stress analysis of 3-D bodies as well as on models of different material like photo-orthotropic materials[6].

2.3 NEED FOR APPLICATION OF SHEAR DIFFERENCE SCHEME IN DIGITAL PHOTOELASTICITY

The main advantage of photoelasticity is that, it can give the stress distribution for the whole field. But it gives this result as an image of fringe patterns. The main task in photoelasticity is the interpretation of these fringe patterns. In conventional methods tedious compensation methods are needed to obtain the fractional fringe orders at any point other than the fringe areas. The number of data points that could be considered is also less. These procedures are quite involved and requires skill in the identification of

isochromatics. Hence, automation of data acquisition and analysis to minimize these problems and to provide fast and most accurate results, has become essential. With the advent of PC based digital image processing systems, considerable success has been achieved in automating the data acquisition from the entire field and it has now become possible to evaluate the total fringe order at every pixel in the domain. With the availability of photoelastic data, at pixel level, it becomes relevant to study shear difference scheme in the context of digital photoelasticity. This would offer scope for improvement in the results as unlike the conventional approach where a coarse data array is selected, the data array size could be much finer, as fine as just one pixel.

2.4 SHEAR DIFFERENCE METHOD

The shear difference method, uses the integral form of the equilibrium equation[7]. In the absence of body forces, the equation of equilibrium when applied to the problem of plane stress are,

$$\begin{aligned} \frac{\partial \sigma_x}{\partial x} + \frac{\partial \tau_{yx}}{\partial y} &= 0 \\ \frac{\partial \sigma_y}{\partial y} + \frac{\partial \tau_{xy}}{\partial x} &= 0 \end{aligned} \tag{2.7}$$

Equation (2.7) may be re-arranged and integrated to become,

$$\sigma_x = (\sigma_x)_o - \int \frac{\partial \tau_{yx}}{\partial y}\, dx \tag{2.8}$$

$$\sigma_y = (\sigma_y)_o - \int \frac{\partial \tau_{xy}}{\partial x}\, dy \tag{2.9}$$

These can be approximated using the finite difference expressions,

$$\sigma_x = (\sigma_x)_o - \sum \frac{\Delta \tau_{yx}}{\Delta y} \Delta x \qquad (2.10)$$

$$\sigma_y = (\sigma_y)_o - \sum \frac{\Delta \tau_{xy}}{\Delta x} \Delta y \qquad (2.11)$$

In eq. (2.8) and eq. (2.9), $(\sigma_x)o$ and $(\sigma_y)o$ represent known stresses at the boundary point chosen as the start of the integration procedure. If the starting point is chosen on a free boundary then $(\sigma_x)o$ or $(\sigma_y)o$ are given directly by the isochromatic parameter. τ_{yx} is then calculated at the interior points and the summation proceeds in a stepwise manner using a fixed grid with each block measuring Δx by Δy. $\Delta\tau_{xy}$ is obtained from the difference between the top and bottom values at each interior point[8]. In the above equations,the convention for positive x is from left to right while for positive y is from bottom to top. Here in the present work, for the horizontal grid the direction of scanning is from outer (ie.boundary of the quadrant of the circular disc) to the interior (ie. line of symmetry). Since this direction of scanning ie. from right to left, is opposite to that of the standard convention as shown in Fig. 2.2, the sign of Δx needs to be monitored. With the sign of Δx being negative eq. (2.10) for σ_x takes the form

$$\sigma_x = (\sigma_x)_o + \sum \frac{\Delta \tau_{yx}}{\Delta y} \Delta x \qquad (2.12)$$

Once σ_x is calculated for a particular point on the grid, σ_y can be calculated based on the relation :

$$\sigma_y = \sigma_x - \frac{NF_\sigma}{t} \cos 2\theta \qquad (2.13)$$

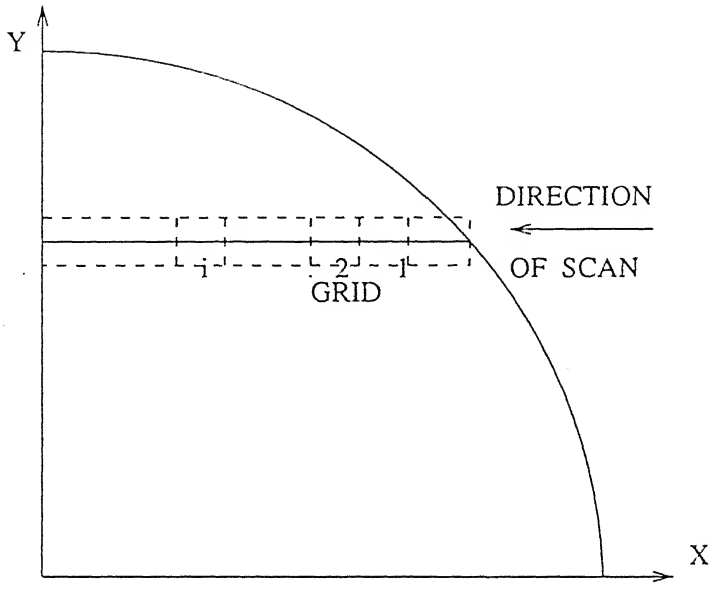

Fig. 2.2 Direction of scan along a horizontal grid.

Hence σ_x and σ_y can be evaluated on each and every point of the grid, while scanning from right to left. It is to be noted that what shear-difference method demands is that the starting values be known. So, once the horizontal scanning is done and σ_x and σ_y at each point of the grid evaluated, these values can now be used as starting values for individual grids being formed for vertical scanning. While scanning vertically, first σ_y is evaluated and then is σ_x. The equations used are either of eq. (2.14) or eq. (2.15), depending on the location of the point of interest.

$$\sigma_y = (\sigma_y)_o - \sum \frac{\Delta \tau_{xy}}{\Delta x} \Delta y \qquad (2.14)$$

$$\sigma_y = (\sigma_y)_o + \sum \frac{\Delta \tau_{xy}}{\Delta x} \Delta y \qquad (2.15)$$

Equation (2.14) is used when the points on the grid above the known point are being scanned while eq. (2.15) is used when those below the known point are scanned.

Once σ_y is calculated σ_x is calculated based on the relation

$$\sigma_x = \sigma_y + \frac{NF_\sigma}{t} \cos 2\theta \tag{2.16}$$

Likewise the stress values σ_x and σ_y are obtained for whole of the quadrant of the circular disc under diametral compression.

2.5 TREBUNA'S METHOD

This method suggests that the shear stress be expressed in terms of the difference of principal stresses, as

$$\tau_{XY} = \frac{1}{2}(\sigma_1 - \sigma_2) \sin 2\theta \tag{2.17}$$

and differentiated it as a product of two functions. Substituting this into eq. (2.10) and eq. (2.11) yields

$$\sigma_x = (\sigma_x)_o - \int \frac{\partial(\sigma_1 - \sigma_2)}{\partial y} \frac{1}{2} \sin 2\theta \, dx - \int (\sigma_1 - \sigma_2) \cos 2\theta \frac{\partial \theta}{\partial y} \, dx \tag{2.18}$$

$$\sigma_y = (\sigma_y)_o - \int \frac{\partial(\sigma_1 - \sigma_2)}{\partial x} \frac{1}{2} \sin 2\theta \, dy - \int (\sigma_1 - \sigma_2) \cos 2\theta \frac{\partial \theta}{\partial x} \, dy \tag{2.19}$$

These can be approximated using the finite difference expressions as,

$$\sigma_x = (\sigma_x)_o - \sum \frac{\Delta(\sigma_1 - \sigma_2)}{\Delta y} \frac{1}{2} \sin 2\theta \, \Delta x - \sum (\sigma_1 - \sigma_2) \cos 2\theta \frac{\Delta \theta}{\Delta y} \, \Delta x \tag{2.20}$$

$$\sigma_y = (\sigma_y)_o - \sum \frac{\Delta(\sigma_1 - \sigma_2)}{\Delta x} \frac{1}{2} \sin 2\theta \, \Delta y - \sum (\sigma_1 - \sigma_2) \cos 2\theta \frac{\Delta \theta}{\Delta x} \, \Delta y \tag{2.21}$$

Again, as for the horizontal grid the direction of scanning is opposite of the

standard sign convention, the sign of Δx needs to be monitored. Hence σ_x is now approximated as

$$\sigma_x = (\sigma_x)_o + \sum \frac{\Delta(\sigma_1-\sigma_2)}{\Delta y}\frac{1}{2}\sin 2\theta\ \Delta x + \sum (\sigma_1-\sigma_2)\cos 2\theta \frac{\Delta\theta}{\Delta y}\ \Delta x \qquad (2.22)$$

$$\sigma_y = \sigma_x - \frac{NF_\sigma}{t}\cos 2\theta \qquad (2.23)$$

Hence σ_x and σ_y can be evaluated on each and every point of the grid, while scanning from right to left. Now again these points act as starting points for vertical scanning.While scanning vertically we first evaluate σ_y and then σ_x.The equation used is either of eq. (2.24) or eq. (2.25), depending on the location of the point of interest.

$$\sigma_y = (\sigma_y)_o - \sum \frac{\Delta(\sigma_1-\sigma_2)}{\Delta x}\frac{1}{2}\sin 2\theta\ \Delta y - \sum (\sigma_1-\sigma_2)\cos 2\theta \frac{\Delta\theta}{\Delta x}\ \Delta y \qquad (2.24)$$

$$\sigma_y = (\sigma_y)_o + \sum \frac{\Delta(\sigma_1-\sigma_2)}{\Delta x}\frac{1}{2}\sin 2\theta\ \Delta y + \sum (\sigma_1-\sigma_2)\cos 2\theta \frac{\Delta\theta}{\Delta x}\ \Delta y \qquad (2.25)$$

Equation (2.24) is used when the points on the grid above the known point are being scanned while eq. (2.25) is used when those below the known point are scanned. Once σ_y is calculated, σ_x is calculated based on the relation

$$\sigma_x = \sigma_y + \frac{NF_\sigma}{t}\cos 2\theta \qquad (2.26)$$

2.6 GENERATION OF THEORETICAL DATA AND APPLICATION OF STRESS SEPARATION SCHEMES

The earlier section discussed the standard form of equations related to shear-difference

method & Trebuna's modification to the shear difference technique. It also discussed their modified form, in case the direction of scanning is opposite to the conventional +x or +y axis. This section discusses the implementation of these equations over the geometry under consideration i.e., disc under diametral compression. In the present analysis only a quarter section of the disc is considered and the whole field analysis of the quadrant is desired.

2.6.1 Physical significance of the grid

One of the essential feature of both the above mentioned methods is that they need to be provided with the starting values of σ_x or σ_y referred to as $(\sigma_x)_o$ & $(\sigma_y)_o$ respectively so that the integration procedure can be applied.

In the case of disc under diametral compression; the isochromatic parameter ie the fringe order on the free boundary is zero & hence $(\sigma_x)_o$ or $(\sigma_y)_o$ can be directly obtained. With the starting point taken on the boundary, we can scan from boundary to the line of symmetry and obtain the state of stress at all points located at specified regular intervals. This interval is at the discretion of the user. The smaller the interval, the better the integration procedure & hence better will be the results. It is noteworthy that these points with known state of stress can now act as the initial point for vertical scanning i.e., each of these points will act as the starting point for the integral procedure in both $+y$ & $-y$ directions, so as to obtain the results over the whole-field.

It's also important to note from eq. (2.8) and eq. (2.9) that for shear-difference method, the variation of shear-stress is averaged over a specified increment along x or y direction. Similarly, in Trebuna's method the variation of $(\sigma_1 - \sigma_2)$ (which implies the

variation of isochromatic parameter N) and the variation of isoclinic parameter θ is averaged over a specified increment along x or y directions, as reflected by eq. (2.18) & eq. (2.19). This physically emphasises the need for grids, wherein the centre line is the line of interest & the adjacent ones are to facilitate the variation of the desired parameter along x or y directions. Figure 2.3 shows the grid system, to be adopted. For better understanding, consider eq. (2.8) for the case of shear-difference method, σ_x at point B would be given by

$$(\sigma_x)_B = (\sigma_x)_o - \frac{(\tau_{yx})_A - (\tau_{yx})_C}{dely}\, delx \tag{2.27}$$

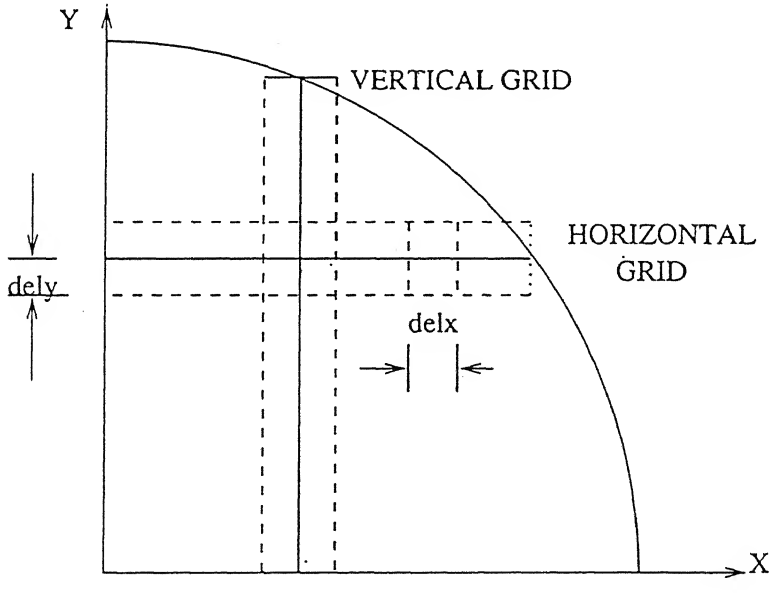

Fig. 2.3 Concept of a grid system.

Similarly, consider eq. (2.18) for the case of Trebuna's method, wherein σ_x at the point B would be given by

$$(\sigma_x)_B = (\sigma_x)_o - \frac{(\sigma_1-\sigma_2)_A - (\sigma_1-\sigma_2)_C}{dely}\frac{1}{2}\sin 2\theta_B \; delx - \frac{(\theta_A-\theta_C)}{dely}(\sigma_1-\sigma_2)_B \cos 2\theta_B \; delx \tag{2.28}$$

The same concept of grid, is applicable for vertical scanning also.

2.6.2 User's input data

In order to obtain the whole field state of stress for the quadrant of the disc under consideration,the pre-requirement is

(i) a known, diameter of the disc.

(ii) a known, line of interest (*yd*).

(iii) a known, increment along *x*-axis.

(iv) a known, increment along *y*-axis.

These parameters in fact constitute the data which is at the discretion of the analyst. Under-given is a detailed procedure with regard to the shear-difference method of stress-separation. It remains exactly the same for Trebuna's method except for the applicable equations.

2.6.3 Scheme for horizontal scanning

(i) No. of data points:

Once the above mentioned set of data has been fed in, the leng ? line of interest

along x axis say xd can be known by the relation :

$$xd = \text{sqrt}(R^2 - (yd)^2)$$

Then the no. of divisions along the line of interest = xd/delx. Based on this value the no. of data points along the line of interest say ndp are evaluated. Two separate cases thus arise, which are shown in Fig. 2.4.

case a) All grids of equal size.

eg. xd = 10.4 mm; delx = 0.52 mm

no. of divisions = 10.4/0.52 = 20

ndp = 21 (each at equal interval)

This is the case wherein all the grids will be of equal size.

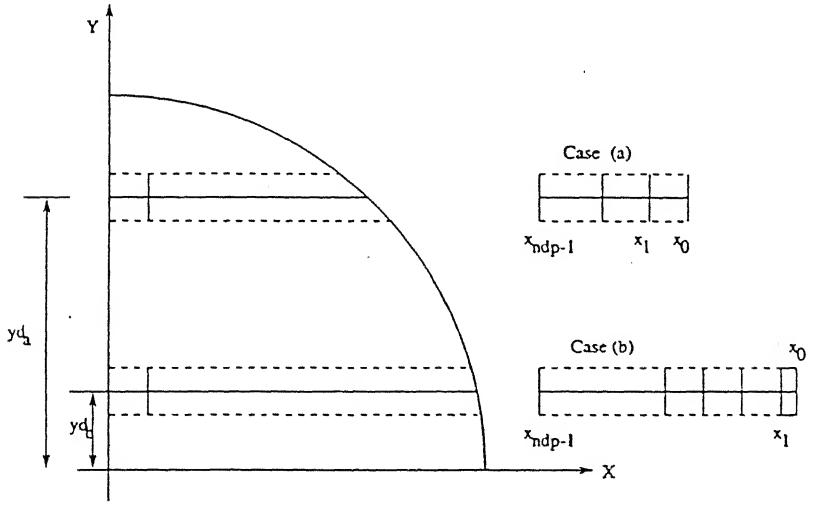

Fig. 2.4 Scheme for horizontal scanning: (a) All grids of equal size (b) Unequal grid at boundary.

case b) Grids of non equal sizes.

eg. xd = 10.7 mm; delx = 0.52 mm

no. of divisions = 10.7/0.52 = 20.576

ndp = 22 (21 at equal interval; one at non-equal interval = 0.576 times of delx)

diffx = 0.576 * delx.

This is the case wherein all grids except one, will be of equal size.

(ii) Generation of co-ordinates:

For any photoelastic analysis over a domain, the x & y co-ordinates, the isochromatic parameter N and the isoclinic parameter θ are necessarily required over each point of interest. The generation of x, y co-ordinates is discussed here.

case a) The coordinates are to be generated over 3 lines.

(i) A line, over the line of interest, referred to as Top line

(ii) line of interest

(iii) A line, below the line of interest, referred to as Bottom line.

As the co-ordinate of the point on the free boundary on the line of interest is known from the relation xd = sqrt(R^2 -$(yd)^2$), the 0^{th} point of the top line can be allocated as it's *x* coordinate the same value as xd and then each time delx can be deducted so as to yield x-coordinates till line of symmetry.

It's true that 0^{th} point of the top line, is rather in free space and not exactly on the free boundary but this is tolerable pertaining to the fact that the top line is just a pixel increment away from the line of interest and hence the error would just be negligible. The y-coordinates for all the points of the top line = yd + dely. Similarly the *x*-coordinates for the line of interest & bottom line can be allocated. For these two lines,

y-coordinates differ, as , for all the points on the line of interest y = yd; while for bottom line y = yd - dely.

case b) In this case, the non-equal increment referred as diffx is to be accounted. It's a better choice to account it near the boundary owing to the fact that the integration procedure starts from the boundary and hence integration performed over a small increment at an initial stage would yield a better solution. The generation procedure for all points remains exactly the same as case a except for the points 1, ndp+1, 2ndp+1 whose coordinates equals to $x_{boundary}$ - diffx and not $x_{boundary}$ -delx.

(iii) Integration Procedure.

case a) σ_x for all the points from 1-j can be determined from eq. (2.12) while σ_y from eq. (2.36).

case b) Determination of σ_x is slightly different for point no. 1 For this Δx of eq. (2.12) is to be replaced by diffx. Once σ_x is determined, σ_y can still be calculated from eq. (2.36).

With the procedure discussed above, being followed, the results obtained for three different scan lines, each measuring approximately y = 0, R/2, 3R/4, respectively have been presented in Fig. 2.5(a), 2.5(b) and 2.5(c) respectively. The results show that the stresses obtained by shear difference scheme and Trebuna's scheme are in close agreement. In fact the stresses evaluated from the two methods, for the line y = 0 (mm), exactly overlap with the stresses evaluated, using the standard formulations for the disc, based on theory of elasticity (refer appendix-I). However slight variation can be observed for the line y = R/2, which further aggravates slightly for the line y = 3R/4. Even for these two lines, the results obtained by shear difference and Trebuna's scheme overlap, though they vary slightly with the theory's.

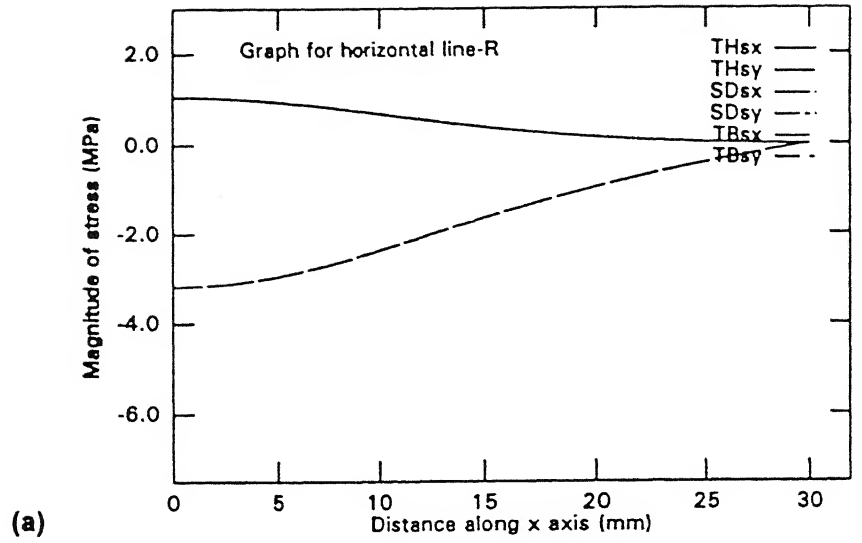

(a)

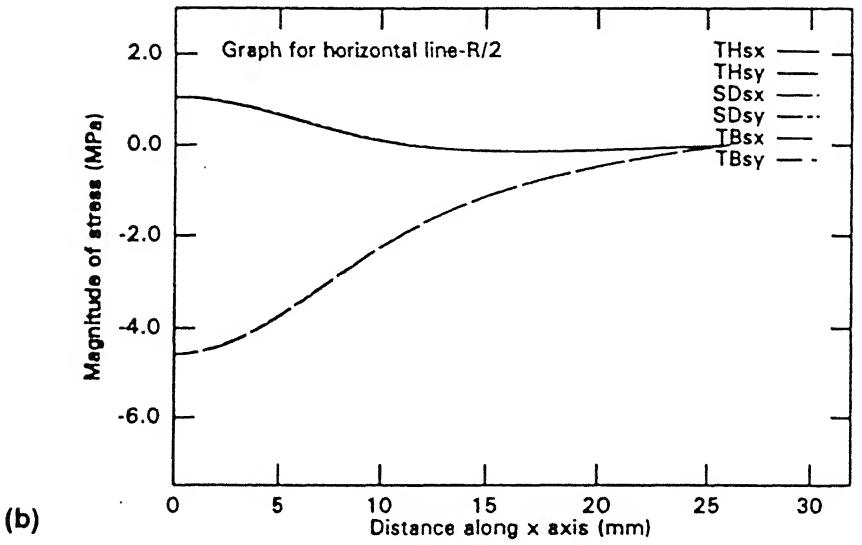

(b)

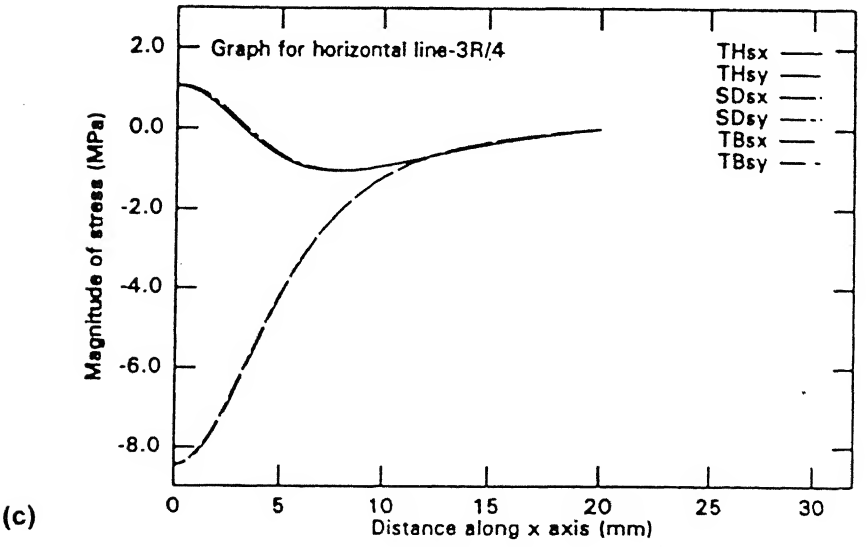

(c)

Fig. 2.5 Variation of stresses over various horizontal lines: (a) y = 0 (mm) (b) y = R/2 (mm) (c) y = 3R/4 (mm).

2.6.4 Scheme for vertical scanning

(i) No. of data points:

By this stage, σ_x and σ_y at all desired points along the horizontal line of interest are known. Consider a general point i and say it's x coordinate is vxd. Now the length of the vertical line of interest can be determined by the relation vyd = sqrt(R^2 -$(vxd)^2$). Two separate cases again arise. Fig. 2.6 physically explains these cases.

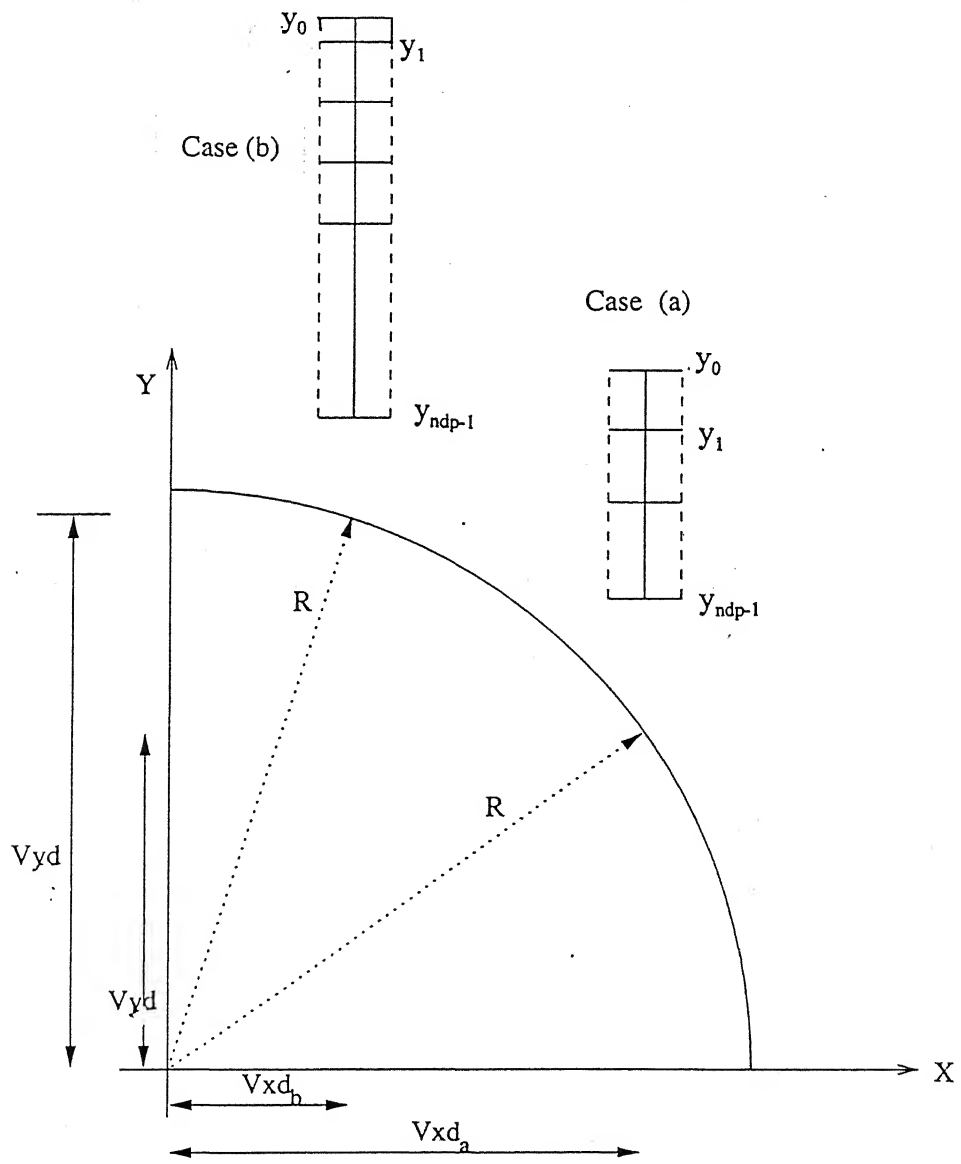

Fig. 2.6 Scheme for vertical scanning: (a) All grids of equal size (b) Unequal grid at boundary.

case a) All grids of equal size.

eg. vyd = 19 mm

dely = 0.76 mm

no. of divisions = 19/0.76 = 25

ndp = 26 (each at equal interval)

This is the case wherein all grids will be of equal size.

case b) Grids of non equal sizes.

eg. vyd = 19.5 mm

dely = 0.76 mm

no. of divisions = 19.5/0.76 = 25.657

ndp = 27 (26 at equal interval; one at non-equal interval=0.657 times of dely)

diffy = 0.657 * dely

This is the case wherein all grids except one, will be of equal size.

(ii) Generation of coordinates:

The procedure of generation remains exactly the same as for the horizontal scanning. The lines are referred as Right line, line of interest & the Left line. The x coordinates for all points along :

Right line = vxd + delx

Line of interest = vxd

Left line = vxd - delx

The y coordinates are allocated from the boundary towards the line of symmetry (x-axis). For case(a) mentioned above, this allocation is uniform while for case(b). diffy is to be accounted close to the boundary.

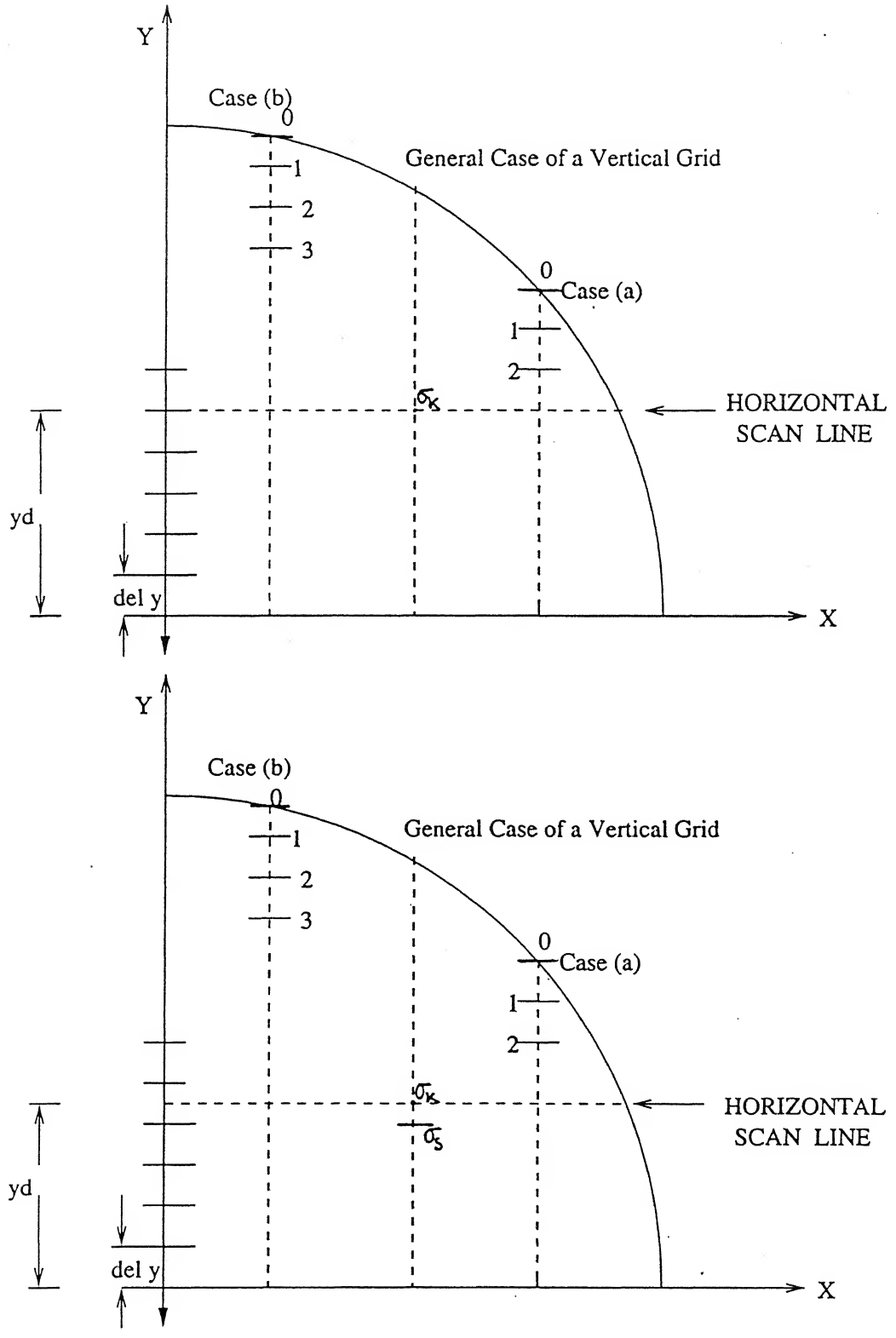

Fig. 2.7 Assignment of starting point in vertical scanning.

(iii) Integration procedure:

The integration procedure for vertical scanning is relatively more involved. Four considerations are to be made. First two corresponding to the cases (a) and (b) as mentioned above, i.e, the grids being of equal or non equal size; while the next two corresponding to the assignment of the values of the known points on the horizontal line of interest as the starting values for vertical integration for each individual grid.

It's worthy to realize that the dist. yd fed in by the analyst may not necessarily be an integral multiple of dely. So, the direct assignment of the known values of the horizontal points as the starting values for vertical integration may not be possible; forcing two new aspects into consideration.

Aspect(i)

yd = n * dely ; where n : integer

As shown in Fig. 2.7(a), the known point say 'k' (known from the horizontal scanning) by virtue of it's overlap as one of the point of interest along the vertical line; can be directly used as the starting point for the integration procedure. Now with the starting value known, utmost care should be exercised while determining the applicable equations for calculation of σ_x & σ_y for points below and points above the known point. As mentioned and justified in earlier section eq. (2.14) & eq. (2.16) are valid for points above while eq. (2.15) & eq. (2.16) for points below the known point.

Note: $\sigma_o = \sigma_k$

Aspect(ii)

yd != n * dely ; where n : integer

Fig. 2.7(b) shows that the known point 'k' (known from the horizontal scanning) does not overlap with the point of interest along the vertical line, and hence it cannot be

directly used as the starting point for the integration procedure. Rather, the known value is to be transformed to the point of interest so that it may act as the starting point. This transformation is not done arbitrarily or by approximation but by applying the equations proposed in the shear difference & Trebuna's method for vertical directions. As a predetermined convention, the known values are transformed to a point of interest which is just below the known point & also happens to be at a dist. which is an integral multiple of dely.

For better illustration of this transformation, consider the known point k and the point of interest which also has to be the starting point. The transformation is as follows:

$$(\sigma_y)_s = (\sigma_y)_k + \frac{(\tau_{yx})_a - (\tau_{yx})_c}{delx}\, dely \qquad (2.29)$$

σ_x can be calculated using eq. (2.16).

Note: $\sigma_o = \sigma_s$

Now again as the starting values are known, attention must be focused on the permissible equations corresponding to :

- different scan directions (above or below known point)
- two different cases: case a) and case b) respectively.

case a):

For evaluation of points below the starting point, eq. (2.15) & eq. (2.16) are valid, while eq. (2.14) & eq. (2.16) are applicable for points above starting point.

case b):

As for case a) eq. (2.15) & eq. (2.16) provide the stresses for points below the starting point while for points above the starting point, the strategy is slightly different. Equation (2.14) & eq. (2.16) are applicable till the point just below the free boundary.

but for calculation of the point on the free boundary, the term dy in eq. (2.14) for relation of σ_y is to be replaced by diffy; diffy being the non equal increment accounted at the boundary.

The discussion over the vertical scanning, conveys the sense that once the horizontal scanning is done and stresses at the points along this line obtained, then each of these points can act as the initial point for vertical scanning. Depending on the location of the horizontal line of interest, the scanning in vertical direction can be performed both along the +y and -y directions to cover the region of interest. Fig. 2.8(a), 2.8(b) and 2.8(c) present the results for three vertical lines, measuring approximately $x = 0, R/2, 3R/4$ (mm) respectively, with the horizontal line at $y = R/2$, taken as reference. The results for the horizontal line at $y = R/2$ have already been presented in Fig. 2.5(b). Along this line, the points at $x = 0, R/2$ and $3R/4$, with known stress values were taken and integrated in +y and -y directions according to the shear difference scheme and the Trebuna's scheme. It can be observed that the results produced by these methods are ic close aggreement with the theory's.

The complete procedure mentioned so far was for a general point, known over the horizontal line of interest (implying a general case of a vertical grid). The same procedure can be applied to all the known points over the horizontal line of interest, thus enabling the whole field analysis of the disc under diametral compression. Figure 2.9 shows the field variation of the stresses. Figure 2.9(a) and Fig. 2.9(b) represent the variation of σ_x and σ_y respectively, evaluated by shear difference scheme. It has been concluded from the results for various horizontal scan lines that with the theoretical data being employed, the results obtained by the standard solution for the disc under diametral compression, the shear difference method and Trebuna's method for stress

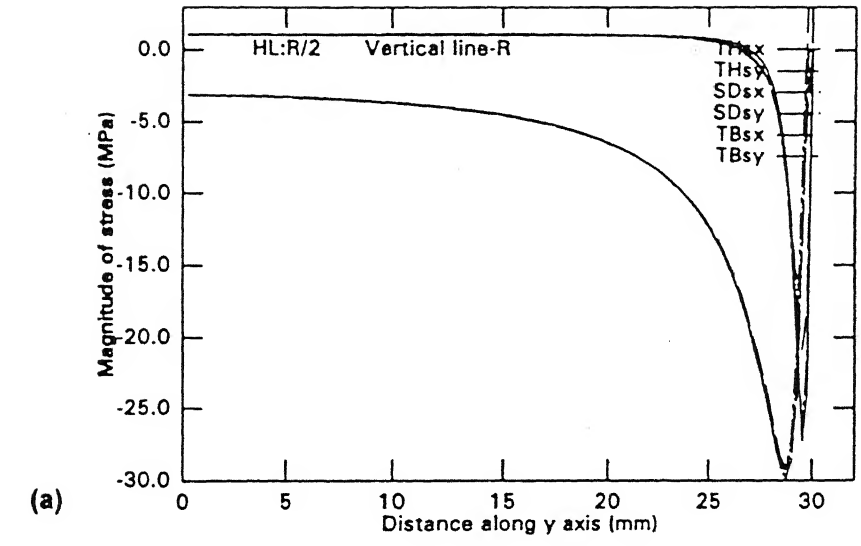

(a)

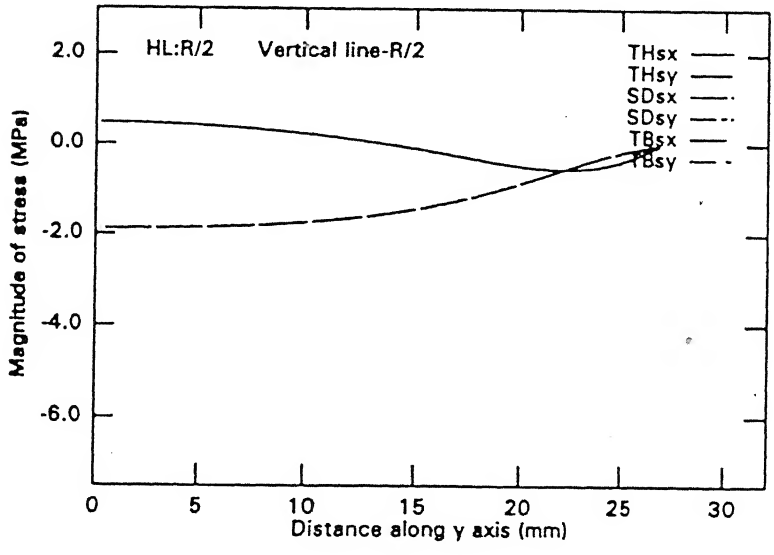

(b)

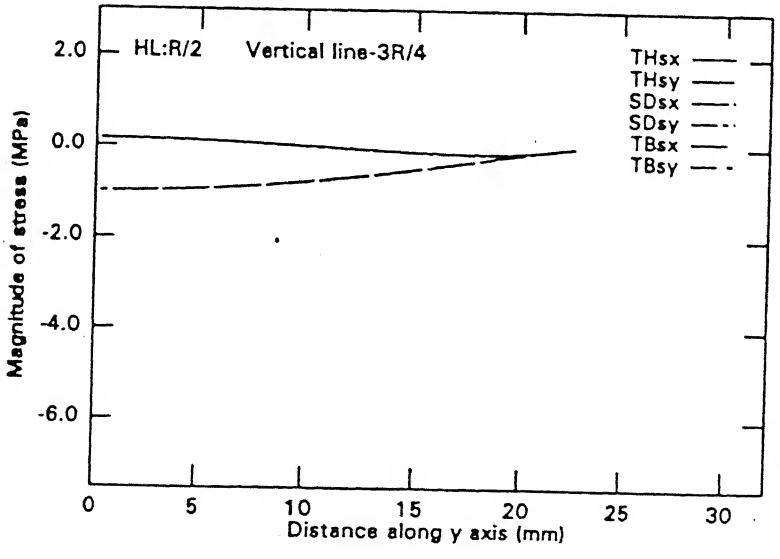

(c)

Fig. 2.8 Variation of stresses over various vertical lines with initial horizontal scan at y = R/2, (a) x = 0 (mm) (b) x = R/2 (mm) (c) x = 3R/4 (mm).

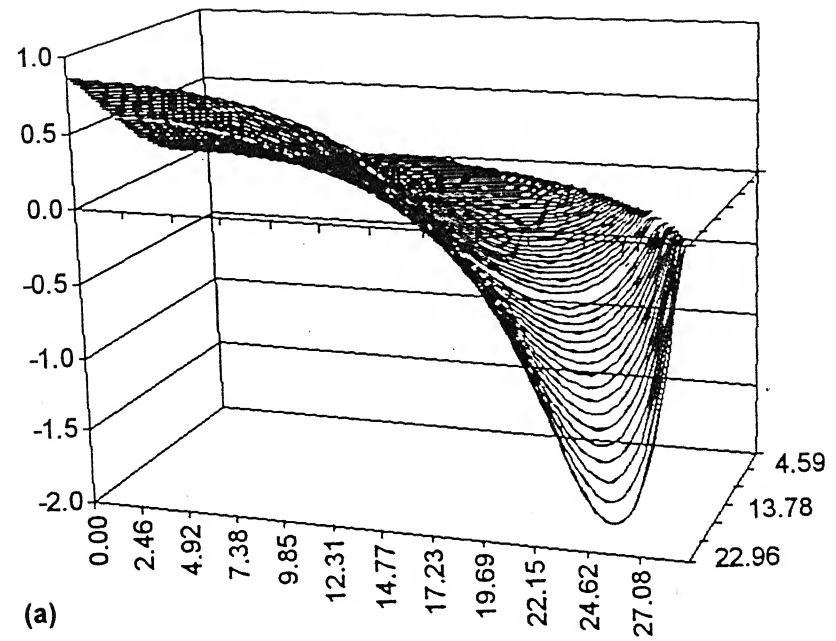

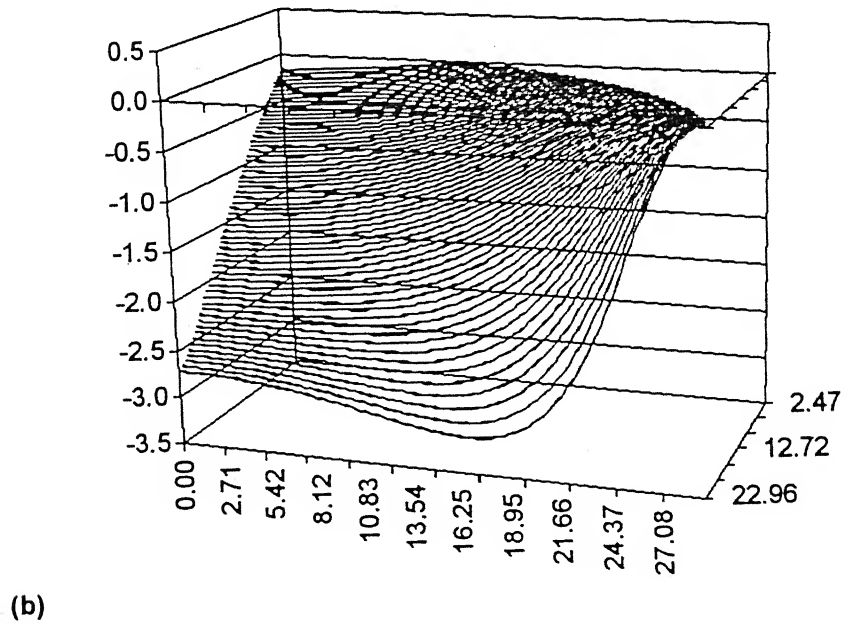

Fig. 2.9 Full field variation of stresses by shear difference method (a) σ_x (b) σ_y

separation, are in complete agreement. As, the field variation of stresses obtained by theory and by Trebuna's method are exactly identical to those of shear difference method, they have not been shown explicitly.

2.7 EFFECT OF GRID SIZE

In this present approach, which aims at the establishment of shear difference and Trebuna's method as reliable stress separation schemes for whole field analysis of stresses, the required photoelastic data is theoretically generated by using standard formulations based on theory of elasticity (refer appendix I). Later, the use of experimentally obtained photoelastic data, is discussed. For this purpose, during experimentation, the images of the model under analysis are captured and the intensities of the recorded images are processed. The fact that the intensity information is processed for each pixel in the region of interest, limits the grid size to the pixel increment only. However there is no such restriction in this approach as the photoelastic data can be theoretically generated for any grid size. Fig. 2.10 and Fig. 2.11 represent the effect of grid size over the accuracy of the seperated stresses. Fig. 2.10 presents the results for horizontal scan line at y = R/2. It can be observed from Fig. 2.10(a), 2.10(b) and 2.10(c) that the accuracy of the separated stresses goes on reducing as the grid size is sequentially raised from pixel dimensions to five times the pixel dimensions and finally to ten times the pixel dimensions. This observation is further supported through the plots in Fig. 2.11 which present the results with varying grid sizes for vertical scanning along the line at x = R/2 with the horizontal line at y = R/2, taken as the reference. It can be concluded that, the smaller the grid size, the better are the results.

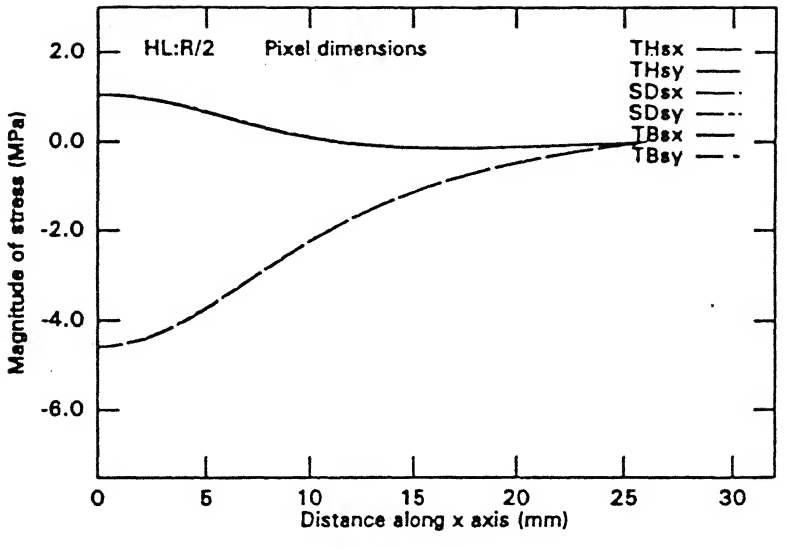

(a)

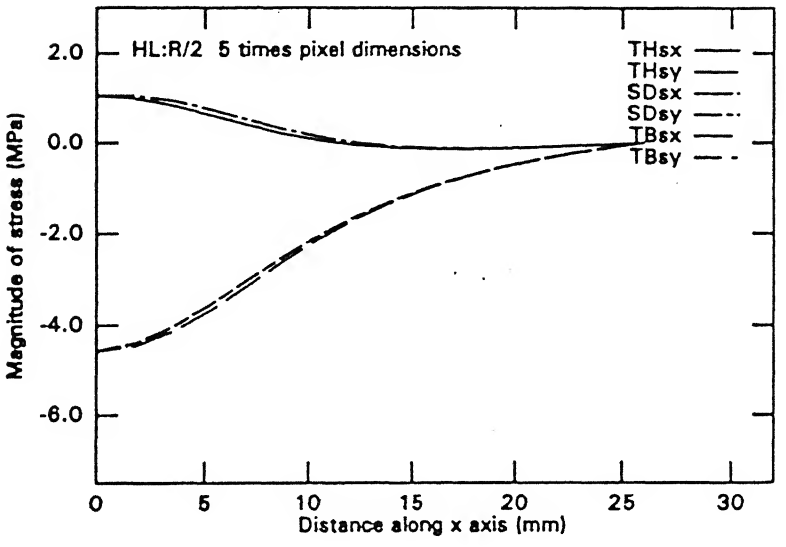

(b)

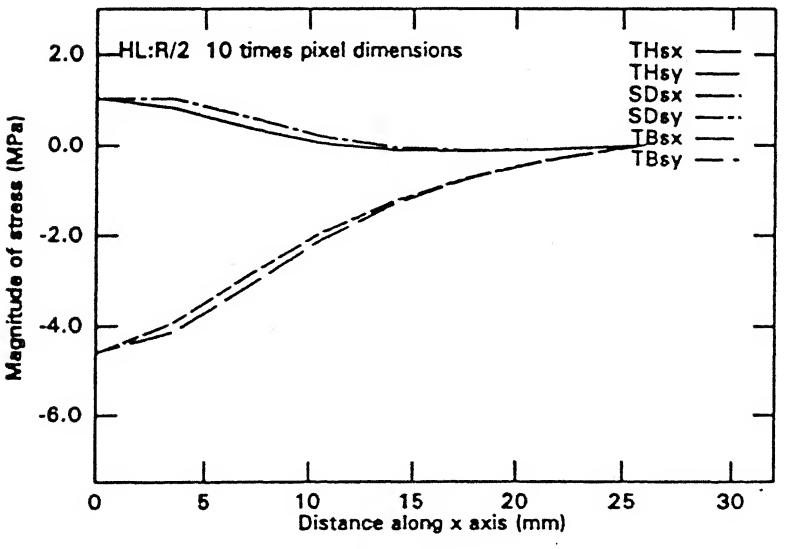

(c)

Fig. 2.10 Effect of grid size over accuracy of stresses for horizontal scan at y = R/2 (mm) (a) Pixel dimensions (b) 5 times pixel dimensions (c) 10 times pixel dimensions.

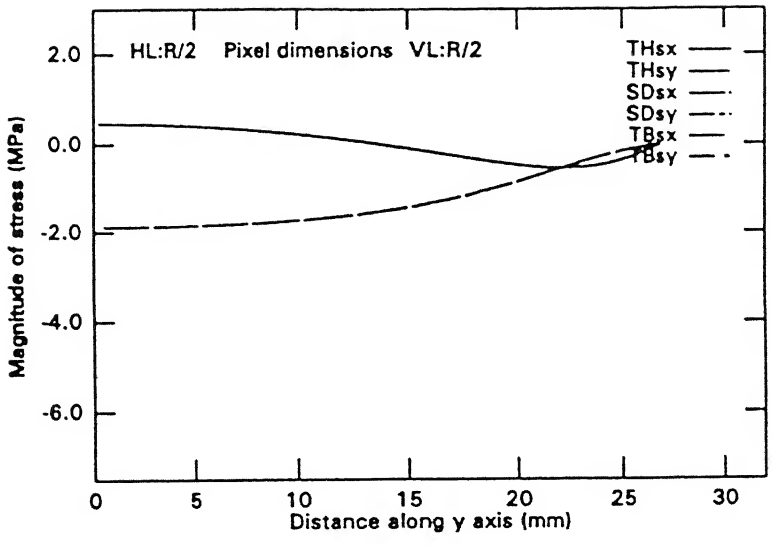

(a)

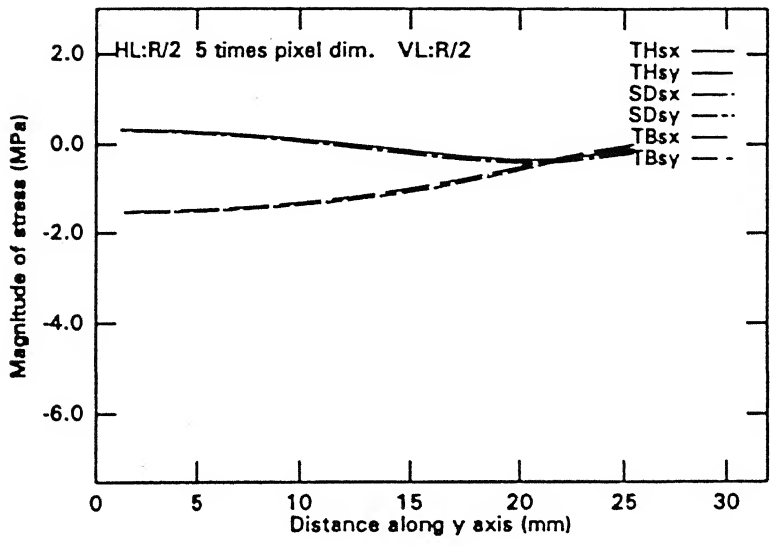

(b)

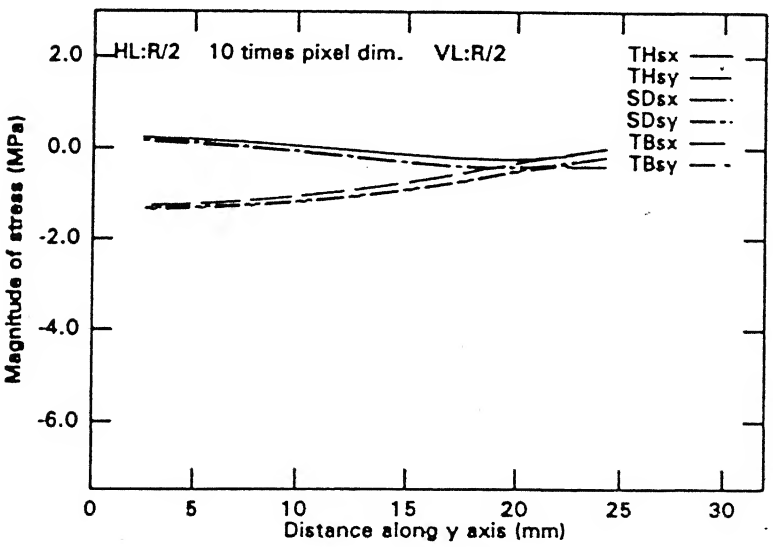

(c)

Fig. 2.11 Effect of grid size over accuracy of stresses for vertical scan at x = R/2 (mm), for an initial horizontal scan at y = R/2 (mm), (a) Pixel dimensions (b) 5 times pixel dimensions (c) 10 times pixel dimensions.

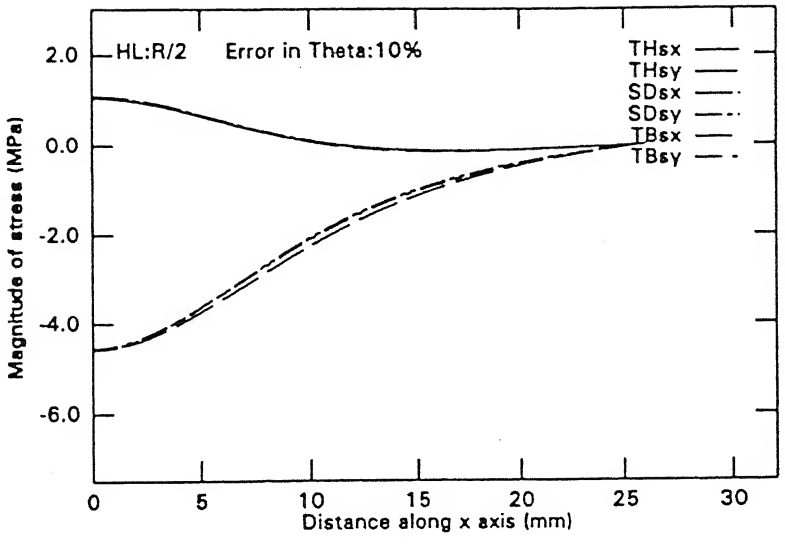

(a)

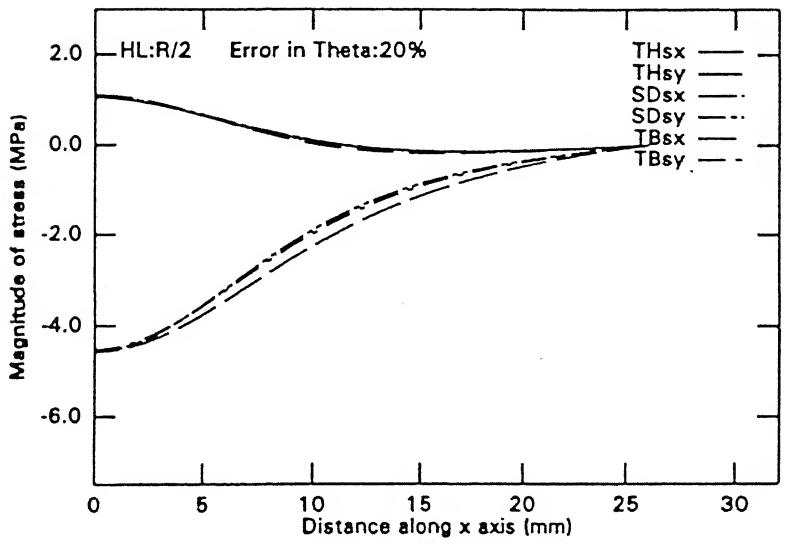

(b)

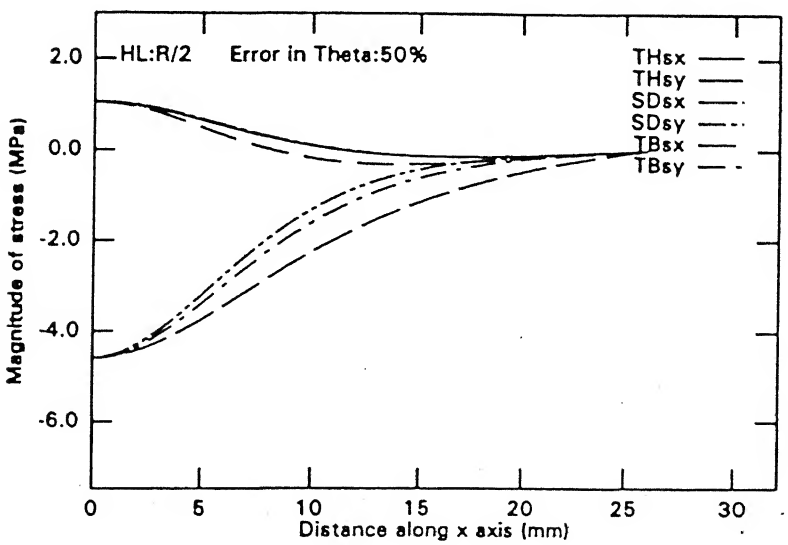

(c)

Fig. 2.12 Comparitive study of Trebuna vs Shear difference method for horizontal scan at y = R/2 with erroneous Isoclinic data: (a) 10% error (b) 20% error (c) 50% error.

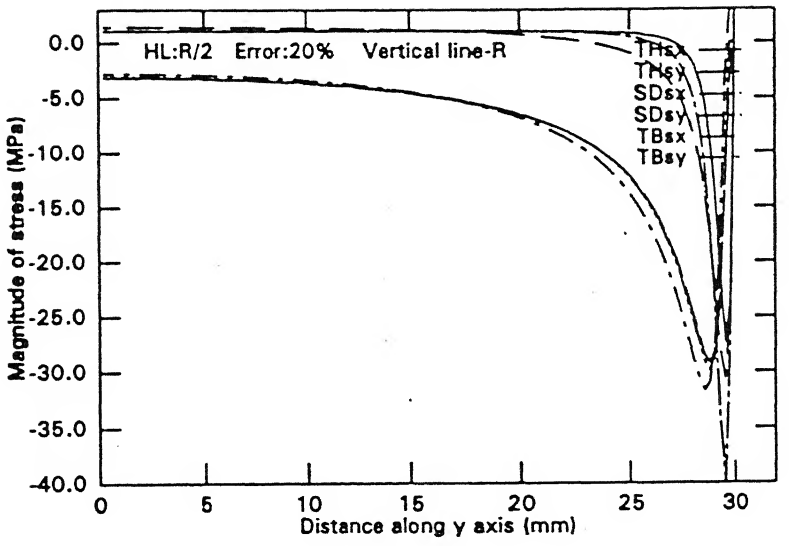

(a)

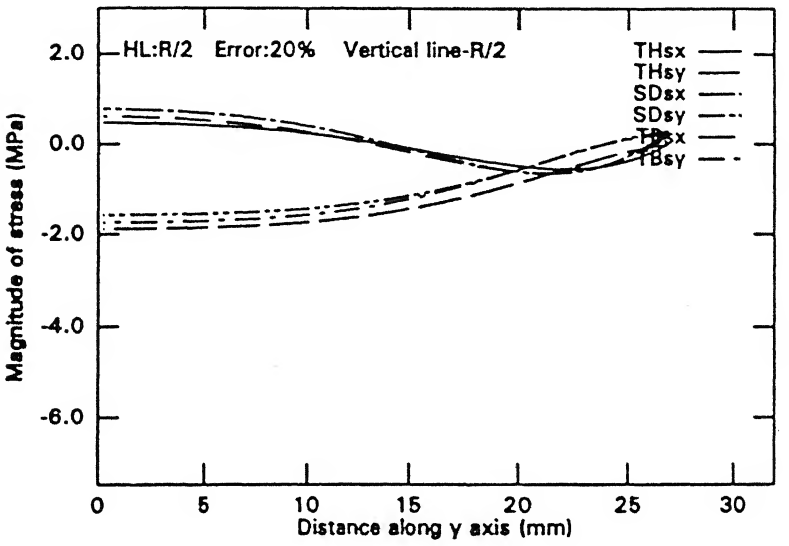

(b)

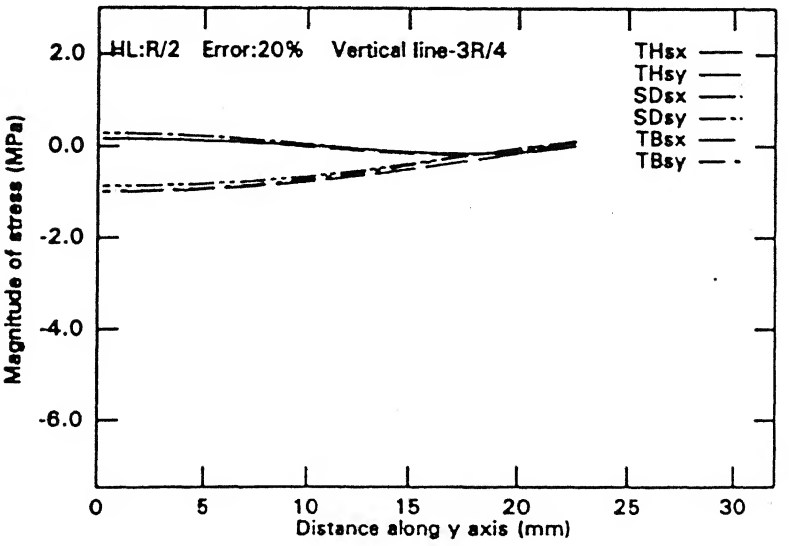

(c)

Fig. 2.13 Comparitive study of Trebuna vs Shear difference method for vertical scans with: 20% error in isoclinic data, Initial horizontal scan at y= R/2. (a) x = 0 (mm) (b) x = R/2 (mm) (c) x = 3R/4 (mm).

2.8 COMPARATIVE ANALYSIS OF ACCURACY ASPECTS OF SHEAR DIFFERENCE AND TREBUNA'S METHOD

Trebuna's method is supposed to be more accurate as the isoclinic parameter is averaged along the three lines of the grid over the model and assumed to represent the isoclinic along the centre line. The purpose is to "smooth out" any noisy points of isoclinic data. Here, in the present approach, as the isoclinic data is theoretically evaluated it is already good and hence its averaging does not introduce any improvement in (Trebuna's) the solution over the shear difference solution. When error in isoclinic parameter is intentionally introduced and trebuna's method then employed, it yields a solution which is more accurate than the one attained by shear difference. This effect has been reflected by Fig. 2.12 and Fig. 2.13. It is observed that with the isoclinic parameter turning erroneous, the results obtained by Trebuna's scheme are more accurate than those obtained by shear difference scheme. Fig. 2.12(a), 2.12(b) and 2.12(c) reveal that, as the error in the isoclinic parameter goes on increasing, the level of additional accuracy that trebuna's modification offers, also goes on increasing. Fig. 2.13 in support of the above observation shows the results for three different vertical scan lines, for the moderate value of error in the isoclinic parameter.

CHAPTER 3

STRESS SEPARATION IN DIGITAL PHOTOELASTICITY

3.1 INTRODUCTION

The recent advances in digital photoelasticity[9] have offered promise for full automation of data acquisition in two dimensional photoelasticity. Following this, a new whole field technique for determination of isochromatic and isoclinic parameters using phase shifting methodology is discussed and implemented. In this technique, a few images corresponding to different optical arrangements, are to be captured. Each of these different optical arrangements, introduces a specific phase-shift and hence the technique is referred as phase shifting. Phase-shifting generally provides the value of isochromatic parameter (N) with a high degree of accuracy. However, the determination of isoclinic parameter (θ) by the existing methods needs to be further improved for its practical utilisation. To determine (θ), two different optical arrangements are discussed. One involves the use of a circular polariscope arrangement and the other, the plane polariscope arrangement.

In this chapter, the use of shear difference technique and Trebuna's method for stress separation is discussed in thecontext of digital photoelasticity. Initially, the stress separation algorithm is verified by using the theoretical values of (N) and (θ) for the

problem of a disc under diametral compression. Later stress separation is effected using the data of N obtained by phase shifting and (θ) by theory. Finally the usefulness of the technique by using the data fully from experiment is investigated.

3.2 NEED FOR AUTOMATION OF DATA ACQUISITION

The main advantage of photoelasticity is that, it can give the stress distribution for the whole field. But it gives this result as an image of fringe patterns. The main task in photoelasticity is the interpretation of these fringe patterns. In conventional methods, tedious compensation techniques are needed to obtain the fractional fringe orders at any point other than the fringe areas. The number of data points that could be considered is also less. These procedures are quite involved and require skill in the identification of isochromatics. Hence, automation of data acquisition and analysis to minimize these problems and to provide fast and more accurate results, has become essential. With the advent of PC based digital image processing systems, considerable success has been achieved in automating the data acquisition for the entire field. In the early development of digital photoelasticity, the data acquisition is limited to fringe areas. The real potential of DIP hardware was realized only when the concept of identifying the fringe fields as phase maps came into existence. This introduced new concepts in data acquisition. It is possible to evaluate the total fringe order at every pixel in the domain and not restricted to just fringe skeletons alone.

3.3 Phase shifting In photoelasticity

The phase stepping concept can be simply described as "changing the absolute phase of the reference wave in equal steps and measuring the local light intensity after each step". The change in phase, is in practice, achieved by rotation of the output optical elements of the polariscope. By varying the phase difference between the beams involved, in known steps, it is possible to generate sufficient number of equations to solve for the parameters involved. The phase shifting approach has been applied to many classical interferometric techniques. In most classical interferometers including holography, the path length of the two interfering beams are distinct and separate. In general, phase differences can be added by altering the path length of any one of the light beams. In photoelasticity, the two light beams cannot be treated separately but always go together. This means that a phase shift introduced in one light beam will also introduce a corresponding phase shift in the other beam also[10]. The change in phase, in practice, is achieved by appropriately rotating the optical elements of the polariscope.

The phase shifting concept for photoelasticity was first introduced by Hecker and Morche[11] in 1986. Extending the work of Hecker and Morche, Patterson and Wang[12] reported in 1991 a full automation procedure for photoelastic analysis. In 1992, Sarma et al.[13] reported a methodology using plane polariscope. Later in 1993, Asundi[10] reported a new methodology, which extended the Tardy method of compensation from a point to point approach to evaluate fractional fringe order on all points lying on the isoclinic line. In 1996, Ramesh and Ganapathy[14] reported a comparative study of the above methodologies and reported that among these techniques, the technique proposed by Patterson and Wang is truly a whole field technique.

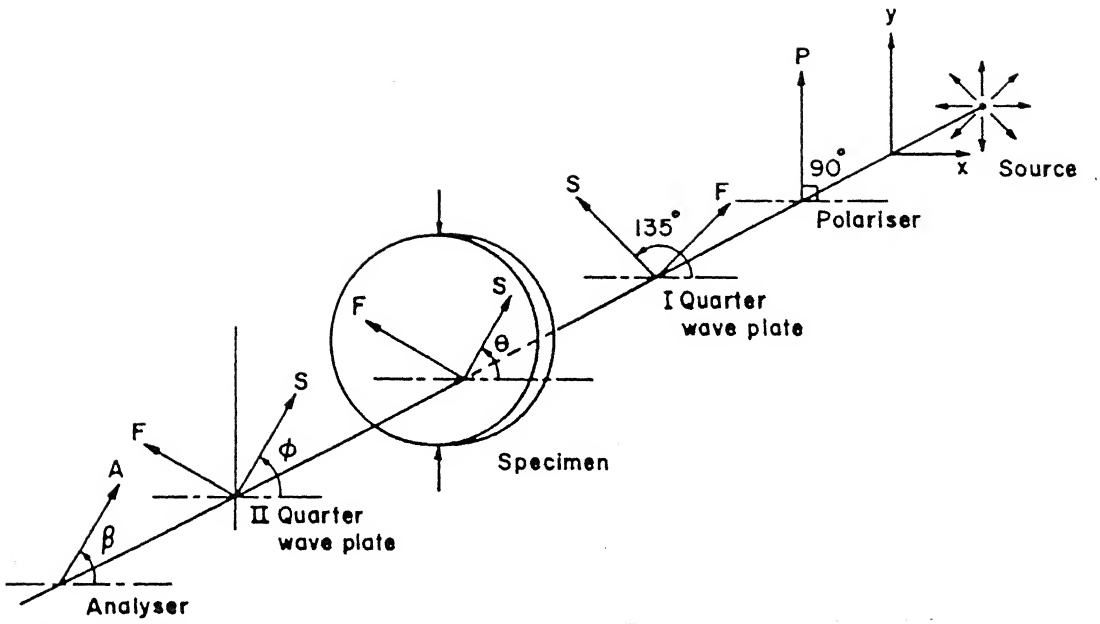

Fig. 3.1 Circular polariscope arrangement for phase shifting technique.

3.3.1 Patterson and Wang's Scheme;Use of circular polariscope.

The Patterson and Wang's algorithm requires a circular polariscope which has a provision to rotate each optical element independently. When circularly polarised light is used to view a photoelastic specimen, the light emerging from the analyser at any point (x,y) takes the form for intensity:

$$i(x,y) = i_m + i_v(sin2(\beta-\phi)\cos\delta - sin2(\theta-\phi)\, cos2(\beta-\phi)\sin\delta) \qquad (3.1)$$

where i_v is the intensity emerging when all the axes of the polariscope and specimen are parallel and the term i_m takes account of the stray light. The angles β, ϕ and θ are angles between a reference axis and the slow axis of the analyser, output quarter wave plate and specimen respectively, as shown in Fig. 3.1. The relative phase δ of the two rays formed when the light is transmitted through the specimen is related to the fringe order N as follows:

$$\frac{\delta}{2\pi} = N = \frac{(\sigma_1 - \sigma_2)\, t}{f_\sigma} \qquad (3.2)$$

where σ_1 and σ_2 are the principal stresses in the plane of the specimen, t is the thickness, and f the material fringe constant. In eq. (3.1) there are usually four unknowns, namely the isoclinic parameter (θ), the relative phase δ and the intensities i_m and i_v. In order to solve for these unknowns a minimum of four phase steps or changes in β and ϕ, the positions of output optical elements, are needed. Hecker and Morche employed increments of $\pi/3$ for β, the position of the analyser with the output quarter plate both aligned to the analyser and at $\pm\ \pi/4$ to it. They suggested that the use of high modulation of the phase produces smoother results. Consequently Patterson & Wang

used increment of $\pi/4$ for both β and ϕ, and combined the resulting six signals in such a way that a modulation of $\pi/2$ is achieved.

Below, are presented in a tabular form, the various possible combinations of Analyser angle β and the angle ϕ, representing the orientation of the second quarter wave plate. The intensity equations corresponding to each combination of β and ϕ are also specified.

Table 3.1 Intensity equations for various optical arrangements used in the phase-shifting algorithm.

S.No	II Quarter wave plate ϕ	Analyser angle β	Intensity equation	Fringe pattern interpretation
1	0	$\pi/4$	$i_1 = i_m + i_v \cos\delta$	circular polariscope bright field
2	0	$3\pi/4$	$i_2 = i_m - i_v \cos\delta$	circular polariscope dark field
3	0	0	$i_3 = i_m - i_v \sin 2\theta \sin\delta$	none
4	$\pi/4$	$\pi/4$	$i_4 = i_m + i_v \cos 2\theta \sin\delta$	none
5	$\pi/2$	$\pi/2$	$i_5 = i_m + i_v \sin 2\theta \sin\delta$	none
6	$3\pi/4$	$3\pi/4$	$i_6 = i_m - i_v \cos 2\theta \sin\delta$	none

Using the above intensity equations, the isoclinic angle (θ) and the fractional retardation (δ) can be evaluated as mentioned below.

$$\theta = \frac{1}{2}\tan^{-1}\left(\frac{i_5 - i_3}{i_4 - i_6}\right) \tag{3.3}$$

$$\delta = \tan^{-1}\left(\frac{i_5 - i_3}{(i_1 - i_2)\sin 2\theta}\right) = \tan^{-1}\left(\frac{i_4 - i_6}{(i_1 - i_2)\cos 2\theta}\right) \tag{3.4}$$

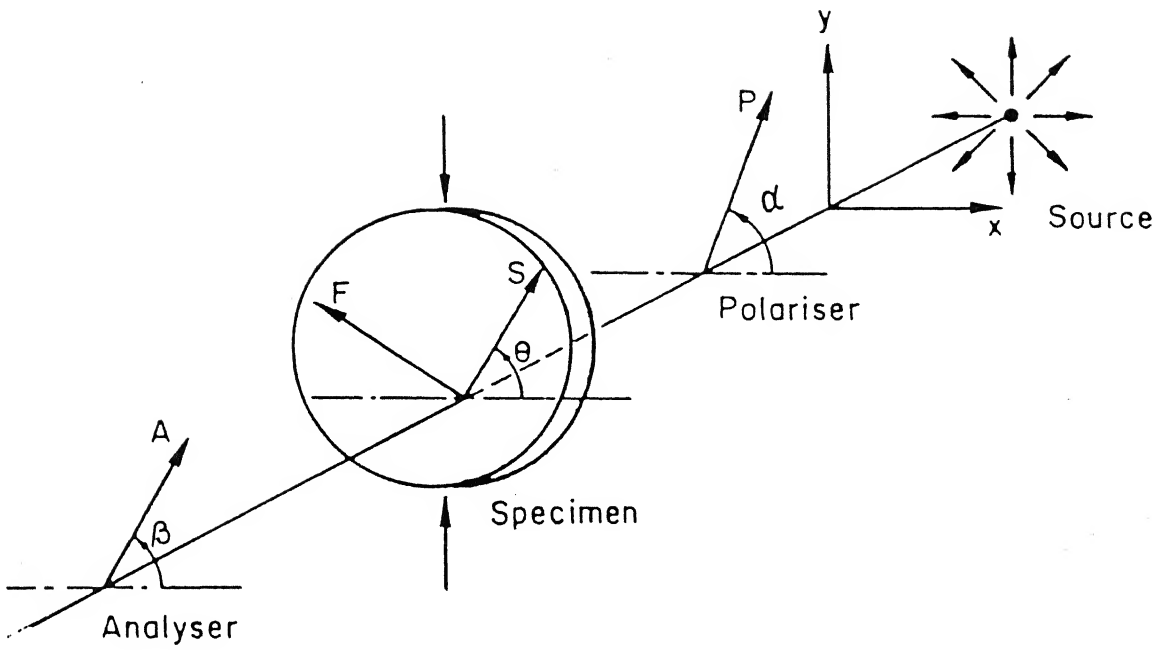

Fig. 3.2 Plane polariscope arrangement for phase shifting technique.

3.3.2 PLANE POLARISCOPE ARRANGEMENT

In phase shifting technique, the relative position of the optical elements play a significant role. Removing the first and the second quarter wave plate from the circular polariscope arrangement and changing the relative orientation of the analyser and the polariser[15], leads to a new arrangement. As only the polariser, the model and the analyser are involved in the arrangement, it is referred as plane polariscope arrangement (refer Fig. 3.2). If the orientation of the polariser is denoted by angle (α) while that of the analyser by angle (β) and the intensities corresponding to these combinations recorded, it is observed that only six intensity equations turn out to be unique for all possible combinations of α and β, in steps of $\pi/4$.

Table 3.2 Table, showing that only six intensity equations are independent.

$\alpha \rightarrow$ $\beta \downarrow$	0	$\pi/4$	$\pi/2$	$3\pi/4$	π
0	i_6	i_3	i_1	i_2	i_6
$\pi/4$	i_3	i_5	i_2	i_4	i_3
$\pi/2$	i_1	i_2	i_6	i_3	i_1
$3\pi/4$	i_2	i_4	i_3	i_5	i_2
π	i_6	i_3	i_1	i_2	i_6

These six intensity equations corresponding to various combinations of the α and β have also been formulated in table 3.3. Using the above mentioned intensity equations, the isoclinic parameter (θ) can be evaluated using the relation:

$$\theta = \frac{1}{4}\tan^{-1}\left(\frac{i_3 - i_2}{i_4 - i_1}\right) \qquad (3.5)$$

Table 3.3 Table showing the intensity equations for the different orientations of the polariser and analyser.

S.No.	Polariser angle α	Analyser angle β	Intensity equation
1	0	$\pi/2$	$i_1 = i_b + i_a \sin^2\frac{\delta}{2}\sin^2 2\theta$
2	$\pi/4$	$\pi/2$	$i_2 = i_b + \frac{i_a}{2}\left[1 - \sin^2\frac{\delta}{2}\sin 4\theta\right]$
3	0	$\pi/4$	$i_3 = i_b + \frac{i_a}{2}\left[1 + \sin^2\frac{\delta}{2}\sin 4\theta\right]$
4	$\pi/4$	$3\pi/4$	$i_4 = i_b + i_a \sin^2\frac{\delta}{2}\cos^2 2\theta$
5	$\pi/4$	$\pi/4$	$i_5 = i_b + i_a\left[\cos^2\frac{\delta}{2} + \sin^2\frac{\delta}{2}\sin^2 2\theta\right]$
6	0	0	$i_6 = i_b + i_a\left[\cos^2\frac{\delta}{2} + \sin^2\frac{\delta}{2}\cos^2 2\theta\right]$

The fractional retardation can still be evaluated using the eq. (3.4).

3.4 Image Processing Set-up

The image processing system consists of a CCD (charge coupled device) camera (TM

560 PULNIX) that has a pixel resolution of 512 x 512 pixels and digitizes the images at video rates. The camera is connected to a PC based image processing system equipped with an image processing card (PIP 1024B, Matrox corporation) connected to a high resolution video monitor. The system has in addition to PC memory, four frame buffers each of 512 x 512 pixels x 8 bits, to store the image being processed and the intermediate results.

3.5 Experimental Evaluation and Whole Field Representation of Fractional Retardation

For the above mentioned experimentation process Sodium vapour lamp is used as monochromatic light source. An epoxy disk with a diameter of 60.06 mm, thickness of 5.04 mm and material stress fringe value (F_σ) of 11.64 N/mm/fringe, which is subjected to a diametral load of 502.57 N is taken up for the analysis. Initially, adopting the circular polariscope arrangement, six images are recorded by keeping the second quarter wave plate and the analyser in six different positions as shown in Table 3.1. Similarly, images are also captured for six different optical positions as proposed in plane polariscope arrangement. These optical positions are referred in Table 3.2. The captured images are shown in Fig. 3.3. The eq. (3.3) produces values of (θ) which are periodic with a wave length $\pi/2$.

It is obtained in a range from $-\pi/4$ through zero to $\pi/4$ which corresponds to the range of 0 to $\pi/2$, obtained from the classical definition of the isoclinic angle given by Frocht7. The value of the phase retardation is expressed in the range of $-\pi$ to π by using atan2 function of C-program library. Dark field isochromatics can be obtained using the

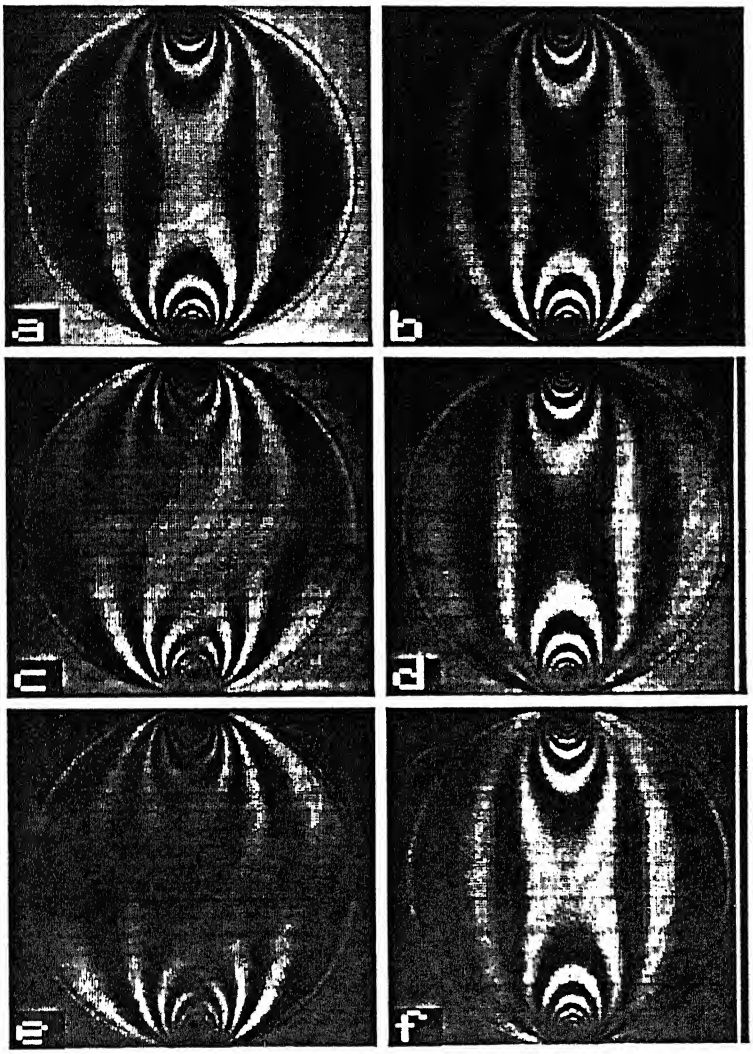

Fig. 3.3 The sequence of six images of a circular disc under diametral compression recorded for phase shifting technique, by plane polariscope arrangement.

following equation.

$$g(x,y) = \frac{abs(\delta)}{\pi} 255.0 \qquad (3.5)$$

Where g(x,y) is the grey level of the pixel at the location (x,y).

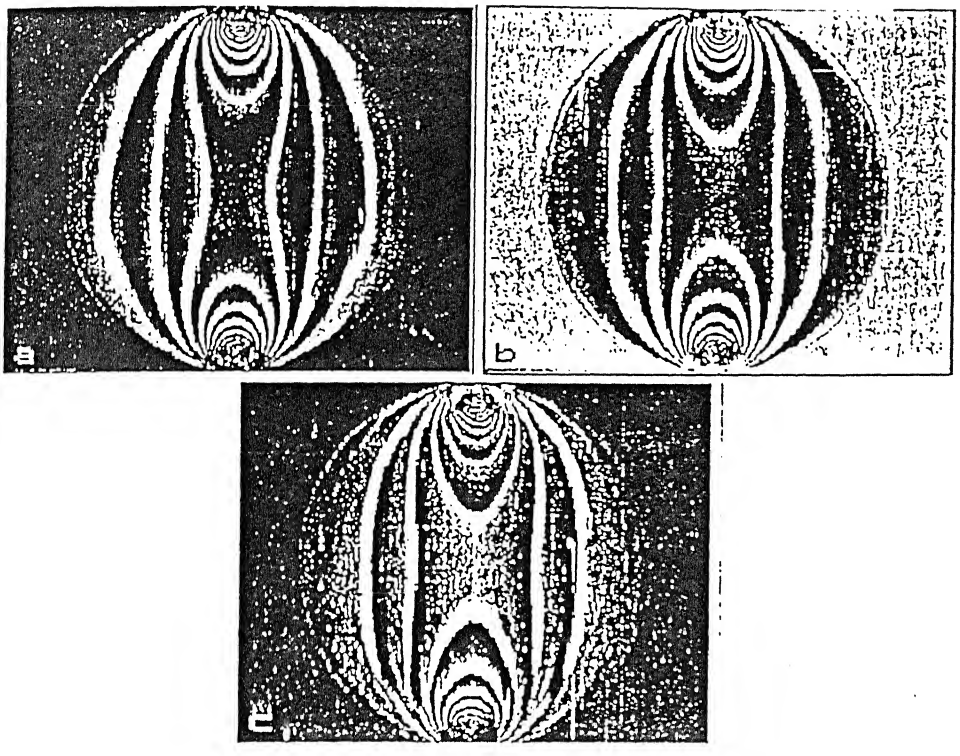

Fig. 3.4 Figure showing the various representations of the phase retardation. (a) Simulated dark field (b) Simulated bright field (c) Phase map.

Figure 3.4(a) shows the simulated dark field isochromatics. The phase map is obtained by converting phase retardation to grey levels. The zero phase retardation corresponds to pitch black and 2π phase retardation corresponds to pure white. So, the phase retardation is to be expressed in the range of 0 to 2π. The phase map can be obtained from the following equations.

$$\delta = \delta$$

$$\delta = \delta + 2\pi \qquad \delta < 0$$

$$g(x,y) = \frac{\delta}{2\pi} 255.0 \tag{3.7}$$

Figure 3.4(c) shows the phase map of the image. The bright field isochromatics for the image can be obtained using the following equations.

$$\delta = \delta + 2\pi \qquad \delta < 0$$

$$g(x,y) = \frac{abs(\delta - \pi)}{\pi} 255.0 \tag{3.8}$$

Figure 3.4(b) shows the simulated bright field isochromatics of circular disk under diametral compression.

3.6 Boundary Detection

To limit the determination of field parameters within the region of interest (within the specimen), the image has to be segmented. The segmentation of the image will result in isolation of the region of interest from the rest of the image. Segmentation of the image is done by detecting the boundary. In general, boundary of the image is detected using spatial filters like Roberts, Prewitt, Sobel etc.. These filters detect the edges based on abrupt change in grey levels. The edge detection algorithms not only detects the boundary, but also detects the regions in the image where there is abrupt change in grey levels. Moreover the primary interest is the detection of the boundary and not the detection of edges. The set of pixels obtained from above filters seldom characterizes a boundary completely, because of noise and breaks in the boundary from non uniform

illumination. These edge detection algorithms typically are followed by other boundary detection procedures designed to assemble and link the edge pixels into meaningful boundaries. This only yield raw data in the form of pixels along a boundary. These filters are helpful to detect the edges of the images obtained in DIP applications like astronomy and defense where image recognition is the only criterion. Accuracy of the boundary is not critical. Unlike the above applications, the experimental mechanics application like photoelasticity, the shape and boundaries of the object are known. This property is used to detect the boundary accurately instead of using the above general edge detection algorithms. To make computations, the data is to be expressed as a suitable representation. In the present study the algorithm proposed by Sreedhar is used. In this the boundary is identified by defining two files one for row-scan and the other for column scan. The area of the analysis is limited by drawing the boundary around the region of interest. In the bright field arrangement of polariscope, the boundary of the image can be seen clearly [Fig. 3.3(a)]. To mark the boundary, primitives have been developed Sreedhar[16]. These are line, circle, ellipse and 3-point arc. The boundary is drawn with an intensity of 255.

In order to quicken the boundary detection process, the algorithm accepts the actual dimensions of the specimen if available. For example to identify the circular disk boundary, one has to specify the centre and the radius. Based on the optical magnification and aspect ratio of the video monitor the boundary is drawn. Figure 3.5 shows the histogram of the bright field image of the circular disk under diametral compression. It can be observed that the maximum grey level of the image over the entire image is 168, which is less than 255 grey level. So, any pixel with grey level value of 255 represents the boundary pixel over the entire domain.

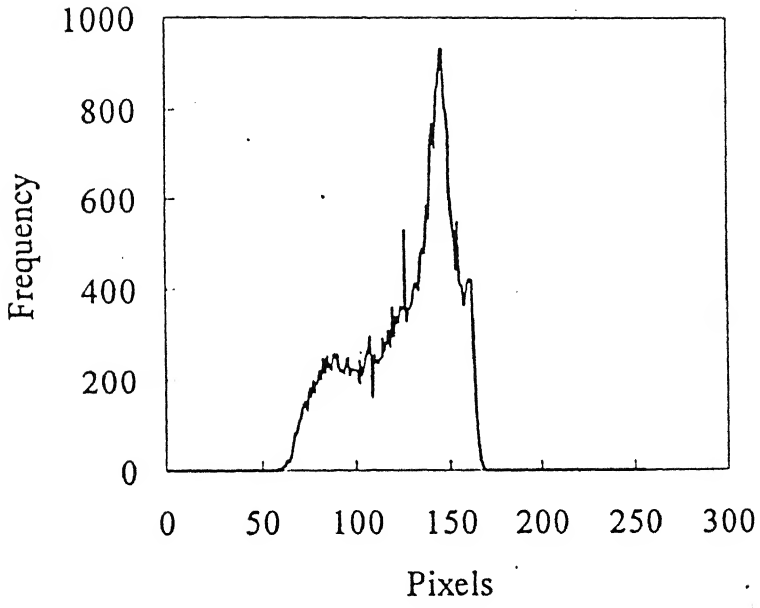

Fig. 3.5 Histogram of the bright field image of the circular disc under diametral compression.

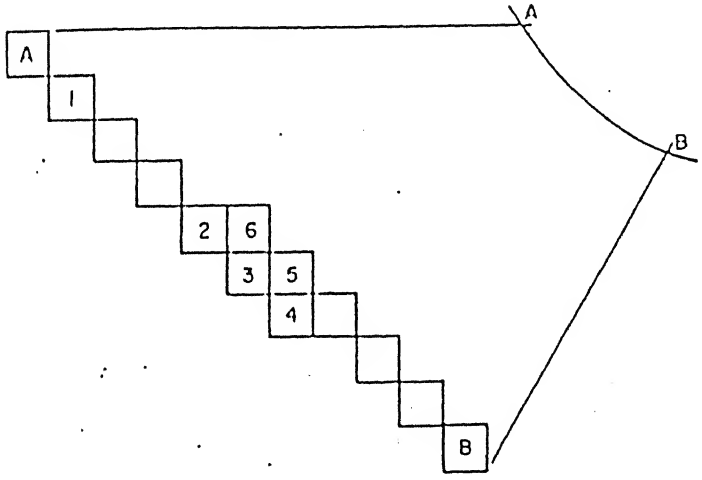

Fig. 3.6 Magnified pixel representation of a curved segment on the screen

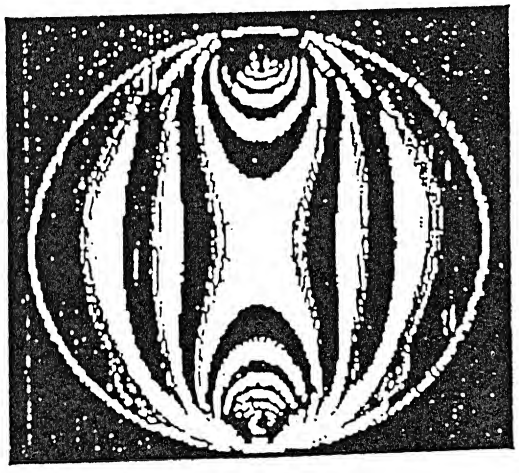

Fig. 3.7 Boundary detection for a circular disc.

The image is represented as a grid of pixels and the representation of a curved boundary is shown in Fig. 3.6. In view of spatial quantization, to represent the curvature more than one pixel is needed. However, for all computational purposes only the outermost pixel must be recognized as a boundary. In order to simulate the actual boundary, the pixel outside the actual boundary but just enclosing it should be marked as the boundary pixel. The boundary is drawn using the primitives developed such that the outer side pixels of the circle represents the boundary of the circular disk. In the ideal case, for the curve shown in Fig. 3.6 only one pixel should represent the boundary. This is achieved by storing the positions of the pixels which have an intensity of 255 into two separate intermediate files (scanx.dat and scany.dat), one for horizontal scanning and the other for vertical scanning. These files will have more than one pixel forming the boundary. Further processing of these files is done in which the first and last columns for every line from these files are extracted and stored into two separate files for horizontal scanning (*.*ybn*) and vertical scanning (*.*xbn*).

In the present study, the analysis of the image is limited to first quarter (256 x 256) of the quadrant. Since, the specimen will not occupy the full quarter of the quadrant, some blank lines appear in scanned files. The boundary pixels corresponding to these blank lines are 0 and 255. Hence, these blank lines are replaced with 0 and 255. The boundary detected by applying the above method on the disk is shown in Fig. 3.7.

CENTRAL LIBRARY
I. I. T., KANPUR
Acc. No. A 128076

3.6.1 UTILITY OF BOUNDARY INFORMATION

It has already been mentioned thus far, that two separate files, one each for horizontal

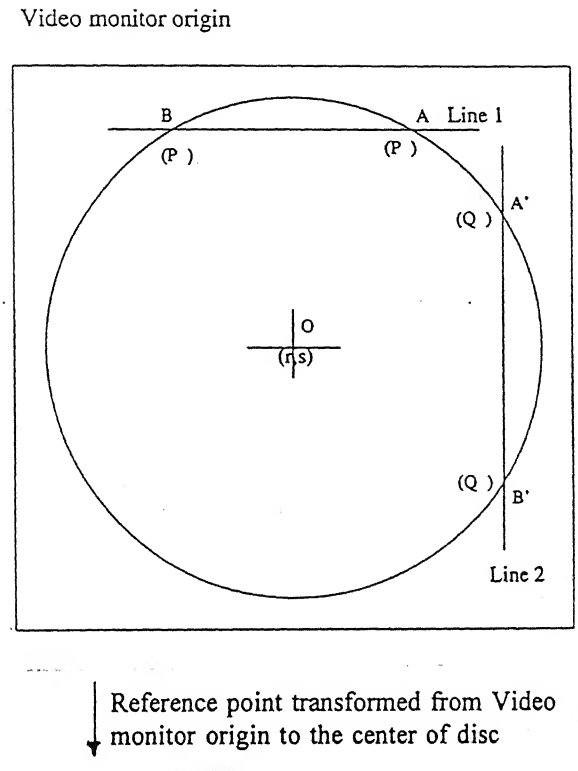

Fig. 3.8 Utility of boundary information.

scanning (*.*xbn*) and vertical scanning (*.*ybn*) are formed to store total boundary information. Consider a disc being scanned over a window size of 256*256 pixels, with the left top corner of the window taken as reference (0,0). Consider two separate lines, *line-1* and *line-2* as shown if Fig. 3.8(a). Let *line-1* intersect the region of interest at points A and B characterized by points P_1 and P_2 respectively. P_1 and P_2 represent the no. of pixels, that points A and B are away from the reference corner (left-top) of the window, along horizontal direction. Similarly, corresponding to *line-2* let the points A' and B' be characterized by Q_1 and Q_2, which denote no. of pixels along vertical direction. The values P_1 and P_2 are known from (*.*ybn*) file while Q_1 and Q_2 from (*.*xbn*) file. The aim lies in determining both the x and y co-ordinates for any general point along the boundary, which is possible through combination of information obtained by (*.xbn) and (*.ybn) files. In this regard if points A and A' are made to coincide, (Fig.3.8(b)) then the point of intersection would be characterized by (P_1,Q_1). Similarly let the centre of the disc be characterized by (r,s). Utilizing the symmetry of the disc, only a quarter section can be analyzed. For ease of analysis the centre of the disc must be regarded as the new origin (0,0). Then the intersection point A-A' will be characterized by $(P_1-r, s-Q_1)$. The actual location of the point A-A',in terms of spatial co-ordinates can be given by (x,y) where

$$x \text{ (mm)} = (P_1-r) * delx$$

$$y \text{ (mm)} = (s-Q_1) * dely$$

Figure 3.9 represents the digitized boundary for the quarter of the disc i.e., the boundary determined based on the spatial location of the pixel on the boundary. It is to be noted that the (*.xbn) and (*.ybn) files determined the boundary in terms of the number of pixels that it is away from the reference taken on the video monitor, which

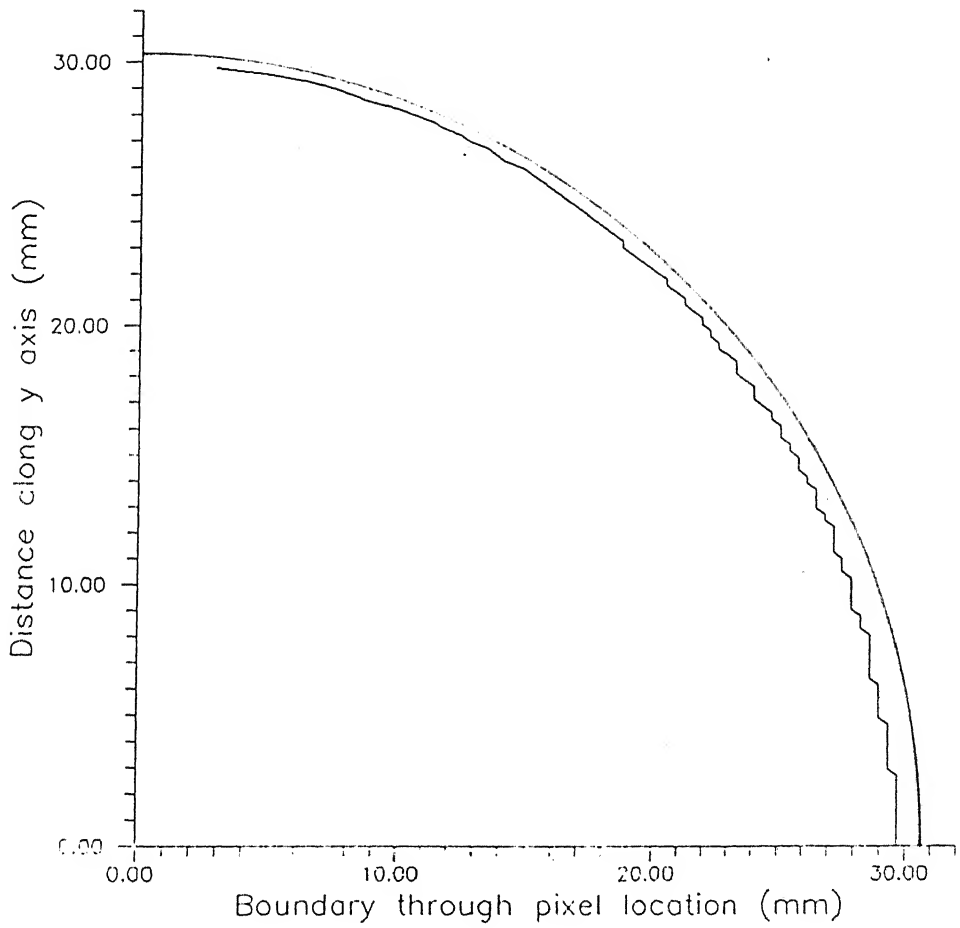

Fig. 3.9 Boundary simulated by pixel location.

is the left top corner of the window containing the image. With the transformation of this reference to the centre of the disc and combining of the information given by (*.xbn) and (*.ybn) files, as mentioned above, the boundary for only the quarter of the disc has been determined and presented in Fig. 3.9. Similarly for all points along the boundary, the spatial co-ordinates are achieved. These known co-ordinates along the boundary help in determination of the co-ordinates of any general pixel inside the region of interest. Thus the boundary information enables the determination of spatial co-ordinates of all points in the region of interest.

3.7 The grid system in digital domain.

With photoelastic data available for each pixel in the region of interest, from different sources as previously discussed, stress separation is performed by scanning the image row by row from top to bottom. The algorithm developed for the implementation of shear difference and Trebuna's Method, visualises the model as being constituted of three separate parts; the top-most part, the central part and the bottom-most part. The implementation of shear difference method and Trebuna's method requires formation of grid constituted of three adjacent rows of pixels, with the central row being the row of interest i.e., the row corresponding to each pixel of which, the stress in x and y direction will be predicted. For the top-most and the bottom-most row of pixel, formation of an exactly identical grid may not be possible due to the absence of physical geometry above the top-most row and below the bottom-most row. Hence to perform the stress analysis over these rows, the averaging scheme of stress separation methods under consideration needs to be modified. Apart from the missing rows above or below, even

with adjacent rows available on both sides difficulty may arise due to non equal number of pixels amongst the available rows themselves. For better understanding consider a fully populated Grid-system as shown below. Referring to the eq. 2.10, eq. 2.11, eq. 2.20 and eq. 2.21, it can be realised that with stresses known at the starting point and photoelastic data available for all other points, the determination of stresses for other points along the direction of scan requires the variation of shear stress or the variation of principal stress difference, to be known in a direction perpendicular to the scan direction. For ease of analysis, refer Fig. 3.10.

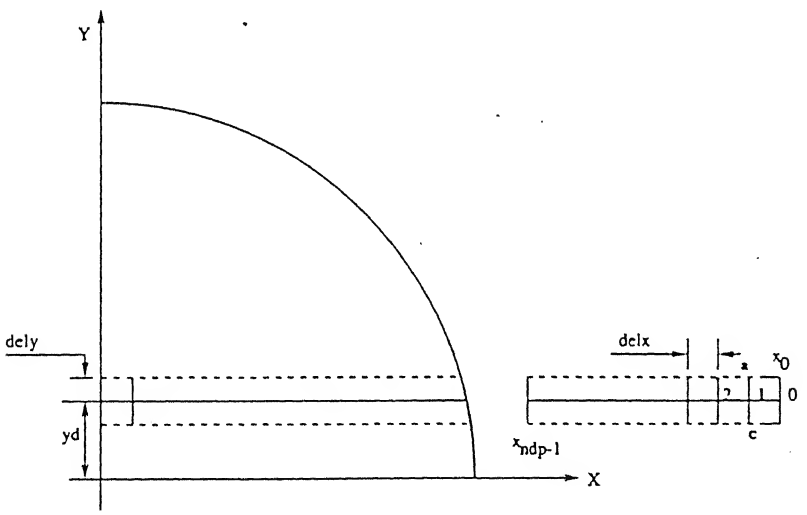

Fig. 3.10 Averaging scheme for a particular grid.

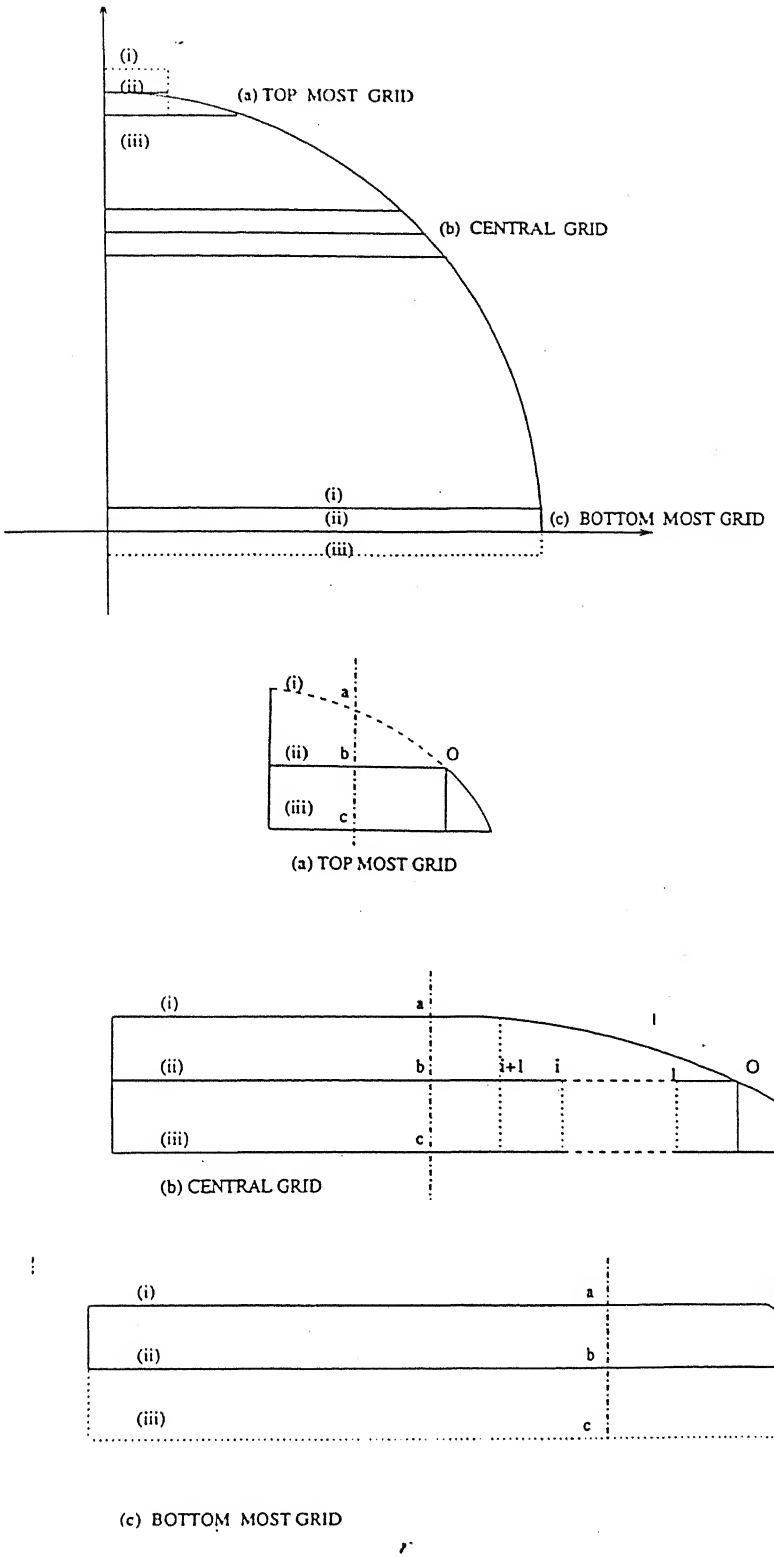

Fig. 3.11 The grid system in digital domain.

3.11(a). Hence the parameter $(\tau_{xy})_b$-$(\tau_{xy})_c$ for shear difference method while the parameters $(\sigma_1-\sigma_2)_b$-$(\sigma_1-\sigma_2)_c$ and $(\theta)_b$-$(\theta)_c$ for Trebuna's method are required. Now, these need to be averaged only over one pixel increment along Y axis.

CENTRAL GRIDS :

Grid structure:	All Rows (i), (ii) and (iii) available.
Row of interest:	Row (ii)
Averaging Rows/Dist.:	(a) For points (1) to (i) : Averaging rows (ii) and (iii); Dist=dely
	(b) For points (i+1) to (z): Averaging rows (i) and (iii); Dist=2*dely

For these grids, though the adjacent pixel rows, both on top and bottom to the pixel row of interest are available, difficulty arises due to non equal number of pixels over these individual rows. This difference in the number of pixels is due to the variation in the size of the disc as traversal is done from top to bottom. Referring to Fig. 3.11(b), it can observed that for a particular section of a grid, if a complete set of three pixels one over the other is not available, the averaging of associated parameters is to be performed over only two rows, which for the disc happen to be the central and the bottom rows.

BOTTOM-MOST GRID :

Grid structure:	Row (iii) missing due to absence of Physical Geometry. Row (i) and (ii) available.
Row of interest:	Row (ii)

Averaging row/Dist.: Averaging rows (i) and (ii); Dist=dely

The bottom-most grid is again constituted of only two rows, as is shown in Fig. 3.11(c). Utilizing the symmetry of the model as only a quarter section is being analyzed, the physical geometry and hence the photoelastic data is not available below the line of symmetry. Due to this feature, the averaging of the associated parameters is done over the line of symmetry and a row of pixels just above it.

3.8 Digital implementation of stress separation technique.

As has also been mentioned earlier that the present analysis adopts theoretical data, partly realistic data and completely realistic data, sequentially to predict the nature of variation of stresses along x and y directions, for the whole field. Theoretical data is one which is obtained by using the standard formulations based on "theory of elasticity" (refer appendix I). The partly realistic data includes (N) obtained from the experimental technique called phase shifting while completely realistic data refers to that combination where (N) is obtained from phase shifting and (θ) from either of the circular polariscope or the plane polariscope arrangement.

3.8.1 Verification of algorithm, using theoretical data

Consider any general pixel (P) in the region of interest as shown in Fig. 3.12.

From the boundary information, it's location in terms of pixels is known, say (px,py). The centre being taken as the origin, it's spatial co-ordinates (x,y) can be generated as:

$$x = px * delx \quad \text{and} \quad y = py * dely$$

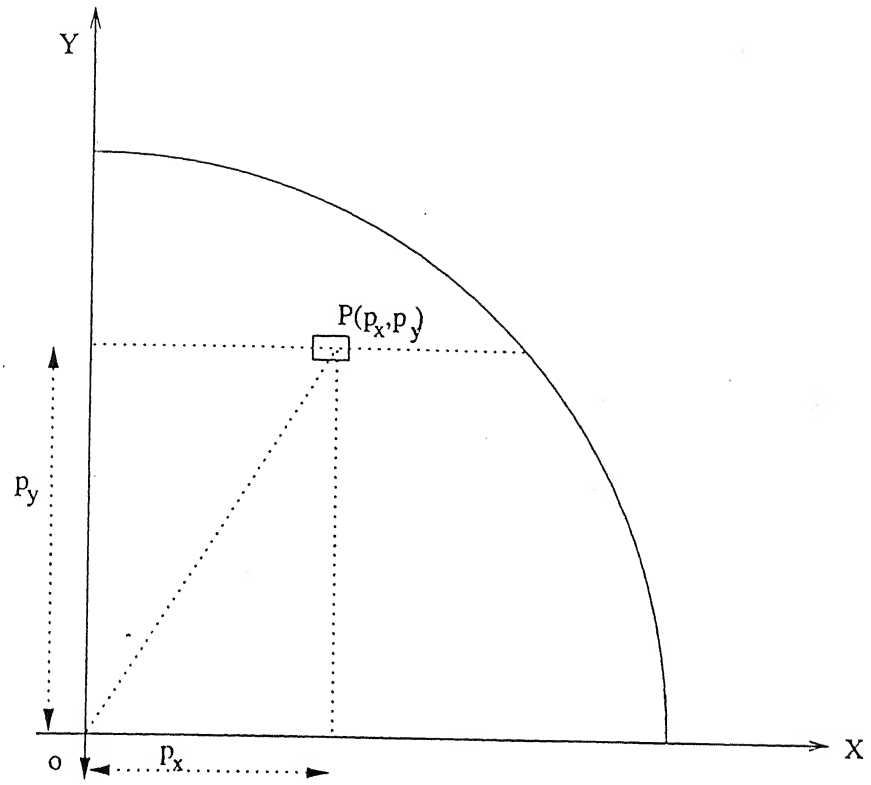

Fig. 3.12 Generation of spatial coordinates for a pixel in the region of interest.

With the spatial co-ordinates known for each pixel in the domain, corresponding fringe order (N) and isoclinic parameter (θ) can be obtained by using the standard formulations for disc under diametral compression (refer appendix I). On this basis, data for the entire field can be obtained and hence stress separation be performed. With the data available for the entire field, the next concern lies in determining the starting value for the integration procedure as proposed by shear difference method and Trebuna's method. For this purpose the concept of stress tensor at the free boundary is applied.

3.8.1.1 TRANSFORMATION LAW

For 2-D case, the stress tensor along x'-y' can be obtained by transforming the stress

tensor along x-y axis (Fig. 3.13).

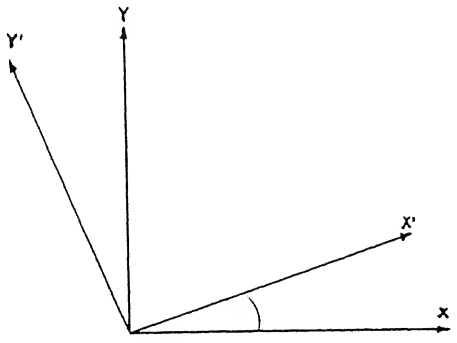

	x	y
x'	$\cos\theta$	$\sin\theta$
y'	$-\sin\theta$	$\cos\theta$

Fig. 3.13 Transformation of stress along a new set of axes.

Hence the transformation matrix [T] is

$$[T] = \begin{bmatrix} \cos\theta & \sin\theta \\ -\sin\theta & \cos\theta \end{bmatrix} \tag{3.9}$$

According to stress transformation law, the transformation matrix can be pre-multiplied while its transpose post-multiplied to the stress tensor along x-y direction to obtain the stress tensor along x'-y' direction.

3.8.1.2 THE FREE BOUNDARY

When a boundary of the model is not loaded directly, it is called a free boundary. The normal and shear stresses on a plane tangential to a free boundary are therefore zero. The principal stress axes are normal and tangential to the boundary (Fig. 3.14). Hence one of the principal stresses, say σ_2, is zero while the non-vanishing principal stress σ_1 is to be found out.

As the direction of rotation here is reverse of the (+) convention, the sign of (θ), needs to be reversed. Also σ_2 and σ_{12} equals to zero. Hence the transformation law shapes up as:

$$\begin{bmatrix} \sigma_x & \tau_{xy} \\ \tau_{xy} & \sigma_y \end{bmatrix} = \begin{bmatrix} \cos\theta & -\sin\theta \\ \sin\theta & \cos\theta \end{bmatrix} \begin{bmatrix} \sigma_1 & 0 \\ 0 & 0 \end{bmatrix} \begin{bmatrix} \cos\theta & \sin\theta \\ -\sin\theta & \cos\theta \end{bmatrix} \tag{3.10}$$

yielding

$$\sigma_x = \sigma_1 \cos^2(\theta)$$

$$\sigma_y = \sigma_1 \sin^2(\theta)$$

where:

$\sigma_1 = N f_\sigma / t$; σ_2 being zero.

N : fringe order on the boundary.

f_σ: Material fringe value.

t : thickness of the model

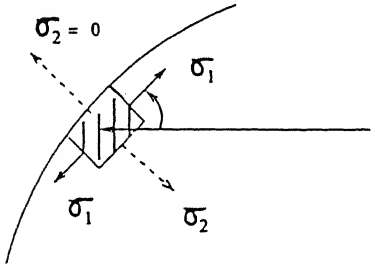

Fig. 3.14 The free boundary.

It is realized by now that the stress tensor at the free boundary can be directly obtained from photoelastic data, if the isochromatic parameter (N) is known at the boundary. In this light, the shear difference method and Trebuna's method are employed for analysis and the results verifying the algorithm, have been presented in Fig. 3.15 - Fig. 3.17. It can be seen that the results obtained by shear difference scheme and Trebuna's scheme are in close conformance with the theoretical results.

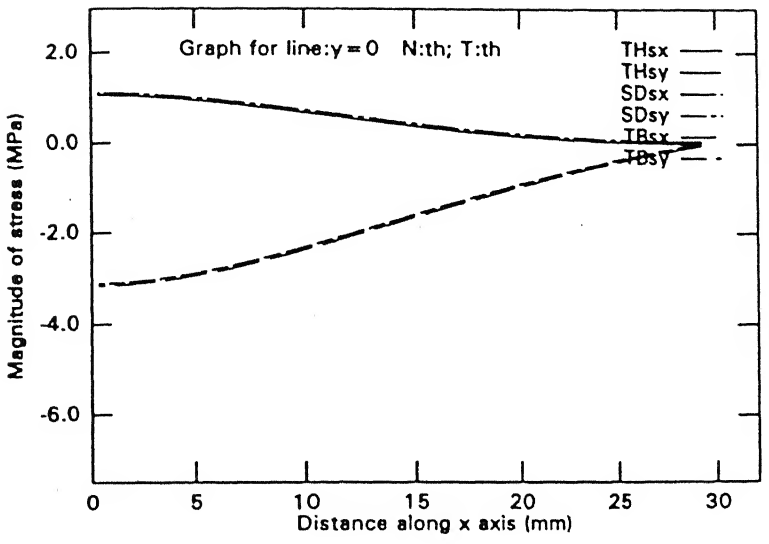

(a)

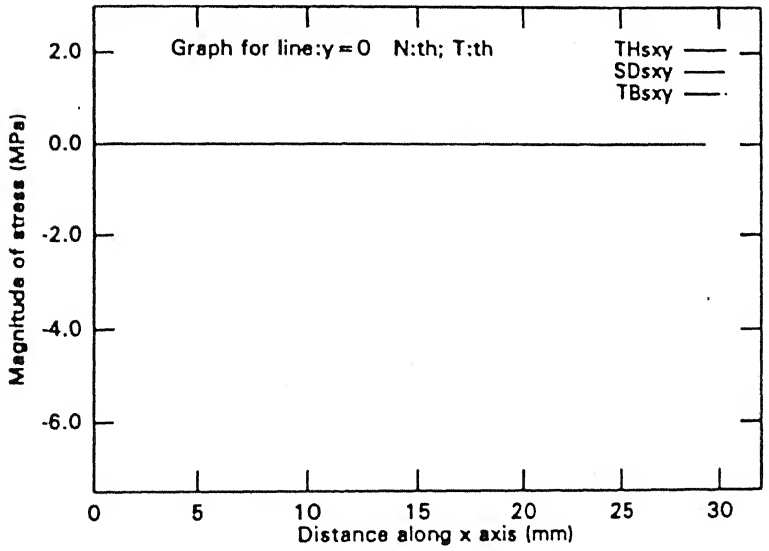

(b)

Fig. 3.15 Use of theoretical data. Variation of stresses over horizontal scan line at y = 0 (mm). (a) variation of σ_x, σ_y. (b) variation of τ_{xy}

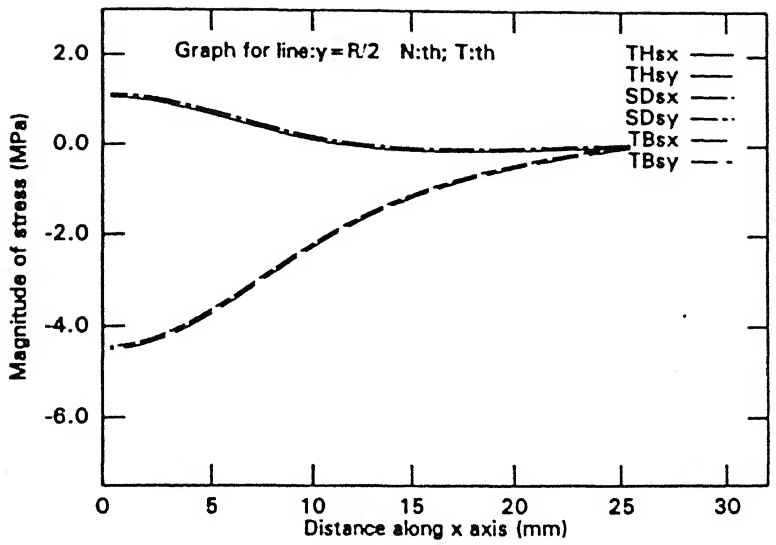

(a)

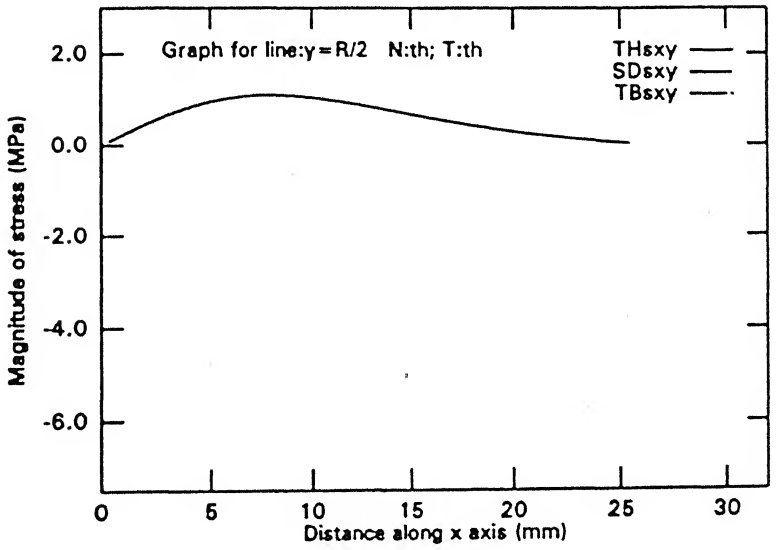

(b)

Fig. 3.16 Use of theoretical data. Variation of stresses over horizontal scan line at y = R/2 (mm). (a) variation of σ_x, σ_y. (b) variation of τ_{xy}

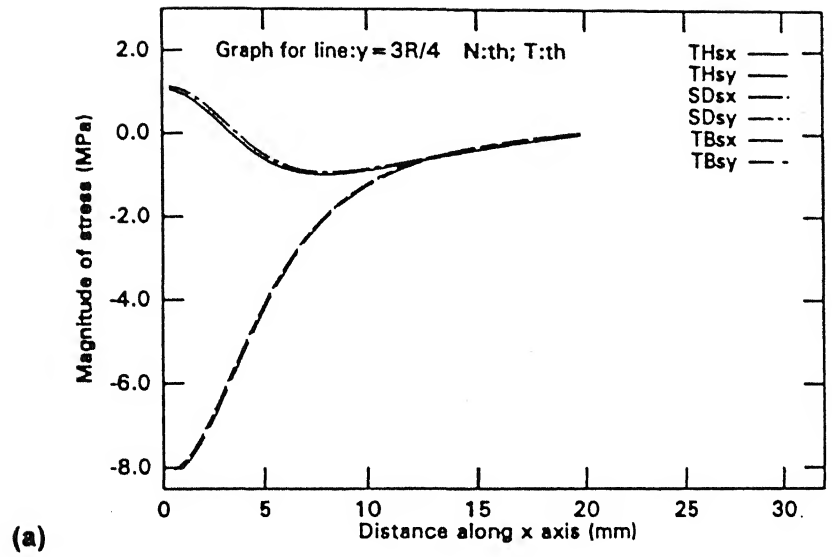

(a)

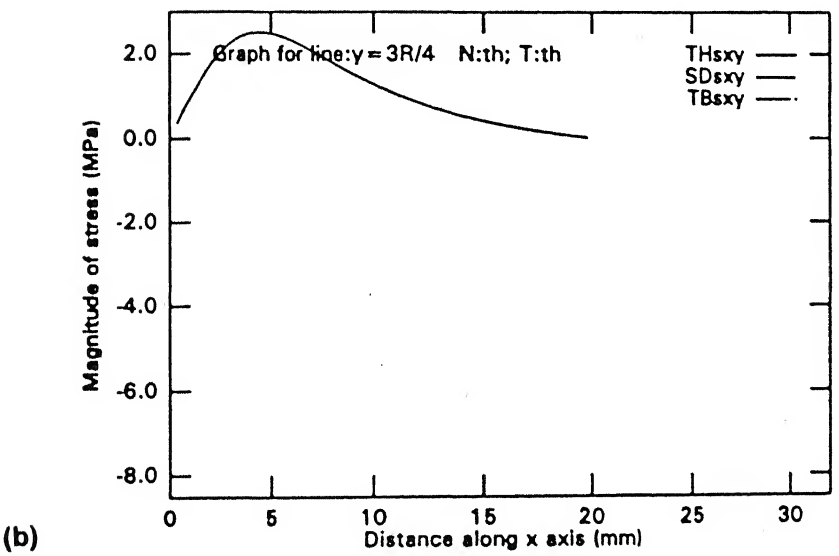

(b)

Fig. 3.17 Use of theoretical data. Variation of stresses over horizontal scan line at y = 3R/4 (mm). (a) variation of σ_x, σ_y. (b) variation of τ_{xy}

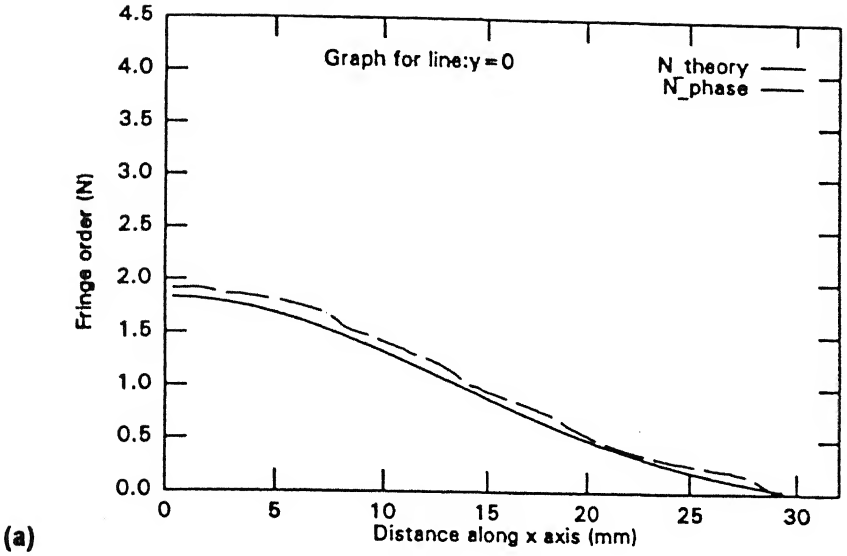

(a)

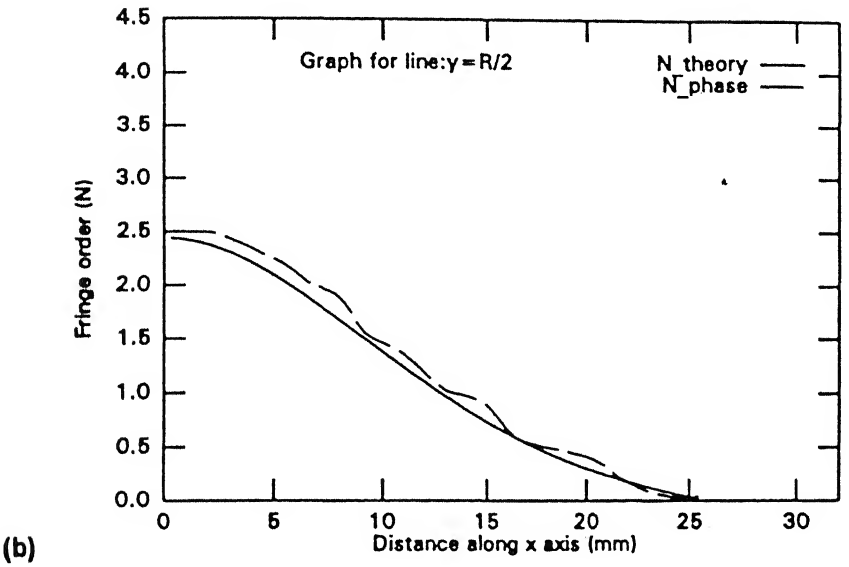

(b)

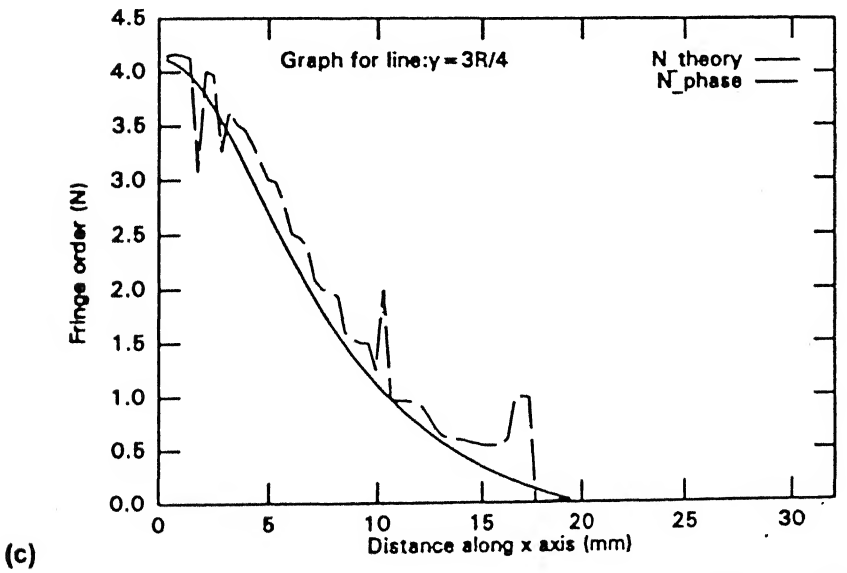

(c)

Fig. 3.18 Variation of Isochromatic parameter (N), obtained from phase shifting technique, for horizontal scan lines at (a) y = 0 (mm) (b) y = R/2 (mm) (c) y = 3R/4 (mm)

3.8.2 Use of *N* from phase shifting; θ from theory.

Fringe order (N) at every pixel can be obtained by digital processing of phase shifting images, as previously discussed. For an estimation of the accuracy of (N), so obtained, comparison with the theoretically generated (N) has been shown in Fig. 3.18, for three different horizontal scan lines. For the disc under diametral compression, the boundary with a known fringe order of zero can also be used as a reference for determining the accuracy of (N) from phase shifting technique. Figure 3.19 presents the value of (N), obtained from phase shifting against theoretically generated (N), along the boundary.

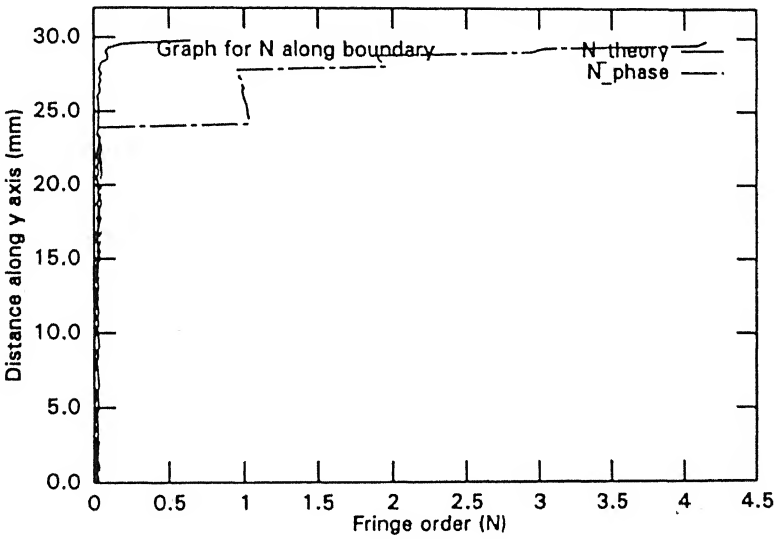

Fig. 3.19 Variation of Isochromatic parameter (N), along the boundary of the quarter disc.

Isoclinic parameter (θ) can still be generated based on theoretical formulation for each pixel. This set of data can be employed to perform, a partially realistic analysis of stress field. The results presented in Fig. 3.20 - Fig. 3.22, for three different horizontal scan

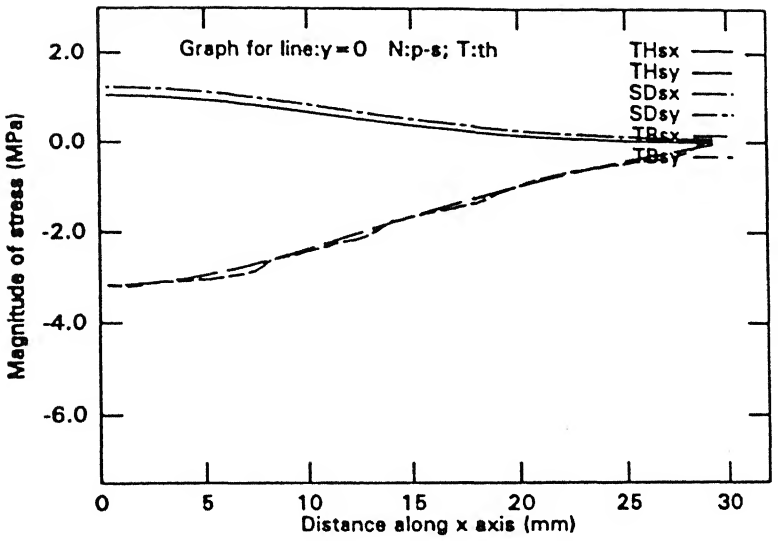

(a)

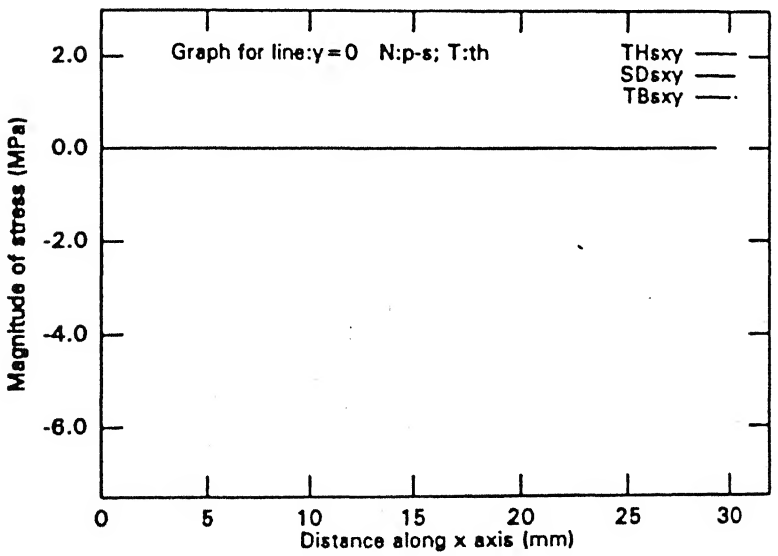

(b)

Fig. 3.20 Use of N: phase shifting; θ: theoretical. Variation of stresses over horizontal scan line at y = 0 (mm). (a) variation of σ_x, σ_y. (b) variation of τ_{xy}

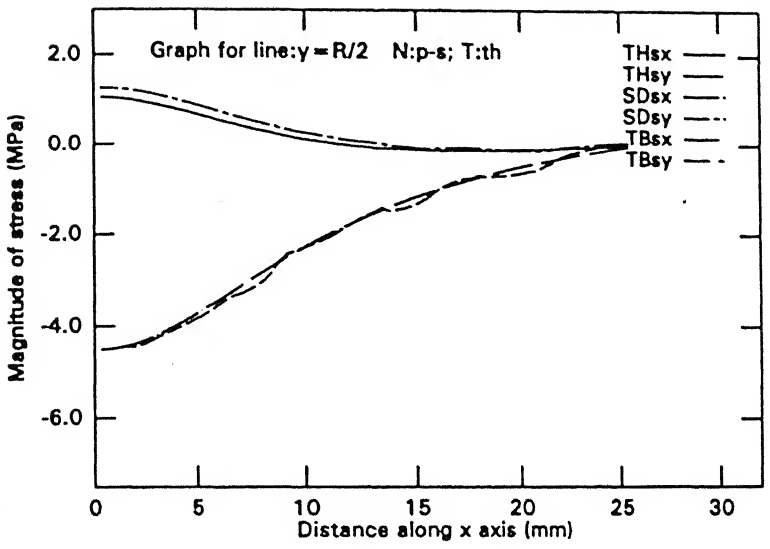

(a)

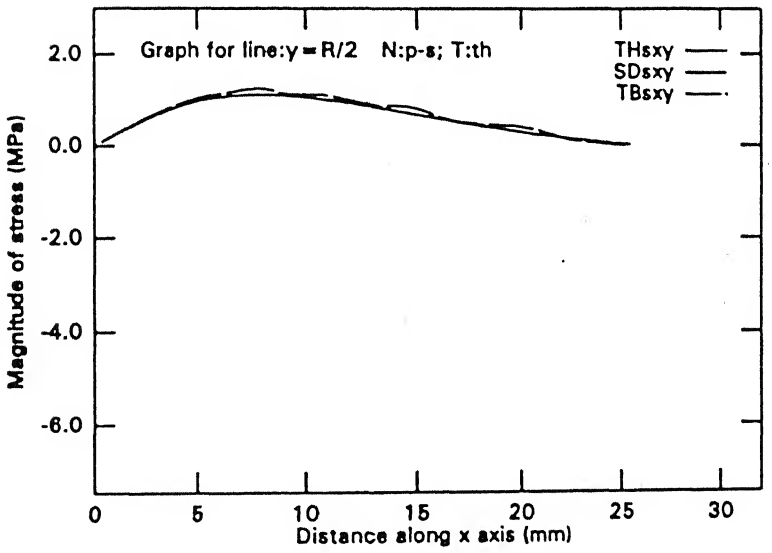

(b)

Fig. 3.21 Use of N: phase shifting; θ: theoretical. Variation of stresses over horizontal scan line at y = R/2 (mm). (a) variation of σ_x, σ_y. (b) variation of τ_{xy}

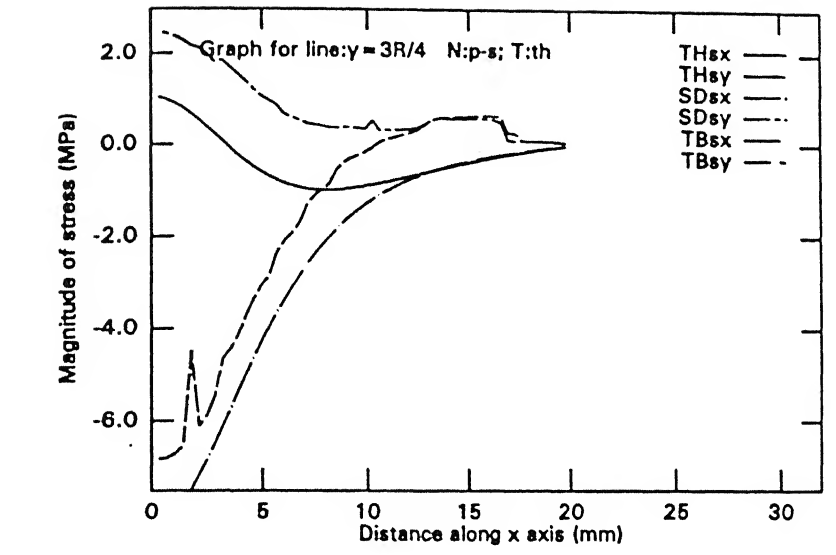

(a)

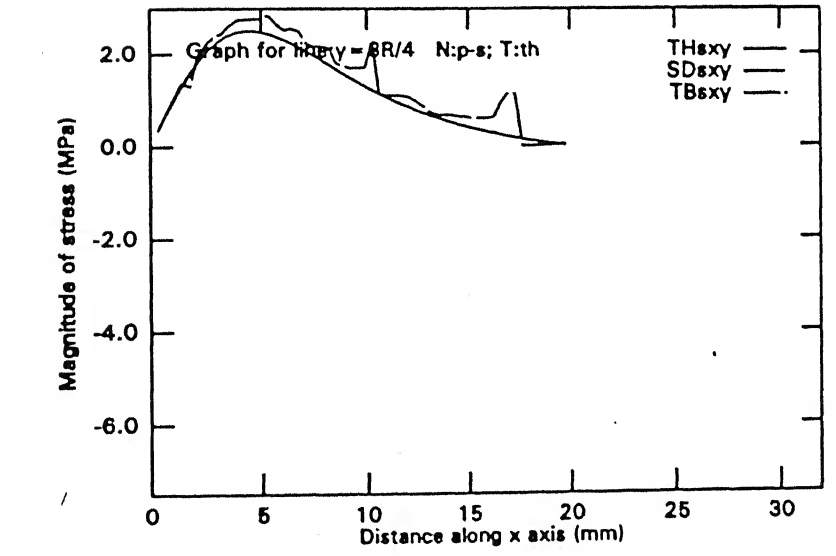

(b)

Fig. 3.22 Use of N: phase shifting; θ: theoretical. Variation of stresses over horizontal scan line at y = 3R/4 (mm). (a) variation of σ_x, σ_y. (b) variation of τ_{xy}

lines, reveal that though the level of accuracy in the stresses, separated by shear difference method and Trebuna's method has fallen with the usage of phase shifting (N), yet, the results are reasonably accurate. This comparison is of significant importance as it helps through, a step ahead in establishment of phase shifting technique as a reliable experimental technique, for determination of isochromatic parameter (N).

3.8.3 Use of N from phase shifting; θ from plane polariscope.

This approach focuses the use of completely realistic data for stress analysis. Here apart from obtaining the isochromatic parameter (N) experimentally, the isoclinic parameter (θ) is also obtained experimentally, using plane polariscope arrangement. The intensities of the recorded images are processed, as mentioned in previous sections and both the isochromatic parameter (N) and the isoclinic parameter (θ), obtained. As (θ) is not defined for fringe orders of 0, 1, 2 etc., excessive noise is present in the corresponding zones. A comparative analysis of (θ) obtained from circular polariscope arrangement and the plane polariscope arrangement, has been presented for three different horizontal scan lines in Fig. 3.23. It can be observed that (θ) obtained from the later is more accurate. It is for this reason that *(θ)* from plane polariscope is further suggested for analysis.

3.8.4 Use of N from phase shifting; θ from plane polariscope; use of multiple loads.

It has been observed that the accuracy of isoclinic determination is very poor near full fringe orders. In general, discontinuous isoclinic fringes are obtained. To bridge the gap,

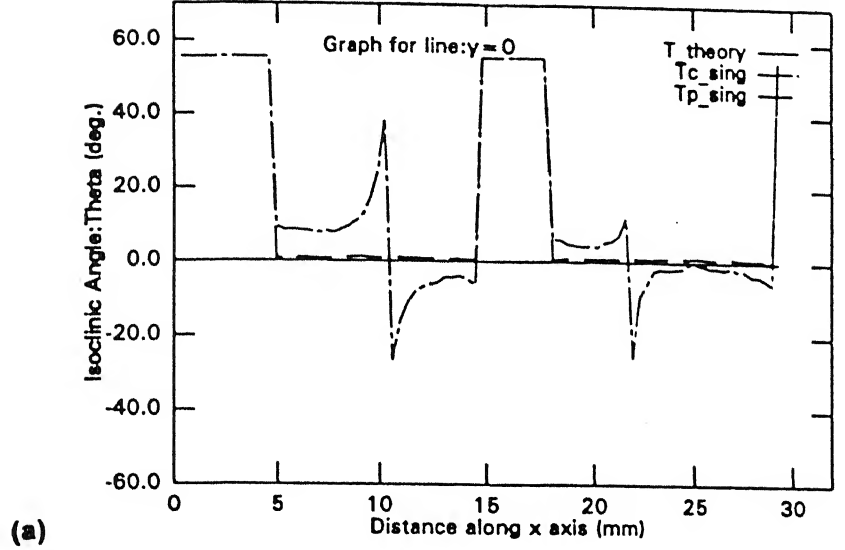

(a)

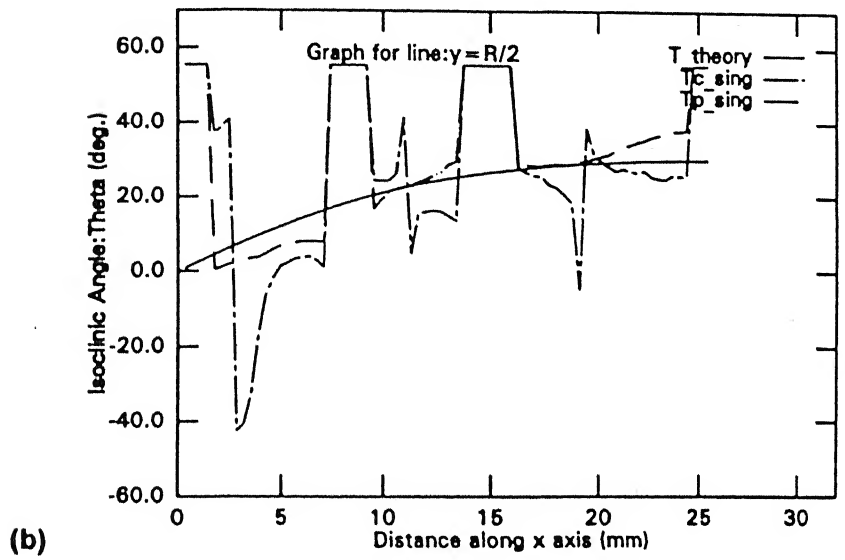

(b)

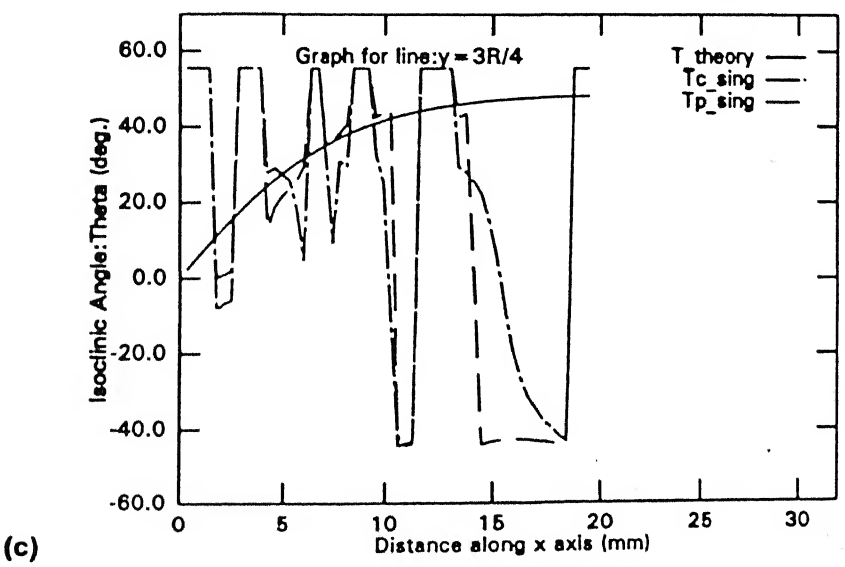

(c)

Fig. 3.23 Comparative study of Isoclinic parameter θ: circular polariscope vs. plane polariscope arrangement, for various horizontal scan lines. (a) y = 0 (mm) (b) y = R/2 (mm) (c) y = 3R/4 (mm).

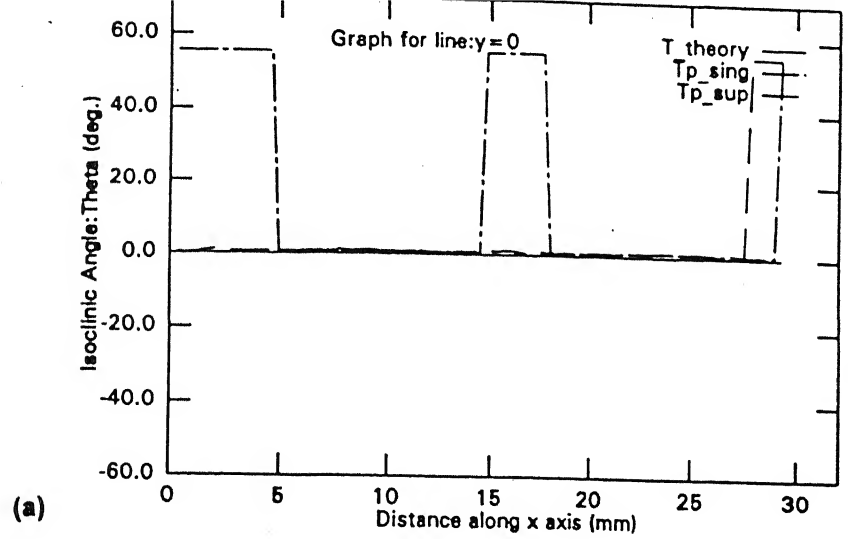

(a)

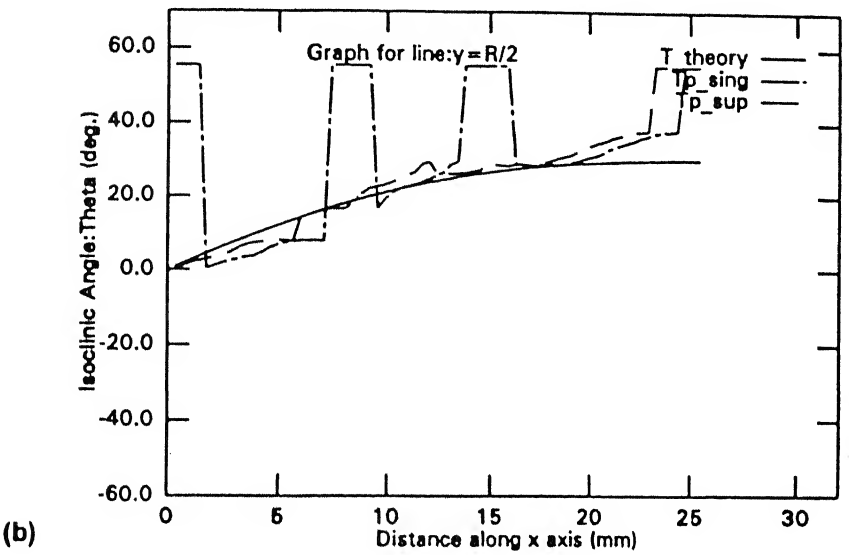

(b)

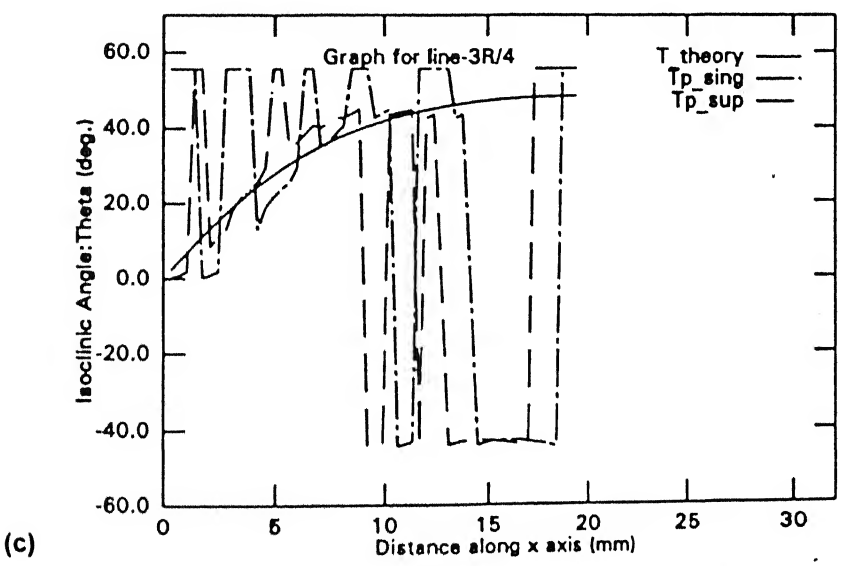

(c)

Fig. 3.24 Comparative study of Isoclinic parameter θ, obtained from plane polariscope arrangement: Single load vs. Multiple load, for various horizontal scan lines.
(a) y = 0 (mm) (b) y = R/2 (mm) (c) y = 3R/4 (mm)

use of interpolation approach[17] or multiple wavelengths[18] is reported. Extending the idea of multiple wavelengths, Petrucci[19] used white light to illuminate the model and extracted isoclinics using the red, green and blue intensity values of the colour image recorded by a colour image processing system. Then Ramesh and Mangal[15] proposed a new scheme, using two different loads to get continuous isoclinic fringes. Using this approach, first, the intensity information from the images corresponding to the load of 335.05 N is processed and isoclinic parameter obtained. Then, the procedure is repeated for the raised load of 502.5 N. Finally, isoclinic for the field is obtained by performing a logical 'OR' operation between the two sets of isoclinic parameter. Figure 3.24 presents a comparative study of isoclinic obtained using single load and that obtained using two loads, for various horizontal scan lines. Isoclinic obtained using two loads, is found to be largely improved over the single load isoclinic. Now with the fact established that the value of (θ) can be best obtained from usage of multiple loads, with plane polariscope arrangement, it's usage for further analysis is suggested, employing the same technique.

Figure 3.25 shows the variation of (θ), obtained from use of multiple loads, along the boundary of the quarter of the disc. It can be observed that the value of θ, along the boundary is a constant whereas the actual variation of θ, along the boundary, should be of the form, as represented by the theoretically generated θ. This difference can be attributed to the fact that θ, given by the eq. (3.3) or eq. (3.5), may be indeterminate, at some points. While processing the intensity information of the grabbed images and obtaining the values of isoclinic parameter θ, for the whole field, the value at such indeterminate points, was arbitarily assigned. The constant value of θ, seen along the boundary is nothing but this arbitarily assigned value itself.

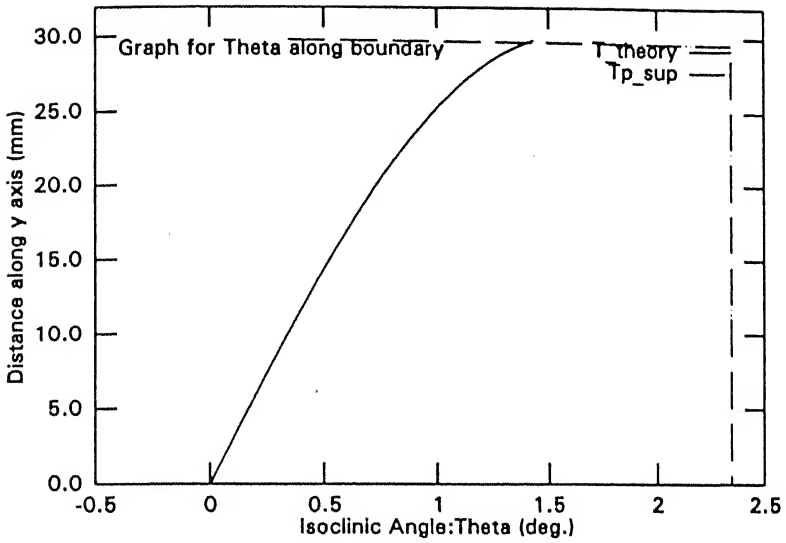

Fig. 3.25 Variation of Isochromatic parameter (N), along the boundary of the quarter disc.

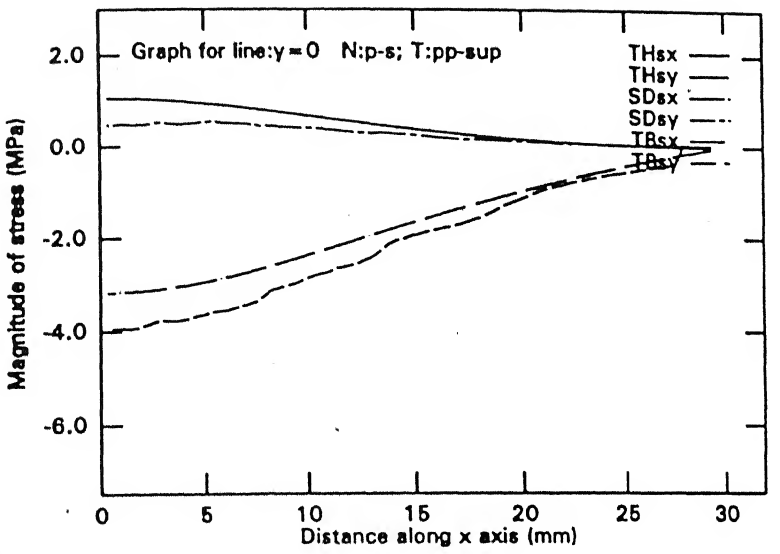

(a)

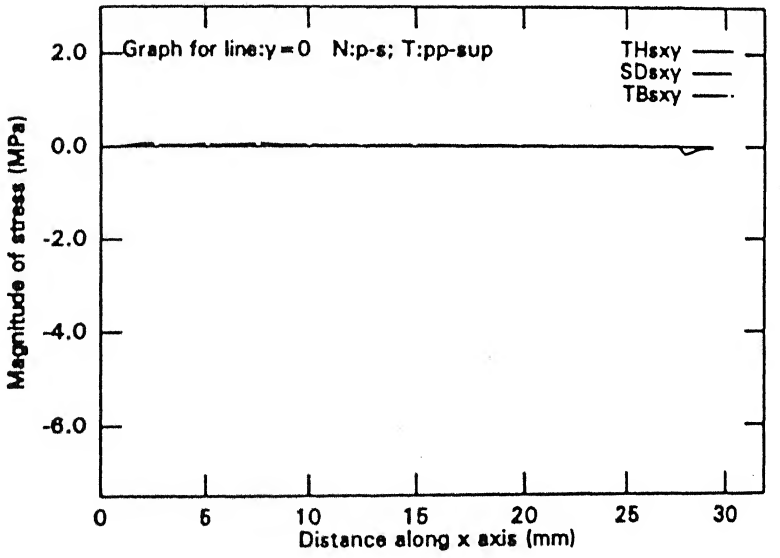

(b)

Fig. 3.26 Use of N: phase shifting; θ: plane polariscope / multiple loads. Variation of stresses over horizontal scan line at y = 0 (mm). (a) variation of σ_x, σ_y. (b) variation of τ_{xy}

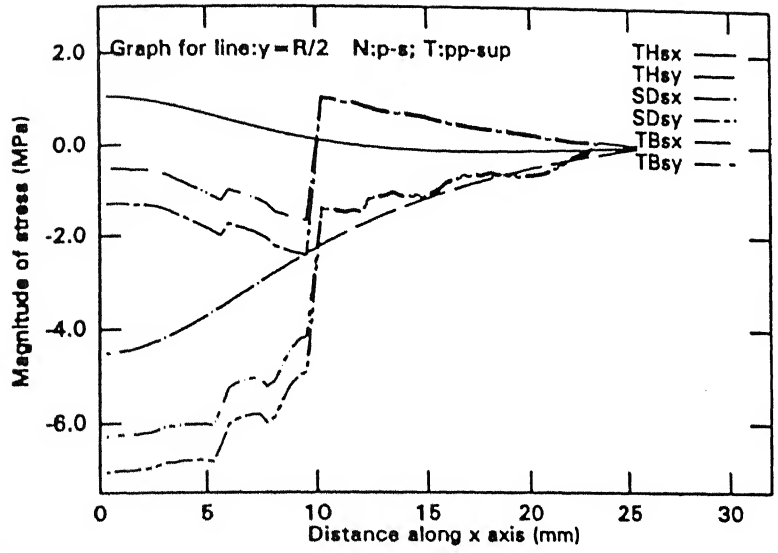

(a)

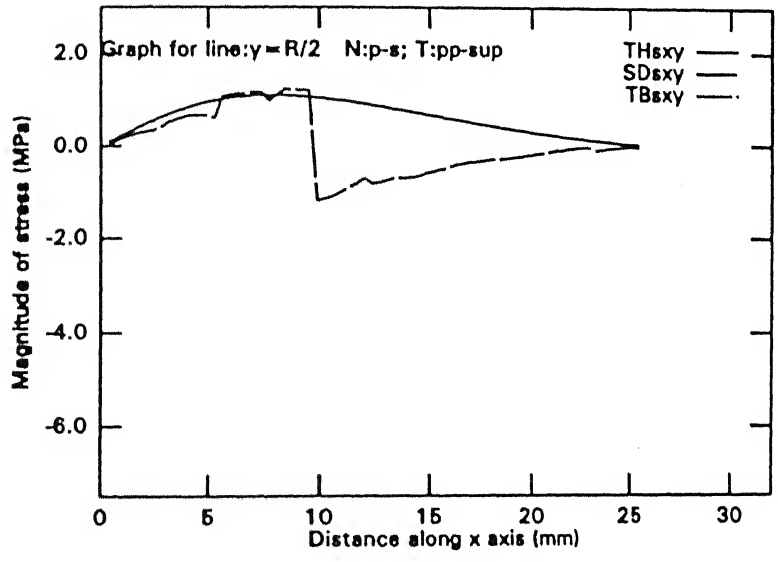

(b)

Fig. 3.27 Use of N: phase shifting; θ: plane polariscope / multiple loads. Variation of stresses over horizontal scan line at y = R/2 (mm). (a) variation of σ_x, σ_y. (b) variation of τ_{xy}

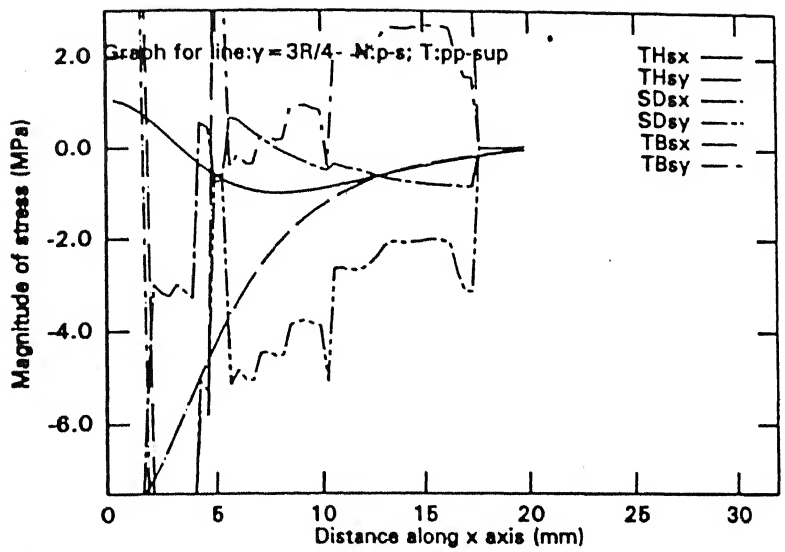

(a)

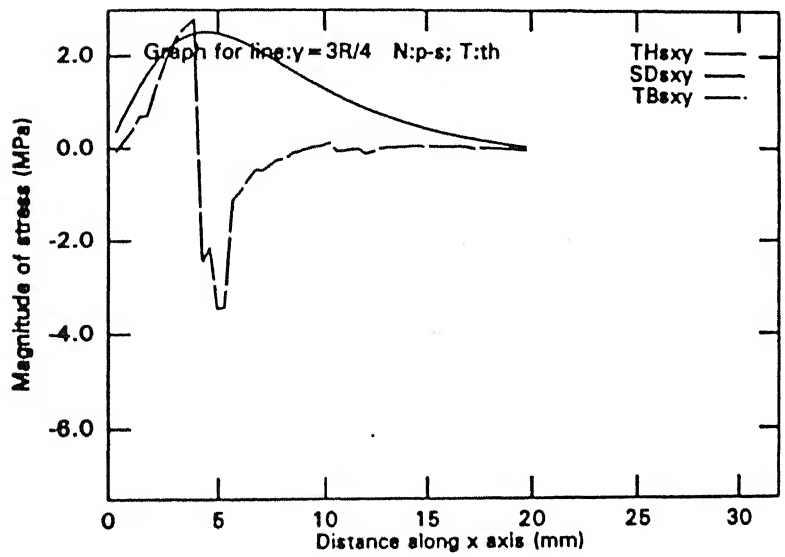

(b)

Fig. 3.28 Use of N: phase shifting; θ: plane polariscope / multiple loads. Variation of stresses over horizontal scan line at y = 3R/4 (mm). (a) variation of σ_x, σ_y. (b)variation of τ_{xy}

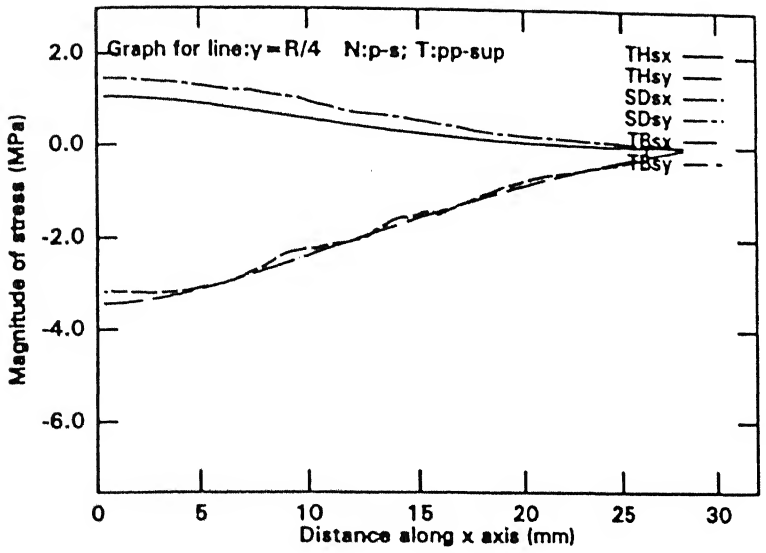

(a)

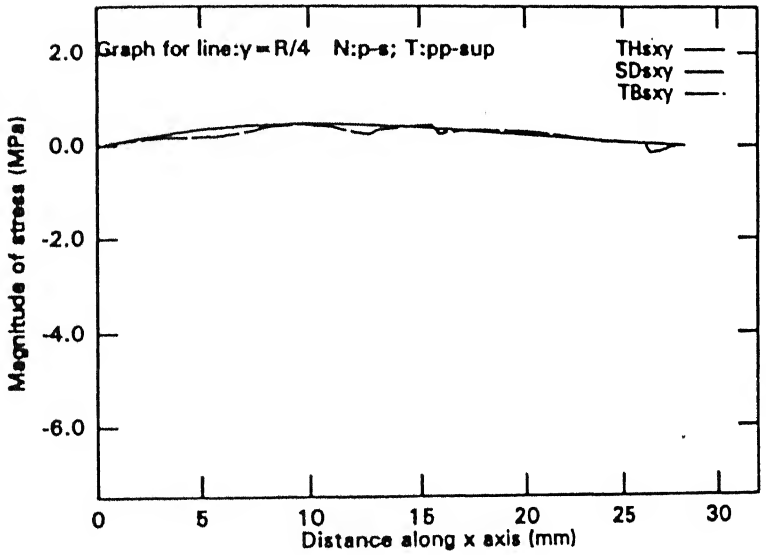

(b)

Fig. 3.29 Use of N: phase shifting; θ: plane polariscope / multiple loads. Variation of stresses over horizontal scan line at y = R/4 (mm). (a) variation of σ_x, σ_y. (b) variation of τ_{xy}

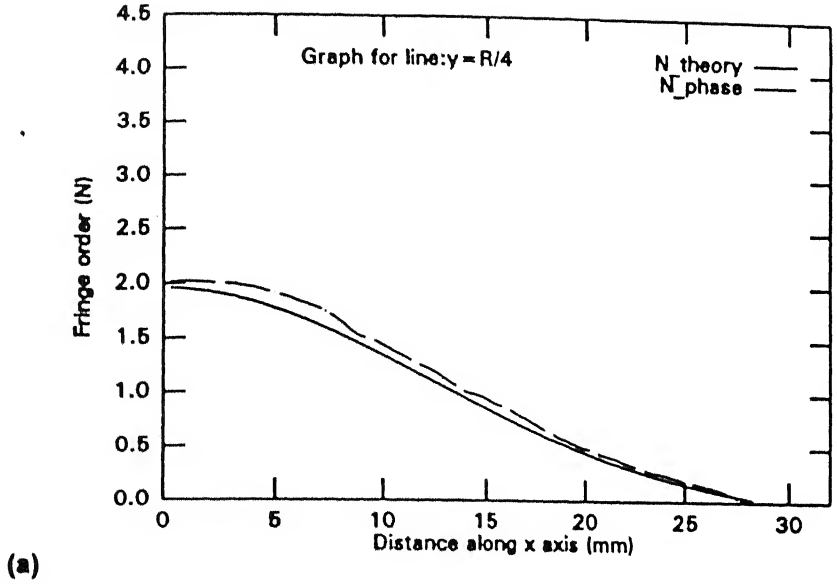

(a)

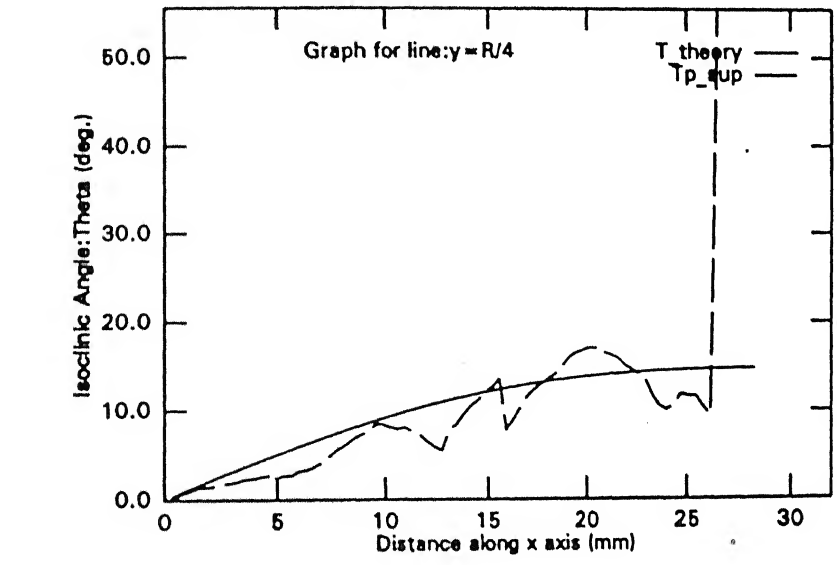

(b)

Fig. 3.30 Variation of photoelastic data for horizontal scan line at y = R/4 (mm). (a)variation of N: phase shifting. (b) variation of θ: plane polariscope arrangement using multiple loads.

The results for various horizontal scan lines have been presented in Fig. 3.26 to Fig. 3.29. It is seen that the stresses evaluated using completely realistic data are not in agreement with the theoretically evaluated stresses. However, the results for the horizontal scan line at y = R/4, are close to the theoretical results. This can be accounted to the better input data, for this particular scan line. The photoelastic data in use for this line is presented in Fig. 3.30.

It is important to realize that the indeterminacy of θ is not restricted to the boundary alone. It could be anywhere across the field also but the indeterminacy of θ, at the boundary has relatively more effect in terms of reducing the accuracy of final solution. If, the value of θ at the pixel on the boundary which also happens to be the starting point for the integration procedure as proposed in shear difference scheme or in Trebuna's scheme, is improved then the corresponding solution can be expected to be better. One possible improvement could be in the form of assignment of a well defined value of θ, closest to the boundary, as the value on the boundary itself. Referring to Fig. 3.11(a), assume a general case where θ at the pixel boundary, say P_a is indeterminate and the closest pixel having a well defined value of θ is P_i. If the value of θ at P_i is assigned to all the pixels towards the boundary, the corresponding solution should be better. Figure 3.31(b), shows the modified θ, along the boundary. The corresponding solutions for arbitrary horizontal scan lines are presented in Fig. 3.32 It can be observed that these results are relatively better than those corresponding to the un-modified θ. Also, the results corresponding to Trebuna's method seem to have improved more than those corresponding to shear difference method.

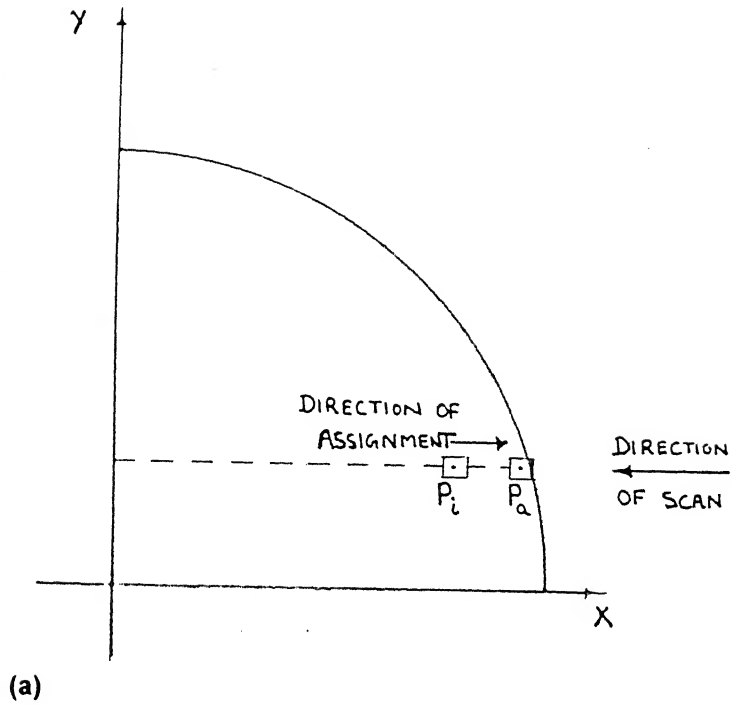

(a)

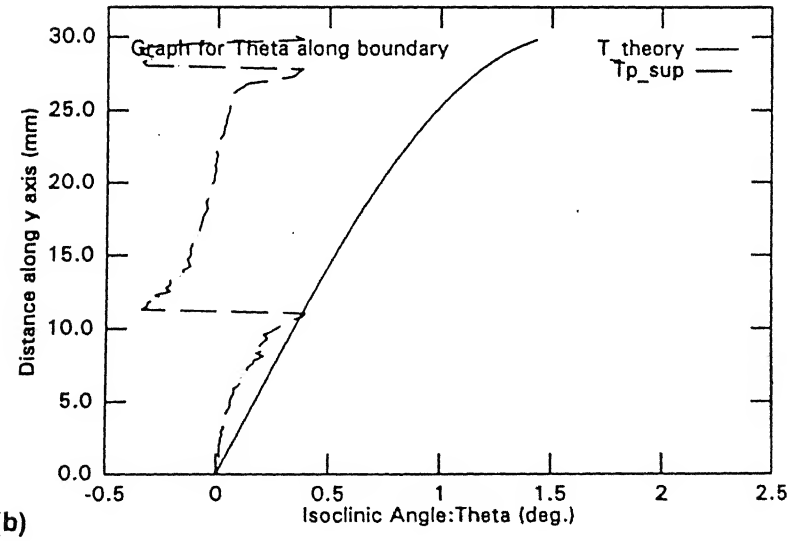

(b)

Fig. 3.31 Modification of Isoclinic parameter (θ), along the boundary (a) the proposed scheme (b) improved variation along the boundary.

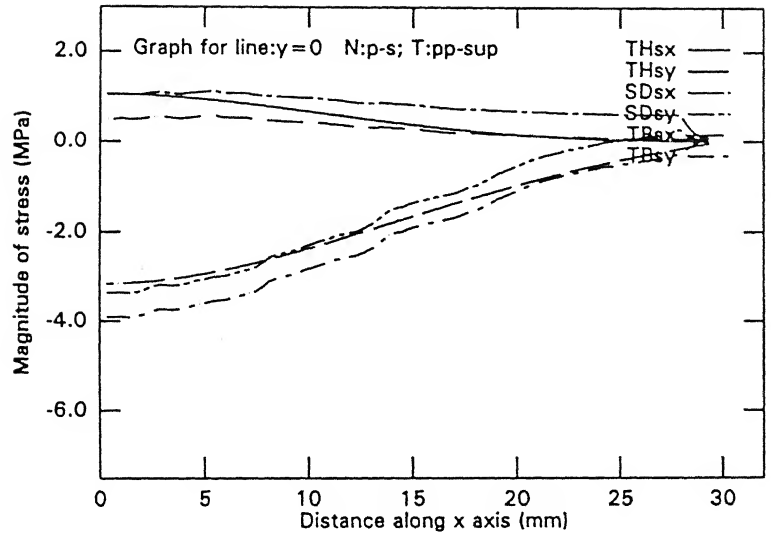

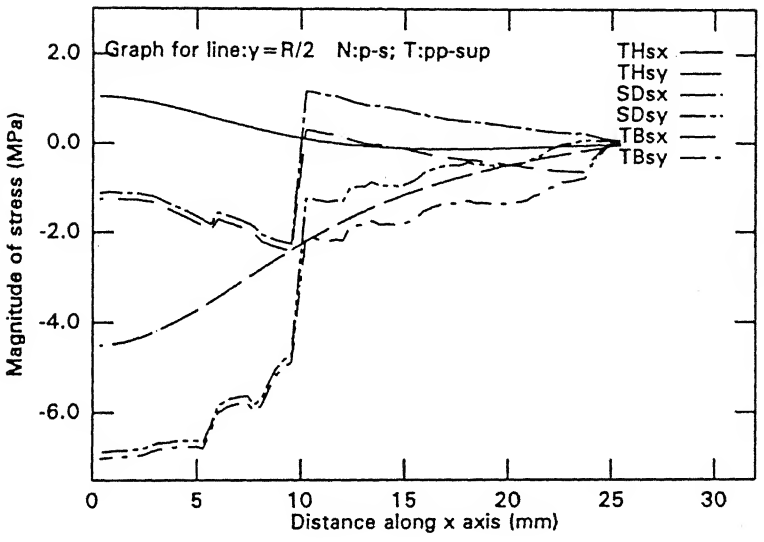

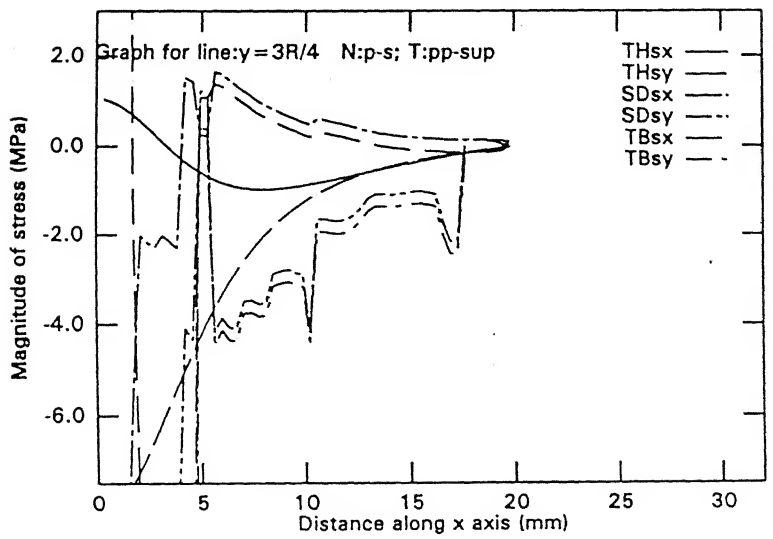

Fig. 3.32 Use of N: phase shifting; θ: modified form of - plane polariscope / multiple loads. Variation of stresses over various horizontal scan lines. (a) y = 0 (mm) (b) y = R/2 (mm) (c) y = 3R/4 (mm)

3.8.5 Whole field representation of the results.

All the results presented thus far have been for a particular horizontal or a vertical scan line. Now, the aim is to represent the variation of σ_x, σ_y and τ_{xy}, for the whole field. The eq. 2.1 relates the difference of principal stresses at a point to the fringe order at that point. Analogous to this, if $(\sigma_1 - \sigma_2)$ is replaced by σ_x, then *(N)* obtained from the equation would correspond to σ_x. If (N) corresponding to σ_x is represented as N_σ, then it can be given by the relation:

$$N_{\sigma_x} = \frac{\sigma_x\, t}{F_\sigma} \tag{3.11}$$

If N_σ is plotted, it would be in one sense the field representation of σ_x itself, the constant (t/F_σ) being the only discriminatory factor between the two. Similarly the plots for N_σ and N_τ can also be obtained. Fig. 3.33(a), Fig. 3.33(b) and Fig. 3.33(c) represent the variation of σ_x, σ_y and τ_{xy} respectively. This solution set is obtained by utilizing theoretically generated photoelastic data, with the standard formulations for the disc under diametral compression. The main emphasis of the thesis apart from the digital aspects of stress separation schemes has been to investigate the trend with which the accuracy of the results vary, as the input data is changed from theoretical to partly experimental and then to completely experimental. Figure 3.34 shows this trend for σ_x. Figure 3.34(a) and Fig. 3.34(b) represent the results obtained from shear difference method and Trebuna's method respectively, using the theoretically generated data. Figure 3.34(c) and Fig. 3.34(d) show the results corresponding to the combination of phase shifting (N) and theoretical (θ). The results can be observed to have detiorated. Finally, the resort being made to completely realistic data, wherein (θ) is also

σ_x : Theory

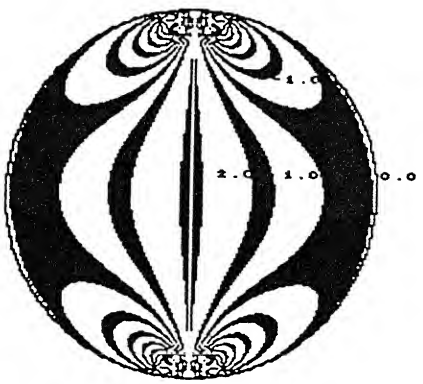

(a)

σ_y : Theory

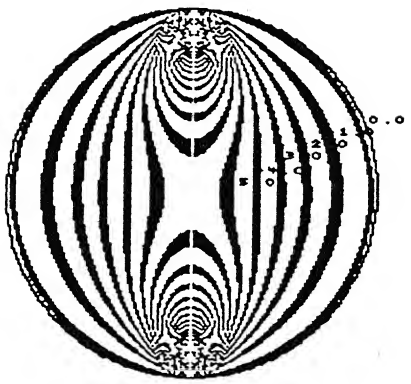

(b)

τ_{xy} : Theory

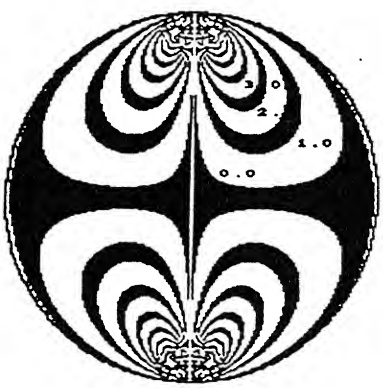

(c)

Fig. 3.33 Pseudo fringe patterns showing variation of stresses, determined using theoretical data and standard solution for disc under diametral compression.

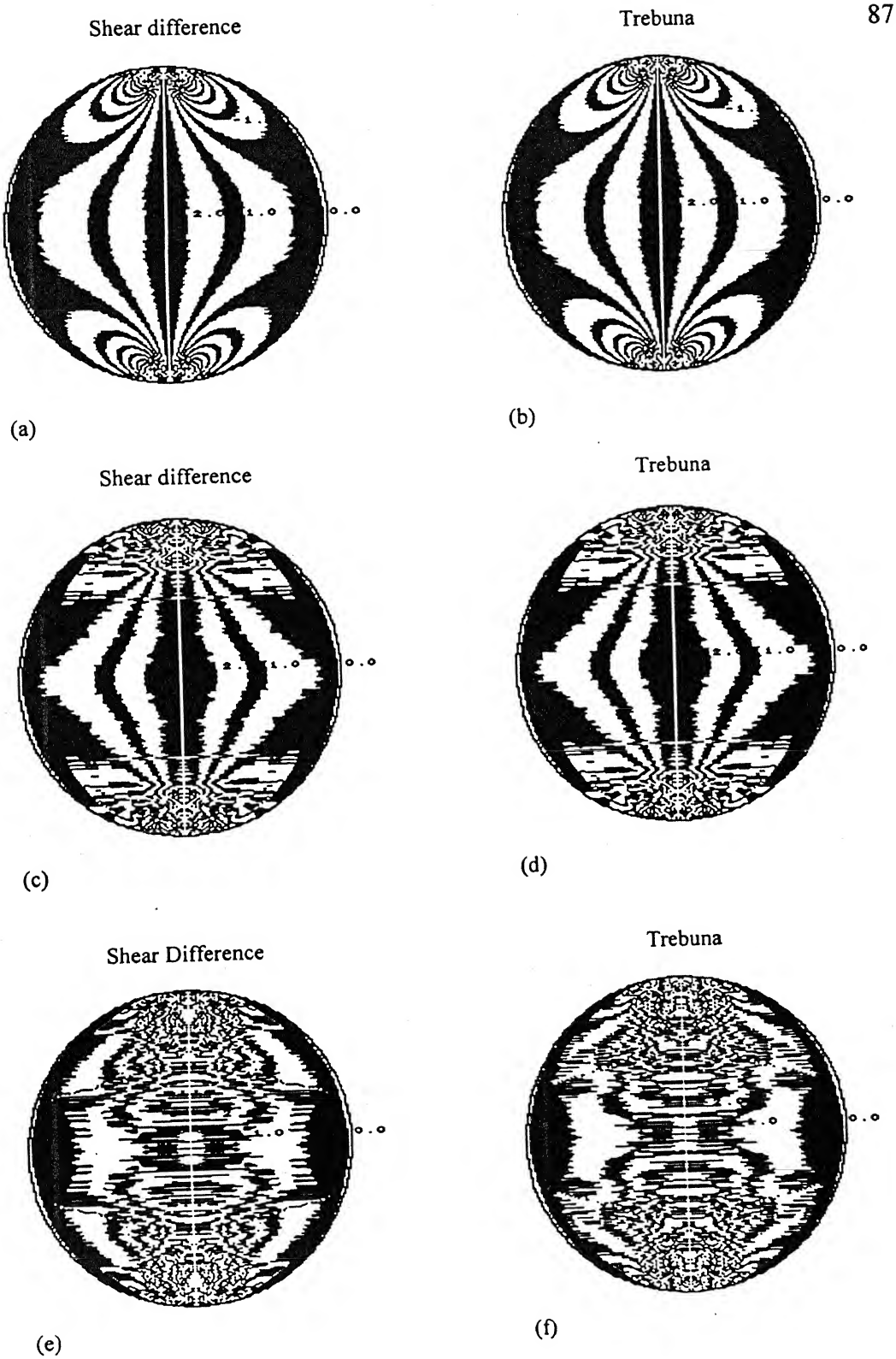

Fig. 3.34 Pseudo fringe patterns for σ_x for various sets of input data.
(a) N:theory; θ:theory - shear diff. (b) N:theory; θ:theory - Trebuna
(c) N:p-sftg; θ:theory - shear diff. (d) N:p-sftg; θ:theory - Trebuna
(f) N:p-sftg; θ:mult.loads - shear diff.(f) N:p-sftg; θ:mult.loads-Trebuna

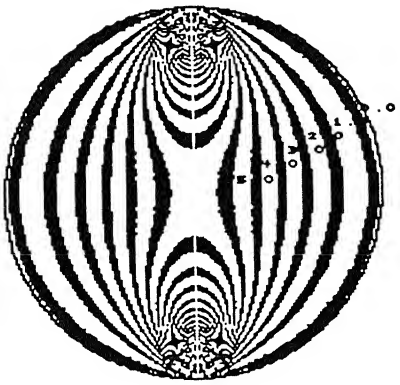

(a)

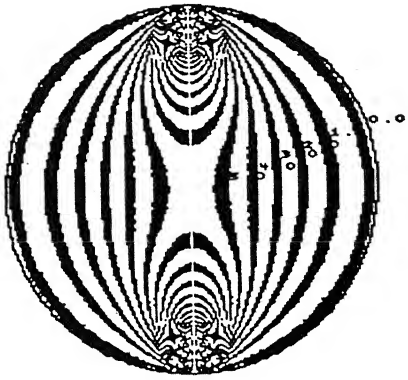

(b)

Shear difference

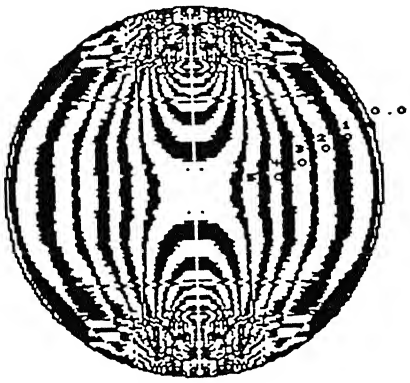

(c)

Trebuna

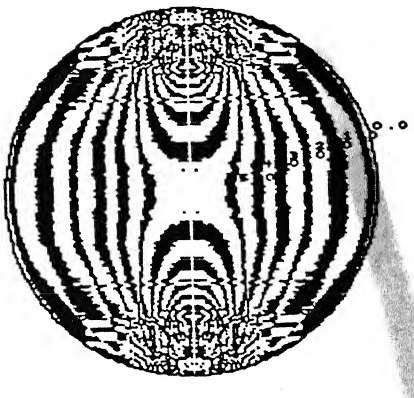

(d)

Shear difference

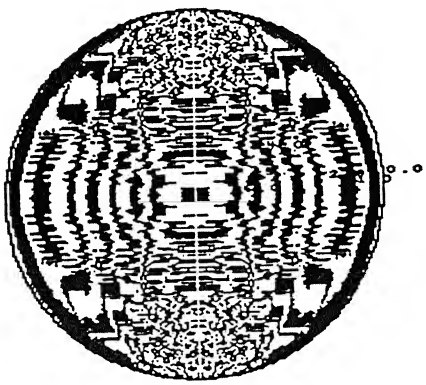

(e)

Trebuna

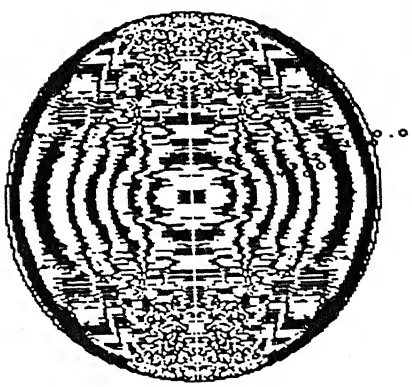

(f)

Fig. 3.35 Pseudo fringe patterns for σ_y for various sets of input data.
(a) N:theory; θ:theory - shear diff. (b) N:theory; θ:theory - Trebuna
(c) N:p-sftg; θ:theory - shear diff. (d) N:p-sftg; θ:theory - Trebuna
(f) N:p-sftg; θ:mult.loads - shear diff.(f) N:p-sftg; θ:mult.loads-Trebuna

Shear difference

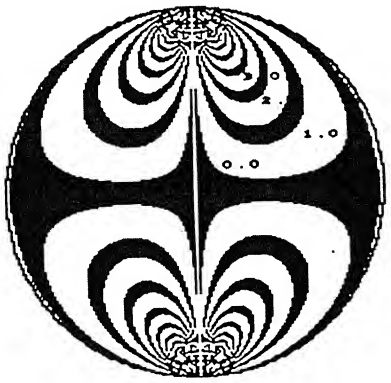

(a)

Trebuna

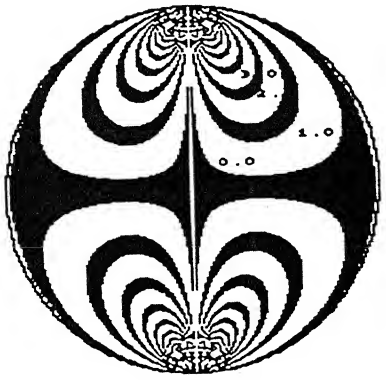

(b)

Shear difference

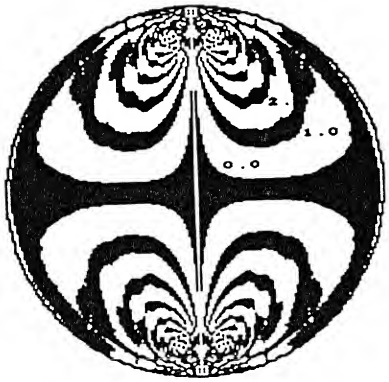

(c)

Trebuna

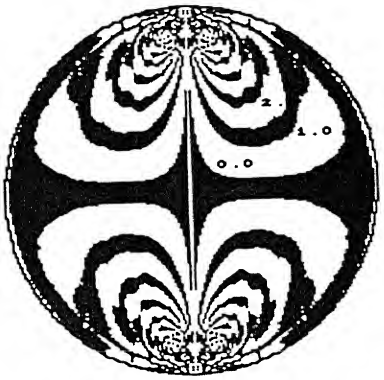

(d)

Shear difference

(e)

Trebuna

(f)

Fig. 3.36 Pseudo fringe patterns for τ_{xy} for various sets of input data.
(a) N:theory; θ:theory - shear diff. (b) N:theory; θ:theory - Trebuna
(c) N:p-sftg; θ:theory - shear diff. (d) N:p-sftg; θ:theory - Trebuna
(f) N:p-sftg; θ:mult.loads - shear diff.(f) N:p-sftg; θ:mult.loads-Trebuna

experimentally obtained , using multiple loads with plane polariscope arrangement, the corresponding results have been presented in Fig. 3.34(e) and Fig. 3.34(f). These results reflect the inaccurate and noisy *(θ)*. Figure 3.35 and Fig. 3.36 present the variation of σ_y and τ_{xy}, respectively. It is worth mentioning here that this mode of fringe plotting is not a true representation of the results, due to the limitation of the plotting code. The stresses being plotted as fringes are only those which lie within a user defined tolerance zone. Any stress value even slightly off this zone, is not plotted, giving a haphazard and a noisy view. Despite of this fact, the fringe representation of the stresses is employed to give a feel of stress variation over the entire field.

3.9 Plate with a hole

The previous sections have discussed the establishment of shear difference scheme and Trebuna's scheme as reliable schemes for stress separation. The trend with which the accuracy of the results vary, as the input data is sequentially changed, first from completely theoretical to partly experimental and finally to completely experimental, has also been discussed. This section discusses the application of above mentioned stress separation schemes over a plate with a hole, subjected to uniaxial tension. The data employed for analysis is completely experimental where (N) is obtained from phase shifting and (θ) from plane polariscope arrangement.

3.9.1 Boundary information

It has earlier been mentioned that in order to detect the boundary of the region of

interest, the maximum grey level over the entire image is detected. The variation of these grey levels can be from 0 to 255. Owing to the fact that the maximum grey level over the image would be less than or equal to 255, any pixel with grey level value of 255 would represent the boundary pixel. Adopting this principle, to mark the boundary, Sreedhar[] had developed some primitives. These are line, circle, ellipse and 3-point arc. Utilising the symmetry of the plate with the a hole, only a quarter section needs to be evaluated. It is to be realised that the complete boundary of the quarter section of the plate, under consideration, cannot be directly determined using any of the primitives mentioned above. For determination of the complete boundary, first the hole in the plate is considered. The boundary of this hole can be detected by simulating it as an ellipse and using the primitive developed by Sreedhar. The spatial location of the three remaining corners of the plate can be known from the grabbed image, in terms of pixels. This information in conjunction with the known hole boundary can be used to determine the complete boundary of the plate with a hole.

As it has been proved in earlier sections that the photoelastic data obtained from plane polariscope arrangement is superior to that obtained from circular polariscope arrangement, images of the plate under consideration (refer appendix III) are grabbed using the plane polariscope arrangement. The sequence of six images grabbed are shown in Fig 3.37. The details regarding the determination of isochromatic parameter (N) and isoclinic parameter (θ) have bben discussed in section 3.3.2. Now, with the boundary detected and the experimental data available for the entire field, the concern lies in determining the starting point for initiation of integration procedure as proposed in shear difference and Trebuna's scheme. For this purpose, again the free boundary is made use of. A boundary which is not directly loaded, is referred as a free boundary. The normal

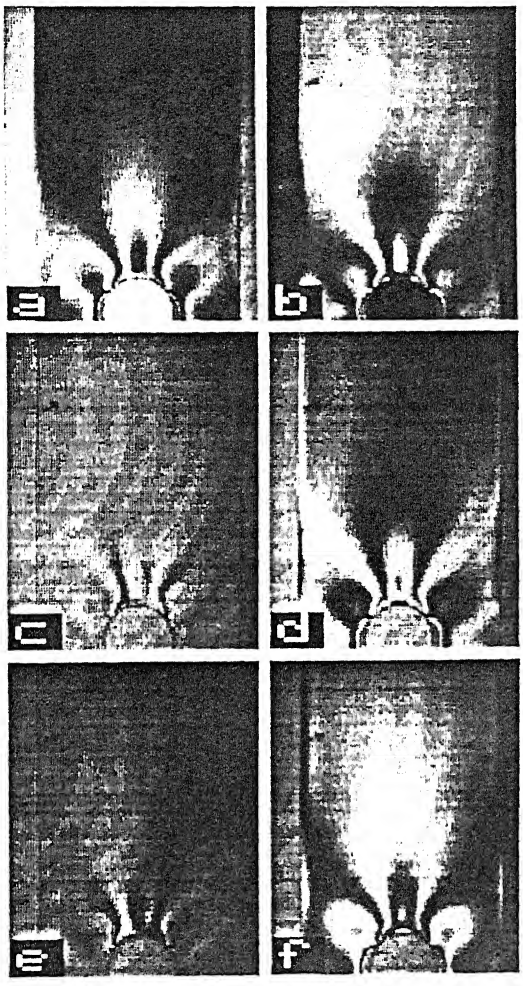

Fig. 3.37 The sequence of six images of a plate with a hole under uni-axial tension recorded for phase shifting technique, by plane polariscope arrangement.

σ_1: FEM

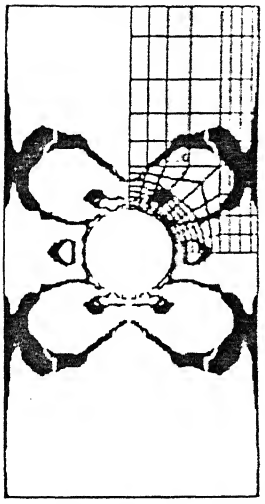

σ_2: FEM

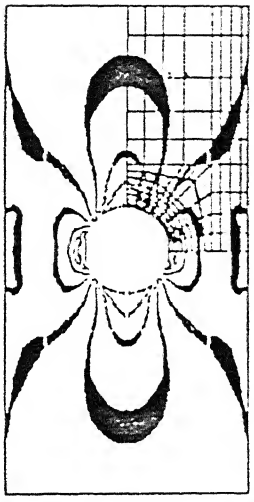

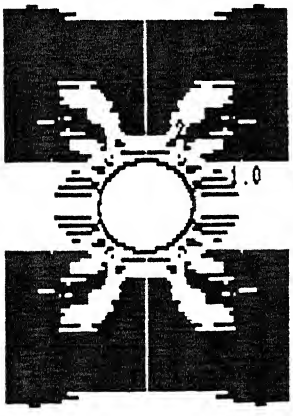

(c) σ_1 : Shear difference

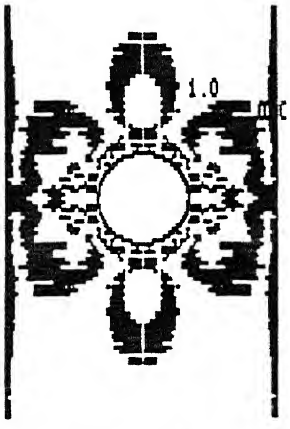

(d) σ_2 : Shear difference

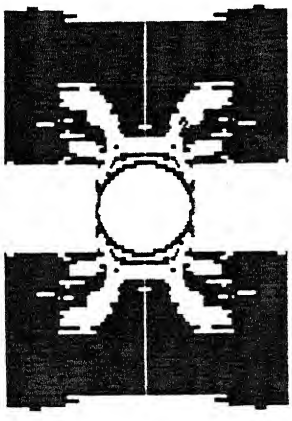

(e) σ_1 : Trebuna

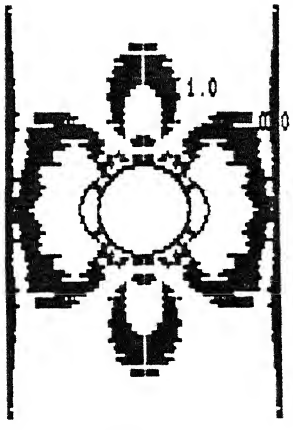

(f) σ_2 : Trebuna

Fig. 3.37 Field variation of principal stresses for the plate with a hole
(a) σ_1: FEM (b) σ_2: FEM (c) σ_1: shear diff. (d) σ_2: shear diff.
(e) σ_1: Trebuna (f) σ_2: Trebuna

and shear stresses on a plane tangential to free boundary are therefore zero. Also, as the principal stress axes are normal and tangential to the boundary, one of the principal stress is zero on the free boundary. Finally, (refer section 3.8.1.2) σ_x and σ_y on the free boundary are given by :

$$\sigma_x = \sigma_1 \cos^2(\theta)$$

$$\sigma_y = \sigma_1 \sin^2(\theta)$$

$\sigma_1 = N f_\sigma / t$; σ_2 being zero.

N : fringe order on the boundary.

f_σ: Material fringe value.

t : thickness of the model

Now, the stress separation schemes are applied and results obtained. Ramesh, Mangal and Pathak[20], had solved the problem of the plate with a hole, using finite element analysis and presented the variation of principal stresses σ_1 and σ_2 in the form of fringes. So, as to present a comparative analysis, the stresses separated by shear difference scheme and Trebuna's scheme have been converted to the principal stresses and plotted in the form of the fringes (refer section 3.8.4) and presented in Fig. 3.38. Figure 3.38(a) and 3.38(b) show σ_1 and σ_2 contours, obtained from finite element analysis. The fringe contours for the principal stresses obtained by shear difference scheme are shown in Fig. 3.38(c) and 3.38(d) while those obtained by Trebuna's scheme are presented in Fig. 3.38(e) and 3.38(f). With, erroneous (θ), Trebuna's method is expected to offer better results, due to the averaging effect of (θ), across the grid lines. It can be clearly seen from the graphs that shear difference's solution has certainly been improved by incorporating Trebuna's modification to it.

form of pseudo fringe patterns.

From the results, for the disc under diametral compression, it is revealed that the results obtained by Shear difference method and Trebuna's method by employing theoretical data are in complete agreement with those obtained by employing the standard formulations, based on theory of elasticity. The results obtained corresponding to usage of phase-shifting (N) and theoretical θ, are reasonably accurate. This establishes phase-shifting as a reliable technique for determining the isochromatic parameter (N). The indeterminacy of (θ), at full fringe orders, poses problems and these points are reflected as noise points. The usage of erroneous (θ) along with the phase-shifting (N) leads to extremely poor results which are in no way reliable. It is shown that the averaging effect of (θ) in Trebuna's method causes improvement in results over shear differences's results. This effect is also reflected in the stress contours for the plate with a hole, subjected to uniaxial tension.

4.2 Suggestions For Future Work

1. Since the role of θ plays an important role on the overall accuracy , newer technique for θ evaluation by phase shifting has to be looked into.
2. Recent studies have indicated that the evaluation of N by phase shifting technique can be improved further. This methodology needs to be incorporated for stress separation.
3. The method should be applied for a variety of problems to improve the ruggedness of the solution.

REFERENCES

1. K.Ramesh and K.Murlidhar, *Short Term Cource On Computer Applications In Experimental Mechanics*, Quality improvement program, I.I.T. Kanpur, 1-13 (1994).
2. James.W.Dally and William.F.Riley, "Experimental Stress Analysis", McGraw-Hill, Inc.
3. K.Chandrashekhar and K.Abraham Jacob, "A method for seperation of stresses in two and three dimensional Photoelasticity", *Journal of Indian Institute Of Science*, Vol 58. No.8,331-340 (1976).
4. L.S.Srinath, M.R.Raghavan, K.Lingaiah, G.Gargesha, B.Pant and K.Ramachandra, "*Experimental stress analysis*", Tata McGraw-Hill (1984).
5. K.Chandrashekhar and K.Abraham Jacob, "An Experimental-Numerical Hybrid Technique For Two Dimensional Stress", *Strain*, 13(4), 25-31 (1977).
6. K.Chandrashekhar and K.Abraham Jacob, "A numerical method seperation of stresses in Photo-orthotropic Elasticity", *Experimental Mechanics*, 18(2), 61-66 (1977).
7. S.J.Haake and E.A.Patterson, "The determination of principal stresses from photoelastic data", *Strain*, 153-158 (Nov. 1992).
8. R.O.Case and A.C.Barkoff, "Computer assisted reduction of two - dimensional photoelastic Shear-difference data", *Experimental Techniques, 32-37* (1986).
9. K.Ramesh and S.K.Mangal, "Data Acquisition Techniques in Digital photoelasticity: A review", *Opt. And Lasers In Eng.*, 53-75 (1998).

10. A.Asundi, "Phase shifting in photoelasticity", *Expl. Techniques*,17,19-23 (1993).

11. F.W.Hecher and B.Morche, "Computer-aided measurement of relative retardations in plane photoelasticity", *Experimental Stress Analysis*, (ed) H.Wieringa, Martinnus Nijhoff Publishers, Dordrecht, The Netherlands, 535-542 (1986).

12. E.A.Patterson and Z.F.Wang, "Towards full field automated photoelastic analysis of complex components", *Strain*, 27, 49-56 (1991)

13. A.V.S.S.S.R.Sarma, S.A.Pillai, G.Subramanian, T.K.Varadan, "Computerized image processing for whole-field determination of isoclinics and isochromatics", *Expl. Mechanics*, 32, 24-39 (1992).

14. K.Ramesh and V.Ganapathy, "Phase-shifting methodologies in photoelastic analysis-the application of Jones calculus", *J.Strain Analysis*, 31, 423-432 (1996).

15. S.K.Mangal and K.Ramesh, "Use of multiple loads to extract continuous isoclinic fringes by phase-shifting technique", *Strain* (in press).

16. D.Sreedhar, *Phase Unwrapping and Optically Enhanced Tiling In Digital PhotoElasticity. M.Tech Thesis*, Dept. of Mech Engg., IIT Kanpur (1997)

17. Patterson E.A., Ji W. and Wang Z.F, "On image analysis for birefringence measurement in photoelasticity", *Optics and Lasers in Engineering*, 28, 1, (1997), 17-36.

18. Haake S.J. and Patterson E.A., "Photoelastic analysis using a full-field spectral analyser", *Proc. SEM spring conf. on Experimental Mechanics,* (1995), 342-345.

19. Petrucci G., "Full-field automatic evaluation of an isoclinic parameter in white light", *Experimental Mechanics*, 37, 4, (1997), 420-426.

20. S.K.Mangal, P.M.Pathak and K.Ramesh, "Use of finite element for stress

separation in digital photoelasticity", *Journal of the Aeronautical Society of India* (communicated).

APPENDIX-I

THEORETICAL STRESS FIELD FOR DISC UNDER DIAMETRAL COMPRESSION

The stress field in a circular disk under diametral compression can be obtained using theory of elasticity from Bousinesque's solution for a compressive load on an half plane and then applying the principle of superposition appropriately. The stress field is obtained as

$$\begin{Bmatrix} \sigma_x \\ \sigma_y \\ \tau_{xy} \end{Bmatrix} = -\frac{2P}{\pi t} \begin{Bmatrix} \dfrac{(R-y)x^2}{r_1^4} + \dfrac{(R+y)x^2}{r_2^4} - \dfrac{1}{D} \\ \dfrac{(R-y)^3}{r_1^4} + \dfrac{(R+y)^3}{r_2^4} - \dfrac{1}{D} \\ \dfrac{(R+y)^2 x}{r_2^4} - \dfrac{(R-y)^2 x}{r_1^4} \end{Bmatrix}$$

where,

$$r_1^2 = x^2 + (R-y)^2$$
$$r_2^2 = x^2 + (R+y)^2$$

P: is the applied load (N).

R: is the disc radius (mm).

D: is the disc diameter (mm).

t: is the thickness of the disc (mm).

APPENDIX-II

MODEL : DISC UNDER DIAMETRAL COMPRESSION

PHYSICAL DIMENSIONS:

(i) Diameter : 60.06 mm
(ii) Thickness : 5.04 mm

MATERIAL PROPERTY :

Material fringe value F_σ : 11.64 N/mm/fringe

IMAGE FRAME SPECIFICATIONS :

Image used : dskplt12.p01
: dskplt12.p02
: dskplt12.p03

Centre : (127,127)

Increment along X-axis, delx : 0.3532941 mm
Increment along Y-axis, dely : 0.2461475 mm

Aspect ratio : 0.6967213

APPENDIX-III

MODEL : PLATE WITH A HOLE UNDER UNI-AXIAL TENSION

PHYSICAL DIMENSIONS:

(i) Width	:	37 mm
(ii) Length	:	174 mm
(iii) Thickness	:	5.26 mm
(iv) Hole Diameter:	60.06 mm	

MATERIAL PROPERTY :

Material fringe value F_σ	:	11.5 N/mm/fringe

IMAGE FRAME SPECIFICATIONS :

Image used	:	platew15.p01
	:	platew15.p02
	:	platew15.p03
Centre	:	(154,225)
Increment along X-axis, delx	:	0.362745 mm
Increment along Y-axis, dely	:	0.257549 mm
Aspect ratio	:	0.710